NATURALLY-DERIVED EXTRACELLULAR MATRIX MATERIALS FOR MENISCUS REPAIR AND REGENERATION

by

JINGLEI WU

Presented to the Faculty of the Graduate School of

The University of Texas at Arlington in Partial Fulfillment

of the Requirements

for the Degree of

DOCTOR OF PHILOSOPHY

THE UNIVERSITY OF TEXAS AT ARLINGTON

August 2017

Acknowledgements

I would like to take this opportunity to express my appreciation to my supervising professor, Dr. Yi Hong, for his guidance, insights, support, and encouragement during my graduate study at UTA for the past years. He provides a great academic environment and valuable resources and devotes his passion and wisdom to my dissertation work.

I would like to thank my dissertation committee, Dr. Liping Tang, Dr. Kytai T. Nguyen, Dr. Baohong Yuan, Dr. Jun Liao, and Dr. Yi Hong, for their great insight and suggestions for me outlining and writing the dissertation. Also, I would like to acknowledge Dr. Tang and Dr. Nguyen for granting me the access to their facilities and their assistance with some of my experiments.

Many thanks to my colleagues, Cancan Xu, Danh Truong, Qing Ding, Ahana Dutta, Xingjian Gu, Victoria Messerschmidt, Roshni Iyer, and Nikhil Pandey, for their support, contributions, and companions for the past years. In addition, I would like to thank Yi-Hui Huang for her assistance with animal studies, histological and immunohistochemical analysis. In addition, thanks to Dr. Connie Hsia, Dr. Ge Zhang, Dr. Priya Ravikumar, Dr. Bryn Brazile, and Megan Jeffords for their excellent work that helps me build more publications.

Finally, I would like to acknowledge my family for their support and understanding. They have always been there for me. This work is dedicated to my father, whose love was unforgettable and never ending. I can always feel your smile and encouragement. You raised me up and devoted all your life to me. I would thank you forever.

Abstract

NATURALLY-DERIVED EXTRACELLULAR MATRIX MATERIALS FOR MENISCUS REPAIR AND REGENERATION

Jinglei Wu, PhD

The University of Texas at Arlington, 2017

Supervising Professor: Yi Hong

Human meniscus plays critical roles in a knee joint by transmitting weight-bearing force, absorbing shock, and stabilizing the knee joint capsule. Meniscal injuries are mainly caused by sports-related activities and age-related degeneration, which significantly reduce the life quality of patients. The injured meniscus has a very limited self-healing capability due to its poorly vascularized nature, specifically in the inner area. Surgical interventions are required to treat the injured meniscus, but the current treatments are not satisfactory because the post-surgery complications are frequently observed. Therefore, tissue regeneration approaches are developed to repair and functionally restore injured menisci. In this thesis, we focus on the development of extracellular matrix (ECM) based materials derived from porcine knee meniscus and investigate their potential in meniscus repair and regeneration.

We firstly decellularized porcine menisci based on a sodium dodecyl sulfate (SDS) protocol, processed the decellularized meniscus ECM into an injectable hydrogel, and then assessed the potential of the ECM hydrogel for meniscal repair and regeneration.

The SDS treatment was effective in DNA removal and resulted in enriched collagen content and an obvious loss in glycosaminoglycan (GAG) content. The meniscus ECM hydrogel had a fibrous structure, tunable mechanical properties, and excellent injectability. It supported cell infiltration and three-dimensional (3D) cell growth *in vitro*. The solubilized meniscus ECM was capable of smoothly injecting into mice and showed good biocompatibility.

Secondly, in order to improve the GAG retention after decellularization, we optimized the meniscus decellularization protocol by comparing three chemical detergents and evaluated the differences among the resulting meniscus ECM hydrogels in material properties and biological performance. It was found that the peracetic acid (PAA) was the most effective in meniscus decellularization. It showed better preservation of ECM structure, maximal DNA removal, and the greater GAG retention compared with the SDS and Triton X-100 (TX) treatments. The PAA-treated ECM (PAA-ECM) hydrogel possessed greatest compressive strength. It promoted significantly higher GAG accumulation of fibrochondrocytes and exhibited the highest biomechanical strength when encapsulated with fibrochondrocytes and cultured for 28 days.

Subsequently, we sought to prepare regionally-specific meniscal ECMs by dividing porcine menisci into three distinctive zones and decellularizing them with the optimized protocol. The inner meniscus ECM contained less collagen and significantly higher GAG compared with the middle and outer meniscus ECMs. These biochemical variations resulted in the varying compressive strengths of the regional ECM hydrogels and greatly influenced the cell behaviors in the hydrogels. Specifically, when

encapsulated with bovine fibrochondrocytes for 28 days, the inner meniscal ECM hydrogel accumulated more GAG, contracted to a greater extent and exhibited higher compressive strength compared with that of the outer meniscal ECM hydrogel.

Based on the above three aims, our future study will focus on illustrating the versatility of meniscus ECM in biomedical applications. Preliminary results demonstrated that decellularized meniscus ECM can be blended with polycaprolactone (PCL) and electrospun to form PCL/ECM hybrid nanofibrous scaffolds. The PCL/ECM scaffolds had better hydrophilicity, greater tensile strengths, and initial moduli compared to the PCL scaffold alone. The PCL/ECM scaffold was cytocompatible to support meniscus fibrochondrocyte growth and was capable of promoting GAG accumulation, indicating its great potential for meniscus repair and regeneration.

In summary, this work demonstrates the development and optimization of decellularized meniscal ECMs. It provides a platform for the preparation of injectable meniscal ECM hydrogels that exhibit meniscal tissue-specific bioactivity and support 3D meniscal cell growth and promote cell-secreted products, which may have opportunities to treat injured menisci through a minimally-invasive manner.

Table of Contents

List of Illustrations

CHAPTER 1

INTRODUCTION

1.1 Structure, function, and pathophysiology of human meniscus

The knee joint contains a pair of crescent-shaped fibrocartilaginous tissues, a medial meniscus, and a lateral meniscus. They are located between the femoral condyle and the tibial plateau and play critical roles in the knee joint in daily activities [1]. The meniscus was defined as “the functionless remains of a leg muscle” over a century ago, and it was totally removed from the knee joint through a surgery called meniscectomy once damaged. Later, the meniscus was found to be capable of partial self-regenerating, and then the strategy for the meniscal damage was replaced by partial meniscectomy that is to remove the injured part and retain the healthy part of a meniscus [2-5]. With the increasing awareness of osteoarthritis (OA) diseases after the total and partial meniscectomy, the importance of meniscus to the knee joint was elucidated in the later studies [6]. The main function of the meniscus is to work with ligaments to stabilize the knee joint and to buffer high levels of load between the femoral condyle and tibial plateau [7]. Most problems of the meniscus are related to acute sports injuries. One of the common cases is traumatic meniscal tear. When the impact force of the femoral condyle and tibial plateau overwhelms the threshold, the meniscus tears in longitudinal or vertical directions. In addition, the age-related degeneration is also associated with the meniscus damage [8-10]. The main reason is reduced proteoglycan in the aged meniscus, which makes the meniscus stiffer and less flexible to resist the vertical pressure in the knee joint [11].

1.1.1 Structure and function of meniscus

The menisci are two pieces of crescent-shaped fibrocartilage discs located in the knee joint, specifically between the femoral condyle and tibial plateau (Figure 1.1A). The knee joint contains a pair of menisci, medial and lateral, with their anterior and posterior horn attached to the ligaments. This combined system can stabilize the joint capsule (Figure 1.1B). The meniscus is a fibrocartilage tissue that exhibits good elasticity to provide mobility and strong mechanical strength to resist tension, compression, and shear stress. Therefore, the meniscus can provide the mechanical stabilization to the whole knee joint, transmit the huge loading stress on a large area to cartilage, and absorb the shock during activities.

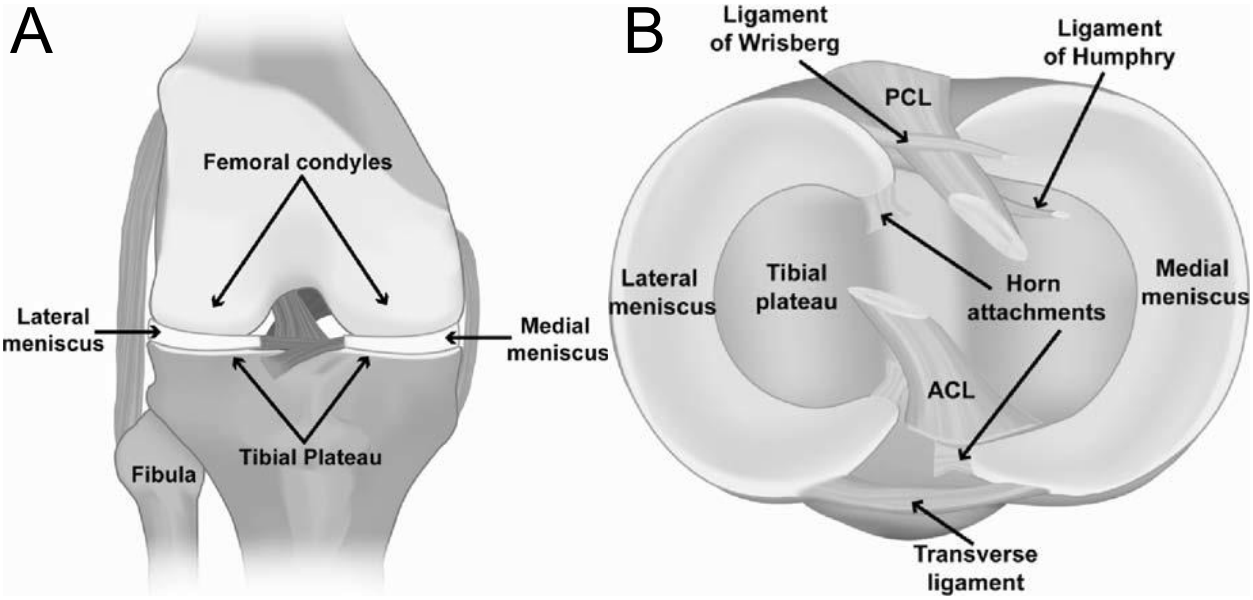

Figure 1. 1 Anterior (A) and superior (B) views of the meniscus in the knee joint. Pictures are cited from [3].

The menisci are generally considered to be partial vascularized because the capillaries infiltrate from the neighboring synovium to the peripheral border and

penetrate up to 30% of the whole width. The capillary infiltrated zone is called as “red-red region” with the overwhelming majority of blood supply and neural presence. The vascularization decreases from the peripheral zone to the middle and inner zones. A distinctive region of the one third inner zone without blood supply or neuron is named as “white-white region” that is totally different from the “red-red region”. The transitional zone between the outer and inner zones is called “red-white region”. It has a limited blood supply, while its vascularization is significantly reduced compared with the “red-red region”. In this thesis, the “red-red region”, “red-white region”, and “white-white region” are designated as “outer zone”, “middle zone”, and “inner zone”, respectively.

The native meniscus contains 70% water, with collagen making up about 60-70% of its dry weight [12]. Along with the variation in the degree of vascularization, the biochemical compositions, and local cell types alter from the outer zone to the inner zone. The extracellular matrix of the meniscus is mainly composed of the collagen with minor proteoglycans and some growth factors [12, 13]. The collagen fibers are predominately circumferential in the meniscus with small quantities of radially-oriented collagen fiber on the surface. Unlike the cartilage that has a uniform distribution of collagen type II supplemented with small portions of collagen type IV and VI throughout the tissue [14], the meniscus has predominant collagen type I with smaller amounts of collagen type II, III, IV, V, and VI. The various types of collagen are heterogeneously distributed inside the meniscus. The outer zone contains only collagen type I with very low amounts of collagen type II and some growth factors.

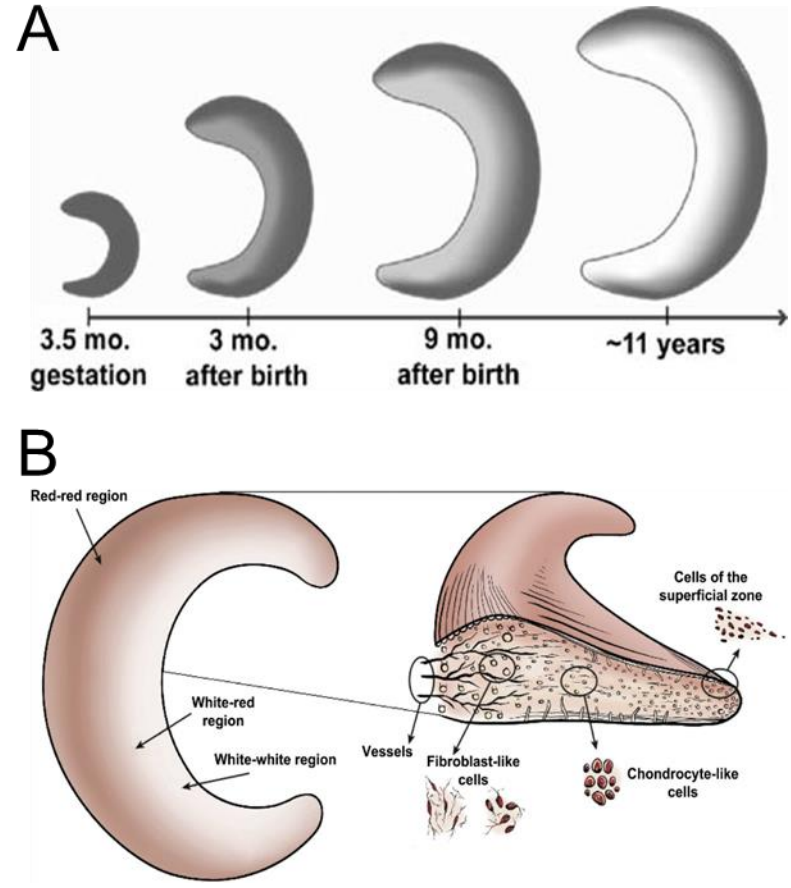

Figure 1. 2 (A) Gradually reduced vascularity of meniscus over time [3]. (B) Cells with distinct morphology within the different zones of meniscus [4].

The collagen composition of the inner zone is 60% collagen type II with 40% collagen type I [15]. Besides, there are some aggregating proteoglycans including glycosaminoglycans (GAGs), chondroitin sulfate, and dermatan sulfate in the inner zone. The middle zone exhibits a transitional feature in chemical composition that contains a major component of collagen type I with increased contents of collagen type II and proteoglycans from the outer to the inner zone.

Similar to the biochemical compositions, the cell types of the meniscus are distinct in terms of size, shape, and secreted products in each zone. The cell physiology of the meniscus is not fully understood, while it is evident that the cellular and vascularity

change over time (Figure 1.2A) [3]. Although there are increasing studies on the meniscal cellular biology and physiology, controversial in the cellular characterization still exists, especially names of the cells of the different zones [4, 16-18]. Generally, by the origination, the cells of the outer, middle, and inner zones were named as “outer meniscus cell”, “middle meniscus cell”, and “inner meniscus cell”, respectively [16, 19]. The cells in the outer zone have a fusiform shape that is similar to fibroblasts (Figure 1.2B). Moreover, like fibroblasts, the cells of the outer zone mainly produce collagen type I. Therefore, they were named as fibroblast-like cells as well. In contrast, the cells in the inner portion are totally different in shape. Those cells in the inner zone are somewhat round in shape and secrete a large amount of type II with higher amounts of proteoglycans compared with that of cells from the outer zone. As the morphology and secreted matrices of the inner meniscus cells are similar to chondrocytes to some extent, they are termed as “fibrochondrocytes” or “chondrocyte-like cells”.

Variations in cellular biology and chemical compositions in the different zones are highly related, and those cellular and chemical alterations of the meniscus are associated with its mechanical properties. The outer region is in fibrocartilaginous characteristic similar to tendon while the inner zone appears to more resemble with the hyaline cartilage in terms of gross appearance and histological properties. These structural and compositional properties enable the meniscus to withstand multiple forces including shear force, tensile and compressive stress. There is a huge difference in tensile strengths in the circumferential and radial directions: the meniscus has a tensile strength of 100-300 MPa in the circumferential direction, but it is around 10-fold lower in the radial direction. This variation is associated with the collagen fiber

orientation [11]. The shear modulus of the meniscus is around 120 kPa [11]. In addition, the meniscus has a compressive aggregate modulus of range from 100 to 150 kPa [20]. In a healthy knee joint, the menisci occupy approximate 50-60% of the contact area between the femoral condyle and the tibial plateau, while transmitting at least 50% of the axial load in the knee joint. Total or partial meniscectomy significantly reduced contact area compared to the healthy knee joints. It was reported that the total removal of the meniscus by meniscectomy resulted in 2- to 3-fold increase in the peak contact load in the knee joint.

1.1.2 Meniscus pathophysiology

The meniscal tear represents one of the most common knee joint injuries and accounts for more than 50% of knee joint surgeries. It has an average incidence of 66 per 100,000 people, in which more than 90% cases require surgical intervenes [4, 21, 22]. The meniscal tears in the outer zone are capable of self-healing to some extent while this capability largely depends on the size of lesions and on the patient age. However, the inner zone of the meniscus has very limited self-healing capability because of its character of avascularization.

The meniscal lesions are associated with sports activities, which mainly occur in young people. Overwhelmed impact forces, hypertensions, and twisting movements are the main causes of the sports-related meniscal injuries. Besides, the meniscal lesions are also attributed to accidents. According to the orientation and shape, the meniscus tears can be categorized into four groups: longitudinal tear, radial tear, complex tear and bucket-handle tear [4, 23-25]. A longitudinal tear takes place along

the direction of circumferential collagen fibers, which partially separates the meniscus along the split. A radial tear is perpendicular to the circumferential collagen fibers. Most radial tears start from the inner edge toward to the outer zone because the inner zone is much thinner than the outer zone. A complex tear has more than one splits that form an irregularly shaped lesion. This kind of meniscal tear is frequently occurred in the aged population due to the degenerative progress. The bucket-handle tears are relatively larger than the longitudinal and radial tears and exhibit huge lesions in the inner zones, leaving the peripheral portion in the shape of a bucket-handle.

The age-related meniscal lesions are not fully understood. It is generally considered that they highly depend on the age-related changes in biochemical compositions [8-10]. Gradually degenerative progress changes the biochemical property of meniscus, making it more vulnerable to injury [26]. The most significant age-related change is the reduced elasticity due to the gradual loss of proteoglycans, which results in decreased flexibility of the meniscus [24]. Degenerative meniscal tears are not directly linked to the pain in the knee, while they play critical roles in knee OA [27].

1.2 Current strategies of meniscus tissue engineering

Tissue engineering offers great potential for meniscus repair and regeneration. The current progress in the development of tissue engineered substitutes for meniscus repair and replacement is expected to reduce the health burden of meniscus diseases. The limited success was made due to the high difficulty in recapturing the nature of meniscus organization in biochemical composition and cellular population [28].

Meniscus tissue engineering aims to prepare the meniscus substitutes that combine scaffolds, cells, and growth factors to recreate the microenvironment of the native meniscus. A good integration of the substitute with the surrounding tissue whilst maintaining biomechanical stability and promoting cellular ingrowth is critical for meniscus regeneration.

Current approaches of meniscus tissue engineering are not perfect as the regenerated meniscus tissue is inferior in quality than the native meniscus tissue, and is prone to failure [29]. The difficulty of repairing the meniscus also presents in the repair of some other dense tissues, such as cartilage and intervertebral dish. Therefore, continuous efforts in preparing engineered scaffolds either using synthetic or natural polymers, or their combination have been made to provide a microenvironment that mimics meniscus ECM to facilitate cell growth and tissue remodeling. In addition, a good understanding of complex of meniscus including cellular physiology and heterogeneous fibrous structure will be highly beneficial for the fabrication of ideal scaffolds and advanced design of cell-integrated implants for meniscus repair and regeneration.

1.2.1 Scaffolds

Engineered meniscus scaffolds provide conducive microenvironment and appropriate mechanical strength to bridge up the meniscal lesions and to facilitate tissue remodeling. Currently, the meniscus scaffolds in the forms of porous sponge, fibrous mat, bulk decellularized ECM, and hydrogel, and they are made from synthetic and biological materials.

1.2.1.1 Porous scaffolds

Porous scaffolds possess large pores, good interconnectivity, and acceptable mechanical strength to provide temporary templates for cellular ingrowth and tissue remodeling. Polyurethane (PU) represents a family of elastic polymers that have been widely utilized for a range of tissue engineering applications [30-35]. The PU porous scaffold with the comparable compressive strength to the native meniscus prepared by salt leaching showed a uniform pore size and isotropic structure [36]. More importantly, the PU scaffold resembles the macrostructure by casting in a custom-made mold. PU scaffolds were shown to be nontoxic to support bone mesenchymal stem cell (BMSC) growth *in vitro* [37]. Another study using PU porous scaffold for partial meniscus defect repair demonstrated successful cellular ingrowth into the implanted scaffolds and at three months in patients with partial meniscectomy surgeries meniscus-like tissue formation [38]. Porous scaffolds made from other synthetic materials such as poly (lactic acid) (PLA) [39] and polycaprolactone (PCL) [40] , and from natural materials such as silk fibroin [41-43] and collagen [44-46]. Preparation of collagen and silk scaffolds is frequently achieved by lyophilizing. For example, collagen sponge scaffolds also called collagen meniscus implants (CMIs), are made from acid-extracted collagen that is solubilized, oriented in a custom-made mold, lyophilized and chemically crosslinked. The CMI is promising in meniscus repair and replacement, as clinical studies in literatures showed that CMI was capable of filling the meniscus defect and supporting cellular infiltration [46, 47]. Follow-up studies showed that after CMI treatment, patients were able to return sports activities, experienced less pain, and did not show progressive osteoarthritis during 6- to 8-year period [47].

As the major component of native ECM, collagen is highly biocompatible and extremely favorable for cellular growth, however, it mechanically weaker than the synthetic scaffolds. While the synthetic scaffolds lack biological cues to direct cell behaviors and guide tissue remodeling. Therefore, scaffolds of the combinations synthetic and natural materials might take the advantages of both materials and overcome their inherent shortcomings of each material, yielding improved performance for meniscus regeneration [48].

1.2.1.2 Fibrous scaffolds

Fibrous scaffolds with fiber size range from nano- to micro-scale that resembles the nature of ECM fibers. Electrospinning is a costless, versatile and feasible technique to produce nano- to micro-scale fiber mats that have been extensively investigated as scaffolds for various tissue engineering applications [49-54], including meniscus [55]. In the past two decades, a great number of studies have demonstrated that electrospun scaffolds are attractive in promoting cellular growth and in manipulating cell behaviors by patterning scaffold texture [56-59]. Human meniscal cells proliferated well on electrospun PCL scaffolds. The cells showed a polygonal shape on randomly-oriented scaffolds, while on aligned fibrous scaffold, they exhibited an elongated morphology along the aligned fiber direction [60]. Similar variation in meniscal cell morphology on electrospun randomly-oriented and aligned scaffolds either made from collagen [61] or PLA [62]. The fiber alignment of electrospun scaffolds promoted the maturation of cell-seeded constructs and contributed to the increase in mechanical strength [63, 64]. Moreover, the total DNA, collagen and GAG contents of the cell-seeded constructs

increased over the *in vitro* culture period, accompanying with much higher stiffness and ultimate load [60-62].

While the above results of are promising, several concerns regarding the utilization of electrospun mats as meniscus filling materials should be addressed. One significant limitation of using electrospun mats to fill meniscus defects or replace resected menisci is associated with the inherent drawback of electrospinning. It is technically difficult to prepare fibrous mats with comparable thicknesses with native menisci, due to the large size and the challenge in replicating the complex geometry of meniscus. In order to increase the scaffold thickness, electrospun mats were layer-by-layer packed to form thick scaffolds that fit the thick meniscus defects [65, 66]. Another shortcoming of the electrospun scaffold is the densely compacted fibers could significantly hinder cellular infiltration into the scaffold and impede tissue ingrowth, which is unfavorable for meniscus repair and regeneration. Great efforts have been devoted to promoting scaffold pore size and loosening fibrous structure of electrospun scaffolds [67], leading a bright future of using electrospun scaffolds toward meniscus tissue engineering.

1.2.1.3 Decellularized ECM scaffolds

The decellularization of tissue/organ through chemical, physical and enzymatic methods or their combinations is elaborately documented in the literature [68-70]. Biological scaffolds derived from tissues have been used pre-clinically and clinically in several tissue engineering and regenerative medicine applications in the past decade [71, 72]. Decellularized ECM scaffolds contain tissue-specific biological and chemical

cues that recruit local cells to the injury sites [73] , facilitate cell growth [74], promote stem cell differentiation into specific lineage [75, 76], guide tissue remodeling and regenerate new tissue/organ [77, 78].

A study using decellularized meniscus ECM as scaffold material was reported by Yamasaki *et al*. in 2005, in which decellularized rat meniscus scaffolds were seeded with autologous MSCs [79]. This study showed the efficacy of repopulating MSCs and differentiating them into chondrocyte-like cells on the rat meniscus ECM scaffolds. A follow-up study by Yamasaki et al. demonstrated that when implanted in the meniscus defects in a rat model, the MSC-seeded rat meniscus ECM scaffolds were capable of providing a chondroprotective effect in the knee joints and promoting maturation of regenerated meniscus tissue within 28 days [80].

Decellularized meniscus ECMs originating from large animals such as sheep [81, 82], pig [83-87], cattle [88], as well as from human [89-91], were prepared and investigated in their material properties and biological performance. The decellularization process almost eliminates the cellular DNA and has negligible effects on the fibrous structure and content of collagen, but it causes a huge loss in GAG [89]. Similar changes in the contents of collagen and GAG could also be found in some other decellularized ECMs. Collagen is more resistant to the detergents or enzymes while GAG is more vulnerable to those reagents. In addition, GAG is water soluble, which makes it be easily washed out during the decellularization process. These might account for the fact that the decellularized meniscus ECM has the comparable tensile strength and failure strain, but significantly lower compressive strength to the native

meniscus [83], as the circumferentially oriented collagen fibers provide the tensile strength, and the GAG mainly contributes to the compressive strength of meniscus.

Decellularized meniscus ECM scaffold is highly biocompatible and bioactive and possesses biochemically meniscus-specific cues to support cell growth. However, cells mainly grow on the surface of decellularized meniscus ECM scaffolds with very limited infiltration, due to the dense structure of the scaffolds [83, 84, 89]. Autologous meniscus cells were injected into the decellularized meniscus ECM scaffolds via a needle and they survived during a culture period of 28 days [81]. This method highlighted a 3D growth of cells with a heterogeneous cell distribution within the scaffold.

1.2.1.4 Hydrogels

The hydrogels made from many natural materials have been used for meniscus tissue engineering. Collagen and alginate are the most frequently investigated natural materials that have been prepared into hydrogels for meniscus repair and regeneration [92-96]. Meniscal cells showed high viability inside those hydrogels because of the high biocompatibility and mild gelling process of those hydrogels. Accumulations of collagen and GAG were identified in meniscal cell-seeded hydrogels, accompanying with a great increase in tensile strength and compressive stress [92]. In addition, it is found that the bovine meniscus fibrochondrocyte behaviors are largely affected by the fiber orientation [93] and the concentration of hydrogels [92], and also are dependent on the external mechanical stimulus [94]. These factors also affect the development and maturation of engineered meniscus *in vitro*. As a non-sulfated glycosaminoglycan that presents in native meniscus ECM, hyaluronic acid has been combined with type I

collagen to form riboflavin-induced photocrosslinking hydrogels for meniscus repair. When encapsulated with tonsil-derived mesenchymal stem cells, the cell-laden hydrogels remained their original sizes and shape, and exhibited a compressive modulus of 582.95 ± 121.85 kPa that is much stronger than the native meniscus [97].

Synthetic polymers have also been processed into hydrogels for meniscus repair. Poly(vinyl alcohol) (PVA) hydrogel with a high water content of 90% was implanted in the knee joints as a substitute replacing the whole meniscus in a rabbit model [98-100]. In a 2-year follow-up study, the PVA hydrogel could execute meniscus function even after 2 years and reduced the compressive strength within the rabbit knee joints compared to the meniscectomy groups [101]. But PVA is a nondegradable polymer and might be not suitable for meniscus tissue engineering.

In addition, copolymer hydrogels made from the synthetic and natural materials have been prepared for meniscus tissue engineering. A thermos-responsive chitosan-graft-poly(N-isopropylacrylamide) hydrogel with comb-like structure was synthesized for the culture of meniscus cells [102]. This injectable copolymer preparation was capable of encapsulating meniscus cells and forming gels *in situ*, can could serve as a coating material to improve meniscus cell attachment and a vehicle for cell delivery [103]. A composite hydrogel made from alginate and polyacrylamide by 3D printing perfectly reconstructed the anatomical shape of meniscus [104]. The composite hydrogel had a comparable elastic modulus (260 ± 20 kPa) to the native meniscus (100 ~ 300 kPa) [28, 105]. However, the researchers' current work merely focuses on the fabrication of the hydrogel, *in vitro* and *in vivo* studies are needed to demonstrate the biocompatibility and capability for meniscus tissue engineering [104].

1.2.2 Cell sources

The cell physiology of meniscus tissue is complex and changed over time as the tissue develops [3]. The meniscus tissue is fully vascularized at the beginning of its formation in the body, and the cells mainly exhibit a circle shape. With the tissue development, the degree of vascularization and cell morphology vary in different zones. Specifically, the outer zone remains vascularized with the cells in a fibroblast-like cell shape. The inner zone exhibits an avascular characteristic. The cells in the inner zone keep a round shape and secrete large amounts of proteoglycans. There are many cell sources including adult cells and stem cells for meniscus tissue engineering in literature as discussed by Makris *et al.* in 2011 [4].

1.2.2.1 Adult cells

Adult meniscal cells are considered as excellent candidates for meniscus tissue engineering, as they are the resident cells of meniscus tissue. Meniscal cells may experience same gene expression profile and produce identical biochemical products in engineered meniscus tissue as that of the cells in native meniscus tissue. Cells isolated from whole meniscus tissue without zonal variations were attempted for this purpose [106-108]. Those studies showed some positive results while they failed to distinguish the cellular altering in different zones of the meniscus. It might be restricted to some technical challenges. For example, rabbits have much smaller menisci compared with that of some large animals [109]. It is not easy to separate rabbit menisci into different zones. Therefore, it is better to perform the studies of regional cellular variations on large animals such as pig and calf.

The variations in cell physiology of meniscus tissue have been noticed and their associations with biochemical and biomechanical properties of tissue are well-documented in the literature [15, 110-113]. There is an increasing effort in separating cells from different regions and applying those regional cells for the repair and regeneration of their respective regions of tissue, and to build up a regenerated meniscus with zonal variations [16, 17, 114-116]. For instance, many studies now focus on fibrochondrocytes, the resident cells of the inner meniscal zone, and apply them toward regenerating the avascular zone of meniscus [117-122]. Fibrochondrocytes are expected to produce more collagen type II and proteoglycans to increase the elasticity of regenerated menisci. The fibroblast-like cell mainly produces collagen type I, which is a good candidate to repair the outer zone of the meniscus.

The use of adult meniscal cells as cell source is advantageous for meniscus tissue engineering, while some limitations still exist. First, the harvest of adult meniscal cells unavoidably results in donor site morbidity of healthy tissue. Additionally, the expansion of those cells is very challenging, as the cells have limited capability of proliferating *in vitro*. Secondly, great difficulties exist when trials are made to isolate and to distinguish those different meniscal cell types *in vitro*, as cell-specific markers are lacked [123, 124]. This challenge is associated with the technical difficulty to exactly define the distinct regions that contain zonally specific cells. Last, similar to the culture of chondrocytes, expansion of fibrochondrocytes through *in vitro* cultivation accompanies with progressive cell dedifferentiation. Specifically, fibrochondrocytes gradually lose their chondrogenesis with a shift from a high level of gene expression of

collagen type II to a predominant collagen type I gene with a low-level collagen type II expression over the cultivation period [125].

Other adult cell sources including fibroblasts and chondrocytes were also attempted for meniscus tissue engineering [42, 82, 83, 89, 90, 126, 127]. Fibroblasts have a high similarity of gene expression profile to meniscus fibroblast-like cells while chondrocytes share the very similar gene expression profile of meniscus fibrochondrocytes. When combined with engineered scaffolds that have laminar channels, fibroblasts grown along the channels and secreted aligning collagen, which mimics the aligned collagen fibers that contribute to the high intrinsic tensile strength of the meniscus tissue [42]. In a proof-of-concept study, fibroblast-seeded scaffolds incorporated in meniscus defect in an *ex vivo* model showed that fibroblasts continuously producing collagen type I, which ultimately formed fibrocartilaginous tissue [127]. Chondrocytes could be the optional cell source to treating avascular zone of the meniscus. They have been seeded with various types of scaffolds including porous scaffolds [42], fibrous mats [116, 118, 128], decellularized meniscal ECM [83, 86, 89, 90] and hydrogels [129], and demonstrated great potential for the meniscus tissue engineering.

1.2.2.2 Stem cells

Stem cells are undifferentiated cells without any tissue-specific tissue function, or with preferential tissue commitment, and could be induced to particular adult cell types under certain conditions [130-132]. Stem cells can be isolated from various sources [133] including bone marrow, adipose, synovium, and muscle, and these cells have

been applied to a wide range of cell tissue engineering applications [134-137]. Like some of the adult cells, the expansion of stem cells is limited, that before stopping proliferation, the cells can only passage a few number of times [133]. For stem cells, the capacity of expansion is also largely determined by the donors' conditions. Stem cells keep an undifferentiated state throughout a lifetime in the body, however, they often undergo an "aging" process and gradually lose the capacity of differentiation under *in vitro* culture. All these conditions are critical for successful tissue engineering and regenerative applications.

The current progress of using stem cells to repairing and regenerating meniscus tissue involve different strategies either with scaffolds or based on scaffold-free injection. A commonly used method is the cultivation of stem cells on engineered scaffolds and induction of those cells into adult cells that produce meniscus-specific tissue ECM. Stem cell proliferation, infiltration, and differentiation can be achieved *in vitro* or by implanting cell-seeded scaffold *in vivo*, with or without the administration of growth factors [64, 138]. A good example the MSC-induced meniscus regeneration is conducted in a rat model, where meniscus ECM scaffolds were seeded with BMSCs and then implanted into meniscus defect. Histological evaluation demonstrated that those BMSC incorporated scaffolds exhibited great chondroprotective effects in the rat knee joints [79, 80]. Another strategy is the administration of BMSC into the defect sites that caused by trauma and degeneration [139-142]. This is a very popular surgical approach due to its high feasibility, minimally invasive manner, and low cost.

1.2.3 Growth factors

Functional tissue formation requires a variety of growth factors that work alone or in combination to stimulate the cell proliferation and differentiation, as well as promote neo-tissue formation. Growth factors are the most critical biochemical stimuli that contribute to meniscus tissue modeling and regeneration [143, 144]. Nine growth factors have been employed to investigate their effects on the growth of meniscus cells [145]. It was found only a few of them (endothelial growth factor (EGF), transforming growth factor-α (TFG-α), basic fibroblast growth factor (bFGF), and platelet-derived growth factor AB (PDFG-AB)) were capable of promoting meniscus fibrochondrocyte growth and enhancing collagen synthesis *in vitro*. Different growth factors might play distinct roles in meniscal cell growth and ECM deposition. It is showed several growth factors can enhance meniscal cell growth however they function in different pathways in regenerated menisci, where only insulin-like growth factor I (IGF-I) could significantly increase the collagen type II accumulation [116]. Angiogenesis, a process of blood vessel formation in tissue, is essential in the healing of injured tissues. This process often accompanies with the producing of endogenous growth factors. A high level of expression of vascular endothelial growth factor (VEGF) was observed during the healing of damaged menisci in a rabbit model [146]. Therefore, it is essential to select the appropriate growth factors for the restoration of meniscus tissue.

1.3 Research goal and specific aims

As discussed in **1.2.1.3**, decellularized meniscus ECM contains the complex of meniscus tissue-specific biological cues and is highly biocompatible and conducive for

meniscus cell proliferation, differentiation, and migration. But it has a densely fibrous structure that significantly hinders cell infiltration. Furthermore, it is technically difficult to make decellularized meniscus ECM perfectly fit meniscus defect. Therefore, in this thesis, we seek to develop and characterize novel decellularized meniscus ECM materials and process them into injectable hydrogels for meniscus repair and regeneration. Three aims of the future work are listed below.

In aim 1, we sought to develop a decellularized meniscus ECM from fresh adult porcine menisci by using SDS treatment. Because the major component of decellularized meniscus ECM is collagen, we speculated that the collagen-based complex is capable of self-assembling and forming a hydrogel when brought it into physiological condition. The material properties including structure, gelation behavior, and mechanical strength, as well as biocompatibility of meniscus ECM hydrogel, was determined to evaluate its capability of meniscus repair and regeneration.

In aim 2, the optimization of meniscus ECM hydrogel was conducted by comparing different chemical treatments of meniscus decellularization. The complement meniscus ECM hydrogel is evaluated by characterizing the hydrogel properties and biological performance. Bovine meniscus fibrochondrocytes will be encapsulated with hydrogels for the *in vitro* test. The growth and GAG accumulation of fibrochondrocytes in the meniscus ECM hydrogel were examined. The biomechanics of fibrochondrocyte-encapsulated meniscus ECM hydrogels were determined.

In aim 3, we investigated and compared the material properties and biological functions of the hydrogels from different regions of the meniscus, which may provide a new sight to understand the meniscus and regenerate the meniscus. The menisci were

regionally divided and decellularized, and then processed into regionally specific ECM hydrogels. The hydrogel properties of the structure, gelation behavior, and mechanical strength were determined.

Finally, we make conclusions based 3 aims and then summarize our future studies in ECM material development. We will further exploit the meniscus ECM materials in various types for regenerative applications. We have preliminarily incorporated the decellularized meniscus ECM with synthetic materials for a hybrid scaffold preparation. The decellularized meniscus ECM was blended with a synthetic polymer (PCL) to fabricate nanofibrous (PCL/ECM) scaffolds via electrospinning. The PCL/ECM scaffolds were characterized in morphology, surface hydrophilicity, and tensile strength. Bovine fibrochondrocytes were seeded with the PCL/ECM scaffold to assess its cytocompatibility and meniscus specific bioactivity. The proliferation and GAG accumulation of fibrochondrocytes on the PCL/ECM scaffold were determined.

CHAPTER 2

PREPARATION AND CHARACTERIZATIONS OF INJECTABLE ECM HYDROGEL DERIVED FROM MENISCUS

2.1 Introduction

Approximately 750,000 minimally-invasive arthroscopic surgeries are performed annually in the United States to treat meniscus diseases [46], that are caused mainly by sports-related injuries and age-related degeneration [4]. The meniscus has relatively low regenerative capability because of limited vascularization. The injured and diseased menisci usually were removed through complete meniscectomy [4], but this treatment resulted in a great increase in contact pressure on the tibial plateau and gradually led to osteoarthritis [4, 147]. Partial meniscectomy developed in 1982 also remains unsatisfactory due to a high risk of osteoarthritis [148-150]. Therefore, a new treatment of regenerating meniscus without osteoarthritis complication is needed, and intensive research efforts have been made to develop tissue engineering scaffolds to repair injured and diseased meniscus [40, 151].

There is an increasing interest in the use of biomimetic, tissue-specific biomaterials to simulate a native tissue microenvironment that can provide appropriate biological and chemical cues for tissue regeneration [152-154]. One approach is to develop extracellular matrix (ECM) scaffolds via decellularization of the native tissues. Such scaffolds contain complex ECM components mimicking with the ECM of the native tissue, and exhibit attractive bioactivity for tissue remodeling and regeneration [68, 155, 156]. The decellularization technique can remove cellular membrane antigens

and nuclear components to minimize immune response, allowing the material to be used safely in clinics. For example, decellularized porcine small intestinal submucosa (SIS) material has been commercialized and clinically used for skeletal muscle treatment [78]. Furthermore, decellularized materials as tissue-specific scaffolds show great promise in repairing and regenerating specific tissues and organs [157]. Among these, the implantation of heart-derived ECM material into an infarcted heart has been shown to promote endogenous cardiomyocyte recruitment and restore heart functions [158, 159]. Thus, it is likely that the complex ECM scaffold derived from meniscus can enhance meniscus regeneration.

The decellularized meniscal materials have been produced as cell-free scaffolds for meniscus repair and regeneration [88, 91]. These scaffolds also were combined with primary cells, such as human primary chondrocytes, murine fibroblasts, and porcine meniscal cells, and stem cells such as rat mesenchymal stromal cells (rMSC) to promote meniscus regeneration [79, 80, 82, 84, 86]. A rat meniscus-derived scaffold seeded with rMSCs was implanted into a rat defected meniscus, that showed better chondroprotective effect than the conventional meniscectomy treatment [80]. However, the decellularized meniscal scaffold partially failed to be recellularized for full thickness meniscus regeneration because of the dense structure [84, 86, 89]. If the solid decellularized ECM scaffold can be processed into an injectable hydrogel, the cells can be easily encapsulated into the hydrogel with uniform distribution. Furthermore, the injectable hydrogel is compatible with popular minimally-invasive arthroscopic meniscectomy surgery in clinics [150], while the ECM scaffold commonly requires surgery with incision. The hydrogel also can deliver cells, drugs, and growth factors, fill

an irregularly shaped defect, and provide a stable microenvironment for cell growth to facilitate new tissue formation [160]. Injectable hydrogels derived from heart [152, 158, 161, 162], dermis [160], bone [163], urinary bladder [164], liver [74], nervous system [165], blood vessel [166], adipose [167], and brain [168], have been reported. It is notable that the porcine heart-derived hydrogel was delivered into the porcine infarcted heart by a catheter, which showed tremendous promise in clinics [158]. But there is no reported study on the meniscus-derived injectable hydrogel, which is the focus of this investigation.

In this study, we processed the porcine meniscus into a flowable solution via modified decellularization and enzymatic digestion. The solution formed a solid meniscus-derived hydrogel at body temperature. The extent of decellularization was evaluated by cellular nuclear staining and DNA quantification. Major components (collagen and glycosaminoglycan (GAG)) of the decellularized meniscal matrix, gelation kinetics, and mechanical properties of the hydrogel were measured. Primary bovine chondrocytes and mouse 3T3 fibroblasts were seeded with the meniscus-derived hydrogel to assess cellular compatibility and infiltration property. Finally, a mouse subcutaneous implantation model was used to evaluate the injectability and *in vivo* tissue compatibility of the hydrogel.

2.2 Experimental section

2.2.1 Materials

Sodium dodecyl sulfate (SDS), ethylenediaminetetraacetic acid (EDTA), phosphate-buffered saline (PBS), pepsin, concentrated hydrogen chloride (HCl),

sodium hydroxide (NaOH), glutaraldehyde, phenol/chloroform/isoamyl alcohol, and sodium acetate were purchased from Sigma and used as received. Collagenase and 4', 6-diamidino-2-phenylindole (DAPI) were obtained from Life Technologies, Inc.

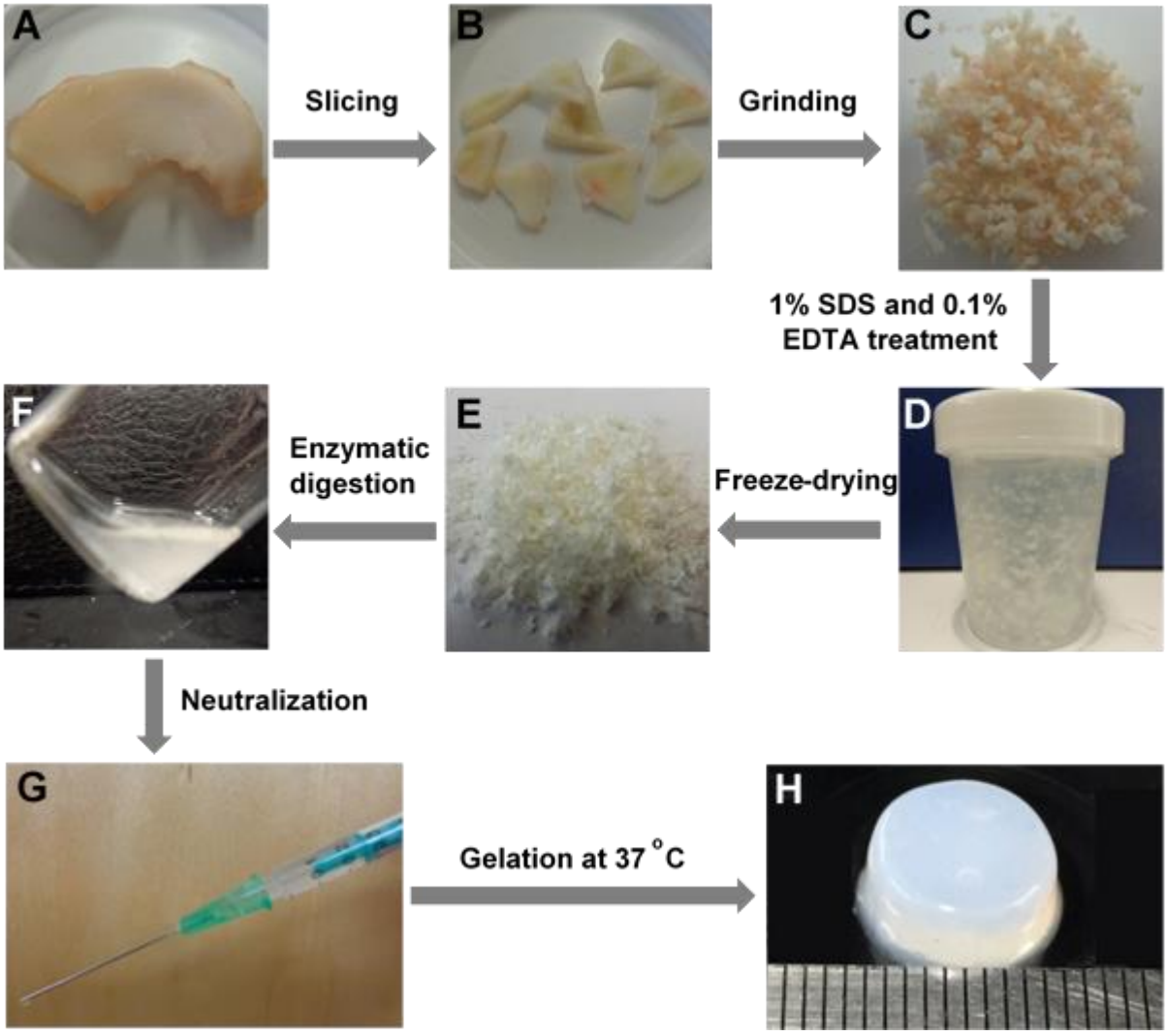

Figure 2. 1 The routine to process the porcine meniscus into an injectable hydrogel. Porcine meniscus (A) was cut into thin slices (B) (1 mm thickness), frozen and then ground into powders (C). The ground tissue powders were then treated with 1% SDS (3 days) and 0.1% EDTA (1 day) (D), followed by freeze-drying to obtain the decellularized meniscal matrix (E). The decellularized meniscal powder was further

digested using pepsin and then neutralized to obtain a flowable solution (F). The solution was loaded into a syringe (G) and then injected into a cylinder model via a 21-gauge needle. After incubation at 37 °C for 30 min, a cylinder-shaped meniscus-derived hydrogel formed (H).

2.2.2 Decellularization of meniscus

The porcine menisci were harvested from fresh knee joints of adult pigs weighing 80~100 kg from a local slaughterhouse. The decellularized meniscal matrix was prepared using a modified protocol according to the ref. [169] (Figure 2.1). Briefly, the meniscus (Figure 2.1A) was cut into thin slices (1 mm in thickness) (Figure 2.1B), frozen at -80 ^{o}C and then ground into coarse powders (Figure 2.1C). The powders were stirred in 1% SDS/PBS (w/v) solution for 72 h (Figure 2.1D). The SDS solution was refreshed every 24 h. The sample was then treated with 0.1% EDTA/PBS (w/v) solution for 24 h and immersed overnight in a large amount of deionized water to remove the residual chemicals. Finally, the obtained decellularized meniscal matrix was frozen at -80 ^{o}C and then lyophilized for 3 d. The decellularized meniscal matrix was further ground into fine powders (Figure 2.1E) and stored at -20 ^{o}C for future use. The sample was embedded in optimal cutting temperature compound (O.C.T) at -20 ^{o}C, and then sectioned into 7 μm thick slices for hematoxylin and eosin (H&E, Sigma) and DAPI staining. The images were taken using a Nikon Eclipse Ti microscope. The morphology of the decellularized meniscal matrix was observed under a scanning electron microscope (SEM, S-3000N, Hitachi).

2.2.3 Preparation of injectable hydrogel

The fine powders of the decellularized meniscal matrix were added into pepsin/0.01 M HCl solution at 15 mg/mL (Figure 2.1F). The pepsin/matrix mass ratio was 1:10. The mixed suspension was stirred at room temperature for 48 h to allow complete digestion (without visible powder) and formed a flowable viscous solution. The viscous solution was neutralized using 0.1 M NaOH and 10X PBS in an ice bath [160], and then the neutralized solution was diluted into a pre-gel solution at a pre-determined ECM concentration using 1X PBS. The pre-gel solution was loaded into a syringe (Figure 2.1G), injected into a cylinder mold and then placed in a 37 ^{o}C incubator for 30 min to form a solidified hydrogel (Figure 2.1H). The hydrogel morphology was observed using a SEM after the hydrogel was frozen in liquid nitrogen, freeze-dried, and sputter coated with silver.

2.2.4 Properties of injectable hydrogel

2.2.4.1 DNA quantification

The DNA content in the decellularized matrix was determined using a reported method [170]. Briefly, the decellularized meniscal matrix and the native meniscus were digested using pepsin (1 mg/mL) in HCl solution (0.01 M) and centrifuged at 2980 xg for 10 min to remove protein remains. The supernatants were then centrifuged at 10,000 xg in phenol/chloroform/isoamyl alcohol (25:24:1, Sigma) for 30 min. The aqueous layer in the centrifuged sample then was extracted for analysis. The DNA was precipitated using 3 M sodium acetate/ethanol solution (v/v=1:20) at –20 ^{o}C overnight. The extracted DNA samples were then dehydrated in a vacuum oven at room

temperature and rehydrated in 1X Tris-EDTA buffer (Life Technologies, Inc). Finally, the DNA amounts were determined using a PicoGreen DNA assay (Life Technologies, Inc) (n = 3).

2.2.4.2 Collagen and GAG quantification

Collagen and GAG in the decellularized meniscal matrix and the native meniscus were quantified using a hydroxyproline assay (Sigma) and a Blyscan Sulfated Glycosaminoglycan assay (Biocolor, UK), respectively. The collagen content was determined by quantifying hydroxyproline, which makes up 14.3% of collagen weight [163, 171]. Briefly, the decellularized meniscal matrix and the native meniscal tissue were hydrolyzed with 6 M HCl at 120 ^{o}C for 3 h and then air dried in 96 well plate at 65 ^{o}C. Next, 100 µL chloramine T/oxidation buffer mixed solution (Sigma) was added to each well, and the plate was incubated at room temperature for 5 min. Each sample then was added with 100 µL dimethylaminobenzaldehyde solution and incubated at 60 ^{o}C for 90 min. The sample absorbance (n=3) then was read at 560 nm on an Infinite M200 plate reader (Tecan, UK). A standard curve was plotted using a series of hydroxyproline solutions at known concentrations.

For GAG measurement, the decellularized meniscal matrix and the native meniscus were fully digested in pepsin solutions (1 mg/mL in 0.01 M HCl solution). The GAG contents were determined using the Blyscan Sulfated Glycosaminoglycan assay (n = 3). Pepsin in 0.01 M HCl solution was used as a negative control.

2.2.4.3 Turbidimetric gelation kinetics

The gelation kinetic of the hydrogel was measured turbidimetrically as described in ref [160]. A pre-gel solution (100 μL) was injected into a well of a 96-well plate, and its absorbance was read at 490 nm at 37 ^{o}C on an Infinite M200 plate reader every 3 min for 1 h. The obtained results were calculated as normalized absorbance = (A-A0)/(Am-A0), where A represents the reading value at each time point, A0 is the initial absorbance and the Am is the maximum absorbance. The time of half gelation ($t_{1/2}$) was set as the time to 50% absorbance; the lag time (t_{lag}) was determined by extrapolating the linear portion of the gelation curve to 0% absorbance (x-axis); and the gelation rate (S) was defined as the slope of the linear portion of the curve [160]. Four samples of each group were tested.

2.2.4.4 Compressive strength of injectable hydrogel

The pre-gel solutions were injected into cylinder molds (10 mm in diameter) and incubated at 37 ^{o}C for 30 min to form solid hydrogels. The cylinder hydrogel (5 mm in height, 10 mm in diameter) was tested on an MTS Insight machine with a 10 N load cell at a crosshead speed of 1 mm/min until failure. Four samples per group were tested.

2.2.5 Biocompatibility evaluation

2.2.5.1 Chondrocyte isolation

Primary bovine chondrocytes were isolated from knee joints of immature calves [172]. Briefly, 2 mm thick articular cartilage pieces were digested overnight using 0.15% collagenase at 37 ^{o}C. After removing tissue residues using a 100 μm filter, the digested

solution was centrifuged at 200 xg for 5 min to obtain chondrocytes. The cells were cultured using Dulbecco's modified Eagle medium (DMEM) supplemented with 10% fetal bovine serum (FBS), 100 U/mL penicillin, and 100 µg/mL streptomycin in a humidified incubator at 37 ^{o}C. The primary chondrocytes were used before passage 3 for all experiments.

2.2.5.2 Cellular growth on the ECM coated surface

Primary bovine chondrocytes and NIH mouse 3T3 fibroblasts (ATCC, Manassas, VA) were seeded separately on the meniscal ECM coated surfaces for cytocompatibility evaluation. The ECM was physically coated on the tissue culture polystyrene (TCPS) [74, 168]. Briefly, the digested ECM (15 mg/mL) solution was diluted into 2 mg/mL using 0.5 M acetic acid. The solution was added onto 24-well cell culture plate surface (1 mL/well) and incubated at 37 ˚C for 1 h to allow ECM adsorption. The coated plate then was rinsed 3 times with 1X PBS to remove unbound components and acetic acid. The chondrocytes and the 3T3 fibroblasts were seeded separately on the ECM coated plates at densities of 5,000 cells/well and 2,000 cells/well, respectively. The culture medium (DMEM supplemented with 10% FBS, 100 U/mL penicillin, and 100 µg/mL streptomycin) was refreshed every 3 d. The untreated TCPS served as a control. An MTT assay (Sigma) was used to assess cellular viability at days 1, 4, and 7. The absorbance (n=4) was detected at 490 nm on a microplate reader, and the absorbance of the TCPS at day 1 was set as 1 for absorbance normalization. A live (calcein-AM)/dead (ethidium homodimer-1) assay (Life Technologies, Inc) was used to visualize cell morphology.

2.2.5.3 Cellular growth within the hydrogel

For cell encapsulation, the chondrocytes (5×10^5 cells/mL) and the 3T3 fibroblasts (5×10^5 cells/mL) were separately blended with the pre-gel solutions (ECM concentration: 10 mg/mL). Next, 300 µL of cell-loaded pre-gel solution was then injected into a well of 24-well culture plate and incubated at 37 ^{o}C for 30 min to form a cellularized hydrogel. The cell culture medium (DMEM supplemented with 10% FBS, 100 U/mL penicillin, and 100 µg/mL streptomycin) then was added and exchanged every 2 d. The live/dead staining was performed at days 1, 4, and 7 to evaluate cell survival inside the meniscus-derived hydrogel. The numbers of the live cells and the dead cells in each image (n = 3) were counted using ImageJ software (National Institutes of Health, USA). The cell survival rate was calculated as live cell number/ total cell number ×100%.

2.2.5.4 Cellular infiltration into the hydrogel

The bovine chondrocytes and the mouse 3T3 fibroblasts were seeded separately on the surface of the meniscus-derived hydrogel (ECM concentration: 10 mg/mL) to investigate cell infiltration behavior. The cells (1×10^4 cells/cm^2) were added to the top surface of the hydrogel and placed in an incubator for 2 h to allow cell attachment. The extra culture medium was then added to the normal cell culture. The culture medium was replaced every 2 d. At each time point (days 1, 7, and 14), the samples (n = 3) were fixed in 2.5% glutaraldehyde solution. The fixed sample was embedded in the O.C.T for cryosection and then stained using DAPI to check cell infiltration depth from hydrogel top surface to bottom. The cell distribution with depths was determined using

a reported method [173]. The cross-sections of the stained samples were divided into five vertical zones. Each zone had a dimension of 300 μm at the vertical direction and 1,300 μm at a horizontal direction. The cell infiltration percentage in each zone was counted as a cell number in each zone/total cell number inside the hydrogel×100%. The immunohistochemical staining of SOX9 was performed to assess the phenotypical characteristic of infiltrated chondrocytes inside the hydrogel after culture for 14 days. Briefly, the chondrocyte-infiltrated hydrogel was sectioned and stained with chondrocyte-specific marker SOX9 (1:200 dilution, rabbit anti-SOX9 polyclonal antibody, Novus Biologicals). The sections then were exposed to a 1:100 dilution of peroxidase-conjugated goat anti-rabbit secondary antibody (Jackson ImmunoResearch Laboratories, PA). Finally, the staining was developed with DAB (Sigma) according to the manufacturer's instructions.

2.2.5.5 *In vivo* subcutaneous implantation

The female Balb/c mice (25g body weight) were used for the hydrogel subcutaneous injection. All animals were treated and used following the protocol approved by the Institutional Animal Care and Use Committee (IACUC) of the University of Texas at Arlington.

The *in vivo* injectability and biocompatibility of the meniscus-derived hydrogel was assessed in a mouse subcutaneous model [167]. To check injectability and gelation *in vivo*, 4 injections (100 μL each) of the pre-gel solution (ECM concentration: 10 mg/mL) were subcutaneously injected into mouse dorsal regions via a 26 G needle. After 30 min, the injected sites were excised to check the hydrogel formation. For *in vivo*

biocompatibility evaluation, the materials with surrounding tissues were explanted at days 3 and 7 after implantation. Four explants were collected at each time point. The explant was directly embedded in O.C.T, frozen at -20 ^{o}C and then sectioned into 7 μm thick slices for H&E staining. The images were taken using a microscope (Eclipse Ti, Nikon). The three zones (100 μm depth each zone) from sample top to center were set on the H&E images and the cell infiltration percentage at each zone was counted as described above.

2.2.6 Statistical analysis

All the data were reported as mean ± standard deviation, and statistically analyzed using Statview software. The statistical analysis of DNA, collagen, and GAG contents was made by student's t-test. The statistical analysis of mechanical properties, cellular viability, and cell infiltration was performed by one-way ANOVA, followed by a Tukey post-hoc test. Significant difference was defined as $p < 0.05$.

2.3 Results

2.3.1 Meniscus decellularization and hydrogel formation

The decellularized meniscal matrix (Figure 2.2A) showed a pink matrix without visible intact purple nuclear dots in H&E stained image, while the native meniscal tissue (Figure 2.2B) showed many chondrocytes with purple nuclei embedded in the matrix. The absence of intact nuclei in the decellularized meniscal matrix also was observed in DAPI stained image (Figure 2.2C), however, the native meniscal tissue showed many DAPI stained blue intact nuclei (Figure 2.2D). The DNA content in the

decellularized matrix was 1.3 ± 0.3 ng/mg dry weight, which is significantly lower than that in the native meniscal tissue (115.6 ± 5.3 ng/mg dry weight) (Figure 2.2E).

Collagen content in the decellularized matrix was 78 ± 22% dry weight, which was significantly higher than that in the native meniscal tissue (42 ± 10%) (Figure 2.2F). The decellularized matrix had a GAG content of 0.54 ± 0.08 μg/mg dry weight, which was significantly lower than that in the native meniscus (14.95 ± 5.57 μg/mg dry weight) (Figure 2.2G).

Macroscopically, a hydrogel with a low ECM concentration (4 mg/mL) (Figure 2.3A, inset) had a cylindrical shape, but it was too weak to be handled. When ECM concentration was 6 mg/mL or higher, the hydrogel showed a cylindrical shape with a sharp edge and it could be handled. All hydrogels showed fibrous morphologies with dense and randomly oriented collagen fibrils (Figure 2.3A-3E). The decellularized meniscal matrix had a nanofibrous structure with some sheets (Figure 2.3F).

The turbidimetric gelation kinetic curves for the hydrogels at different ECM concentrations showed sigmoidal shapes (Figure 2.4A). Hydrogel formation could be observed after a lag period. The times of half gelation ($t_{1/2}$) of the hydrogels at the ECM concentrations of 4, 6, 8, 10, and 12 mg/mL were 15 ± 1, 16 ± 1, 15 ± 2, 14 ± 1, and 13 ± 2 min, respectively (Figure 2.4B), with no significant difference ($p > 0.05$). Similarly, no significant difference was found in either the lag times (Figure 2.4C) or the gelation rates (Figure 2.4D) of the hydrogels at various ECM concentrations ($p > 0.05$).

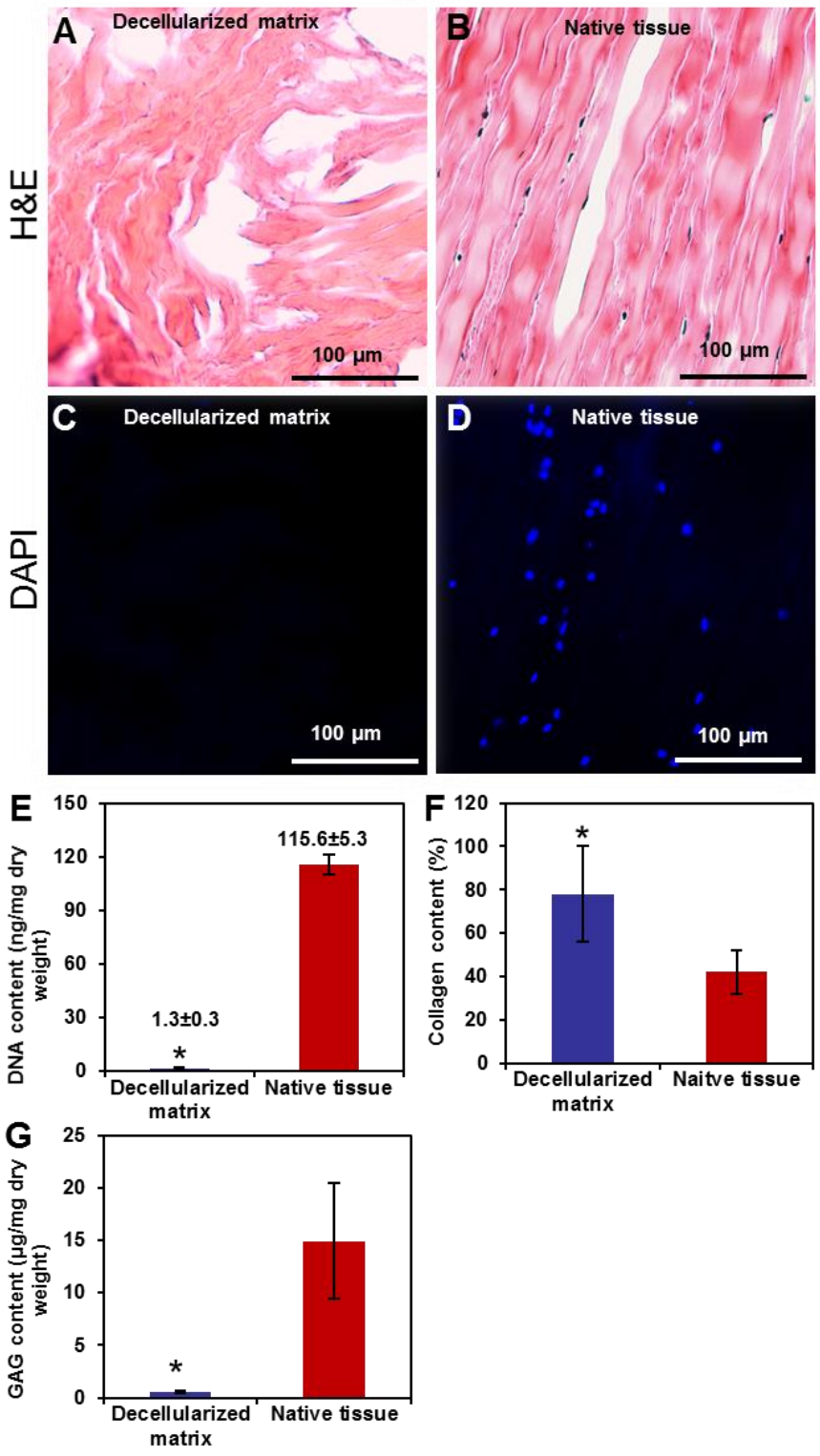

Figure 2. 2 H&E (A and B) and DAPI (C and D) stained images of decellularized meniscal matrix (A and C) and native meniscus tissue (B and D). (E), (F), and (G) show

DNA, collagen, and GAG contents in the decellularized matrix and the native tissue, respectively.

2.3.2 Compressive strength of hydrogels

The compressive strengths (Figure 3G) and the initial moduli (Figure 3H) of the meniscus-derived hydrogels showed an increase trend with increasing ECM concentrations. In Figure 3G, the compressive strength of the hydrogel at 12 mg/mL (838 ± 296 Pa) was significantly higher than those of the hydrogels at 6 mg/mL (101 ± 25 Pa) and 8 mg/mL (322 ± 29 Pa) ($p < 0.05$). The peak compressive strength of the hydrogel at 10 mg/mL showed no significant difference from those of the hydrogels at 8 mg/mL and 12 mg/mL. The hydrogel at 6 mg/mL showed the lowest peak compressive strength. The hydrogel at 4 mg/mL could not be tested due to its weakness and poor handling. In Figure 3H, the hydrogel at 6 mg/mL had the lowest initial modulus (726 ± 77 Pa) ($p < 0.05$). The initial moduli of the hydrogels at 8, 10, and 12 mg/mL showed no significant difference ($p > 0.05$), although an increasing trend of the initial modulus with increasing ECM concentration was shown.

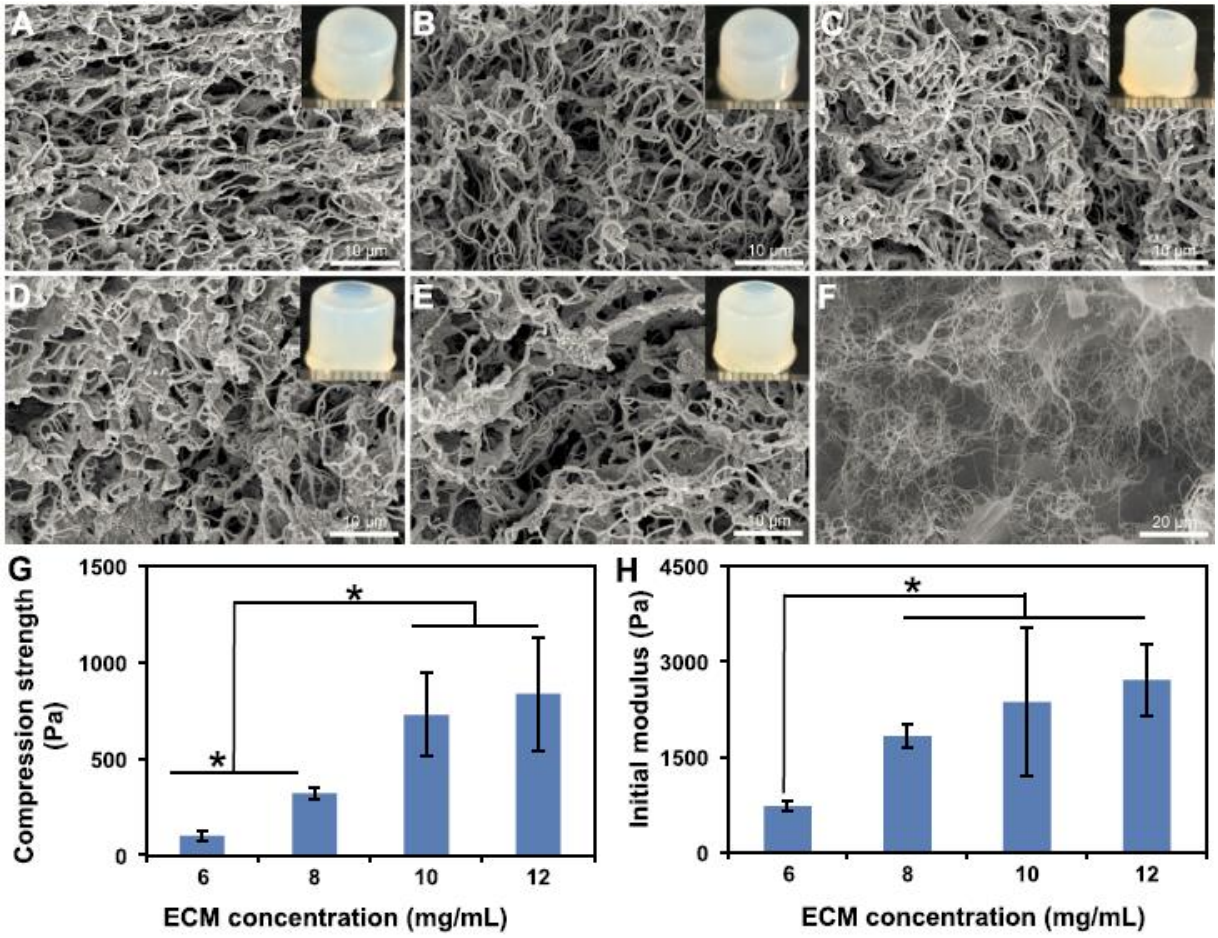

Figure 2. 3 SEM images to show fibrous morphologies of meniscus-derived hydrogels formed at ECM concentrations of 4 mg/mL (A), 6 mg/mL (B), 8 mg/mL (C), 10 mg/mL (D), and 12 mg/mL (E), respectively. (F) is SEM image of the decellularized meniscal matrix. The inset picture is the corresponding macroscopic view of the formed hydrogel. (G) and (H) show the compressive strengths and the initial moduli of the meniscus-derived hydrogels, respectively.

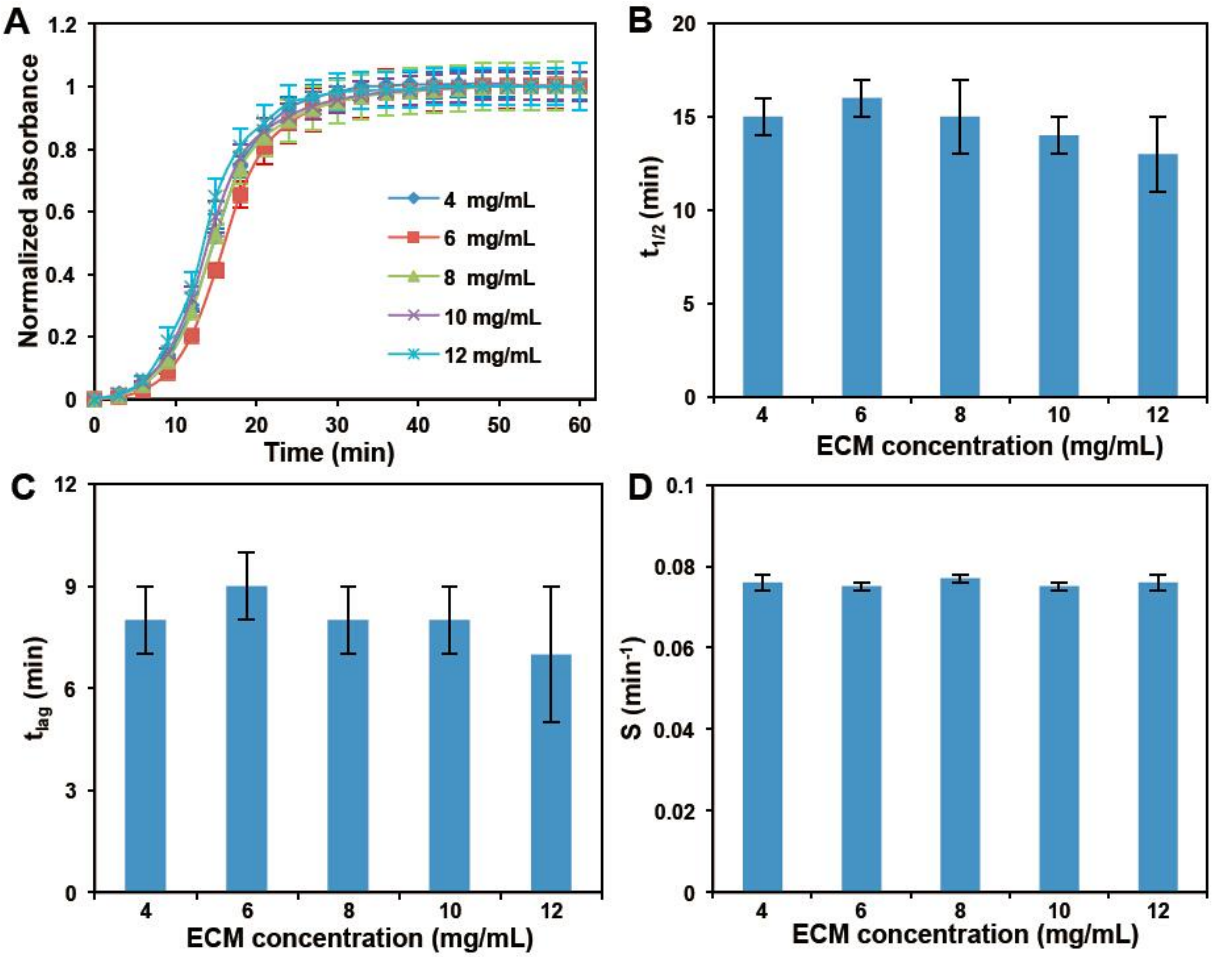

Figure 2. 4 Turbidimetric gelation kinetic curves (A) of the meniscus-derived hydrogels with $t_{1/2}$ (B), t_{lag} (C), and S (D).

2.3.3 Cell growth on the ECM-coated surface

The chondrocytes and the 3T3 fibroblasts were seeded separately on the meniscal ECM coated surfaces to evaluate the cellular compatibility of the hydrogel (Figures 2.5 and 2.6). In Figure. 2.5, the chondrocytes were mostly live (green cytoskeleton without red nuclei) on both TCPS and the ECM coated surface with few dead cells (red dots). At day 1 (Figure 2.5A and 2.5D), the cells were sparsely distributed on the surfaces. Cell growth was obviously seen at day 4 (Figure 2.5B and

2.5E) and cell confluence was found at day 7 on both surfaces (Figure 2.5C and 2.5F). Some chondrocytes on the TCPS, exhibited fibroblast-like morphology with elongated shape at day 7, whereas the normal cobblestone morphology of the chondrocytes was visualized on the ECM coated surface during the whole culture period. The cell viability on the ECM coated surface had no significant difference from that on the TCPS at day 1 and day 4 ($p > 0.05$), but it was 30% higher than that on the TCPS at day 7 ($p < 0.05$) (Figure 2.5G).

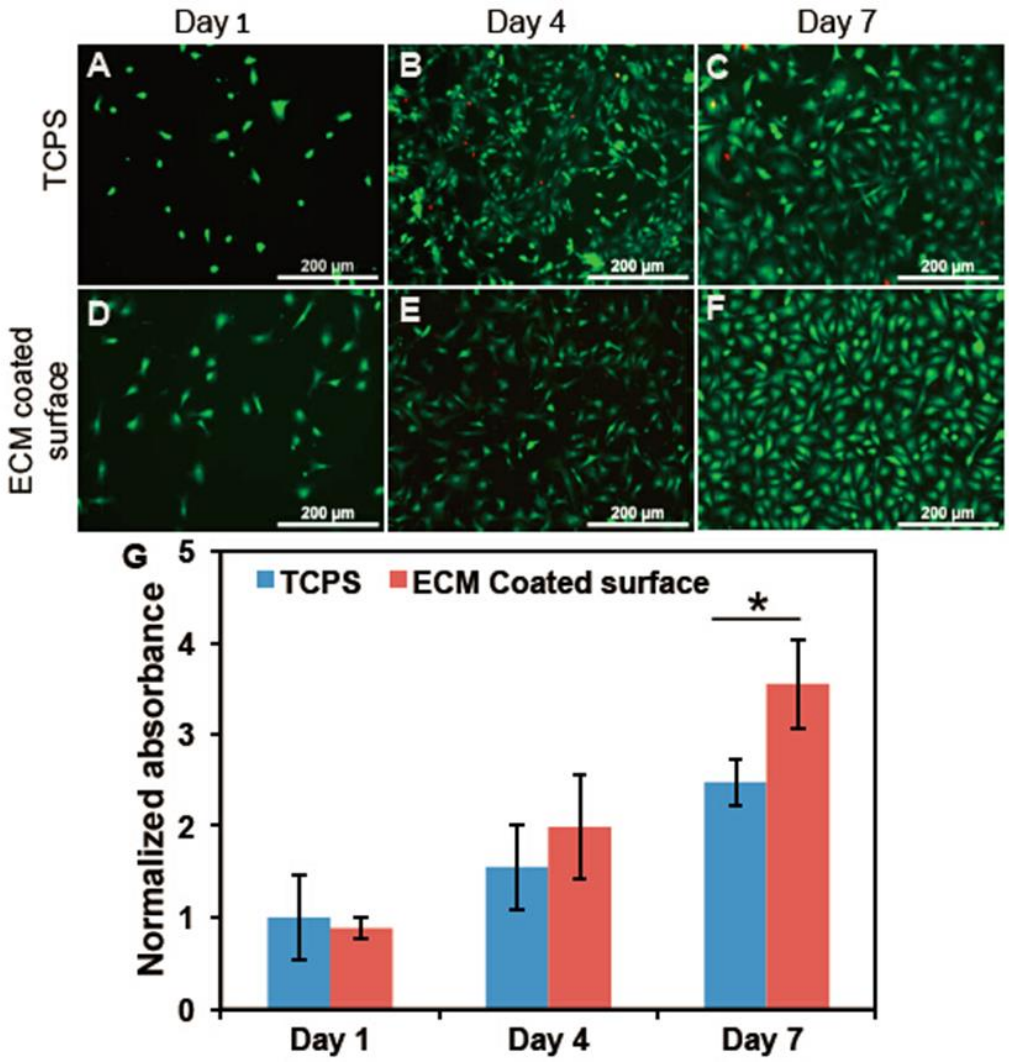

Figure 2. 5 Bovine chondrocyte growth on the meniscal ECM coated surface. The chondrocyte morphology on the control TCPS (A, B, and C) and the ECM coated

surface (D, E, and F) was visualized by live/dead staining at day 1 (A and D), day 4 (B and E), and day 7 (C and F). (G) is the normalized absorbance measured by an MTT assay.

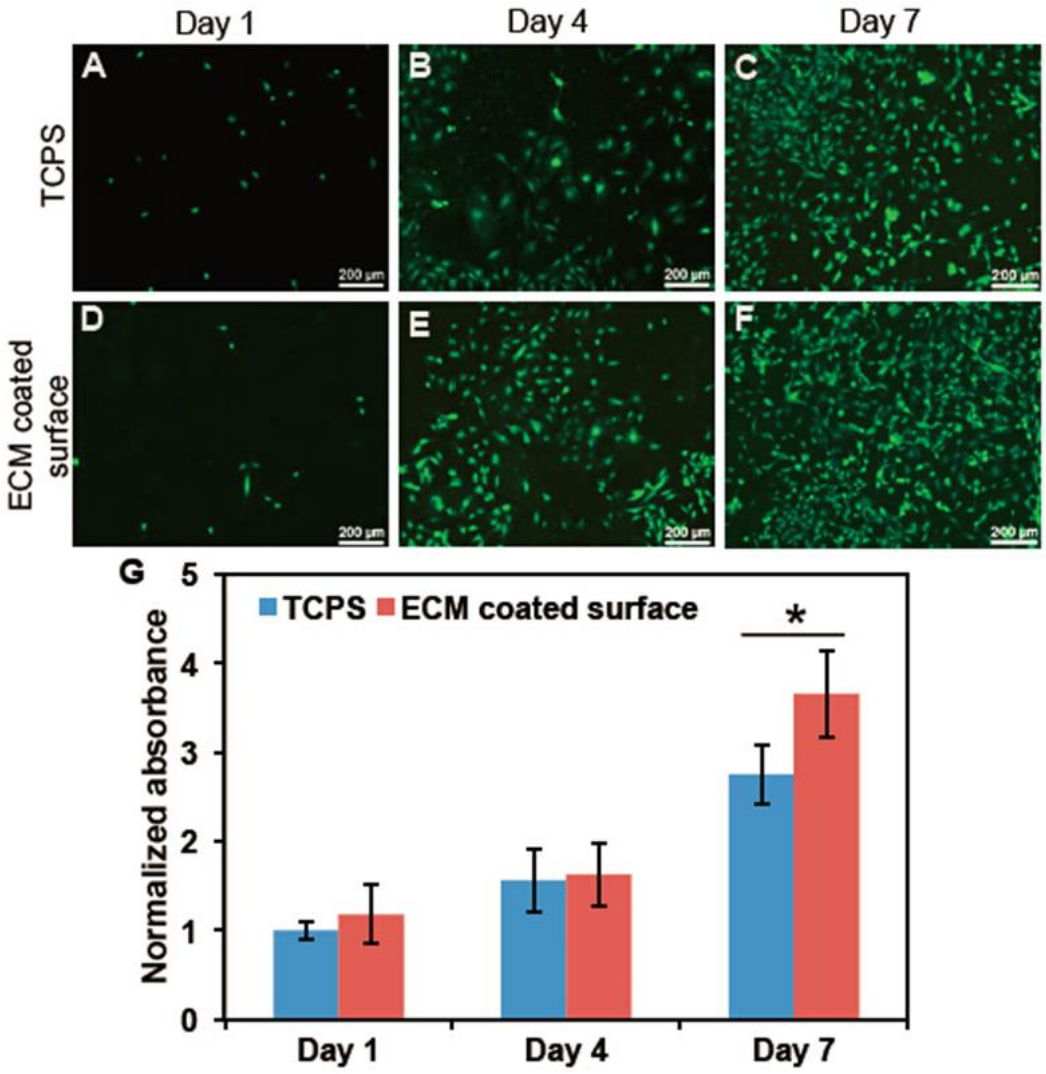

Figure 2. 6 Mouse 3T3 fibroblast growth on the meniscal ECM coated surface. The fibroblast morphology on the control TCPS (A, B, and C) and the ECM coated surface (D, E, and F) was observed by live/dead staining at day 1 (A and D), day 4 (B and E), and day 7 (C and F). (G) is the normalized absorbance measured by an MTT assay.

The behavior of the 3T3 fibroblasts on the TCPS and the ECM coated surface was similar to that of the chondrocytes. We found that the fibroblasts survived and proliferated during 7 d culture without visible dead cells on two surfaces (Figure 2.6). The fibroblast morphologies observed on the two surfaces were similar (Figure 2.6A-F). The cell viability on the ECM coated surface was greater than that on the TCPS at day 7 ($p < 0.05$) (Figure 2.6G).

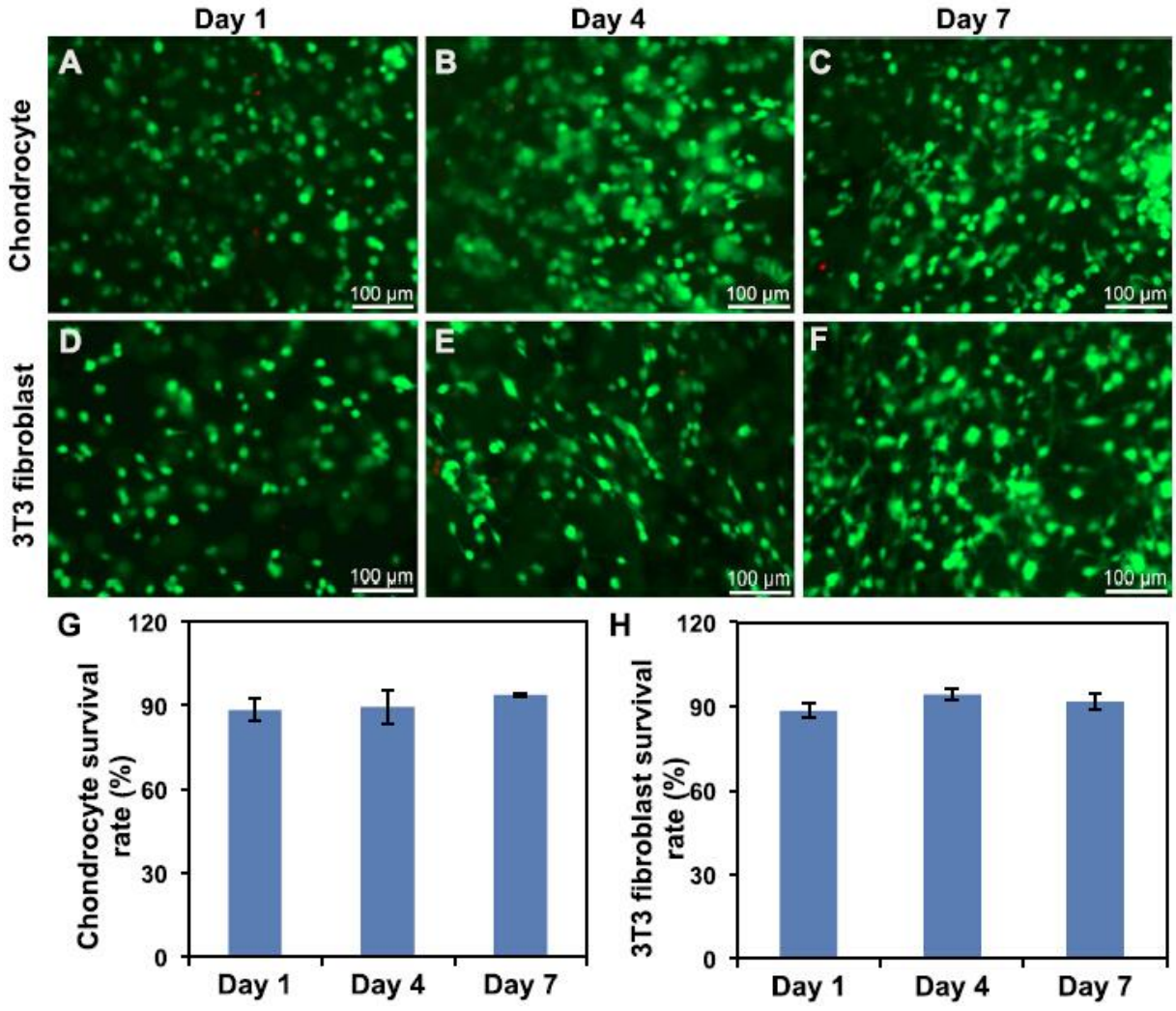

Figure 2. 7 Primary bovine chondrocyte and mouse 3T3 fibroblast growth inside the meniscus-derived hydrogel. The morphologies of the chondrocytes (A, B, and C) and the fibroblasts (D, E, and F) inside the hydrogel were observed using live/dead staining

at day 1 (A and D), day 4 (B and E), and day 7 (C and F). (G) and (H) show survival rates of chondrocytes and fibroblasts inside the hydrogel, respectively.

2.3.4 3D cellular growth within the hydrogel

Cell survival of chondrocytes or 3T3 fibroblasts encapsulated inside the 3D meniscus-derived hydrogel was determined using a live/dead staining during 7 d in culture. The chondrocytes predominantly exhibited a round morphology inside the hydrogel at day 1 (Figure 2.7A) and 4 (Figure 2.7B). A small portion (17 ± 4%) of chondrocytes exhibited a spindle shape at day 7 (Figure 2.7C). The 3T3 fibroblasts had a round morphology at day 1 (Figure 2.7D), and then the major part of 3T3 fibroblasts had an elongated cell morphology at day 4 (Figure 2.7E) and 7 (Figure 2.7F). Both the chondrocytes (Figure 2.7G) and the 3T3 fibroblasts (Figure 2.7H) had cell survival rates of approximately 90% from day 1 to day 7 without significant differences.

2.3.5 Cellular infiltration into the hydrogel

Both the chondrocytes and the fibroblasts exhibited increased infiltration into the meniscus-derived hydrogel with culture time (Figures 2.8 and 2.9). Cell migration distance increased with increasing incubation time. At day 1, 69 ± 10% and 31 ± 10% of chondrocytes were seen at the region 0-300 μm and 300-600 μm away from the hydrogel top surfaces, respectively (Figures 2.8A and 2.9A). No cell was found beyond 600 μm away from the surfaces. At day 7, 29 ± 9% and 17 ± 6% cells were found in the zones of 600-900 μm and 900-1200 μm, respectively (Figure 2.8A and 2.9B). At day 14, 21 ± 4% of the chondrocytes were further observed in 1200-1500 μm zone,

and the cells were evenly distributed in each zone (Figure 2.8A and 2.9C). The chondrocytes showed round morphology with positive SOX9 staining (Figure 2.9G).

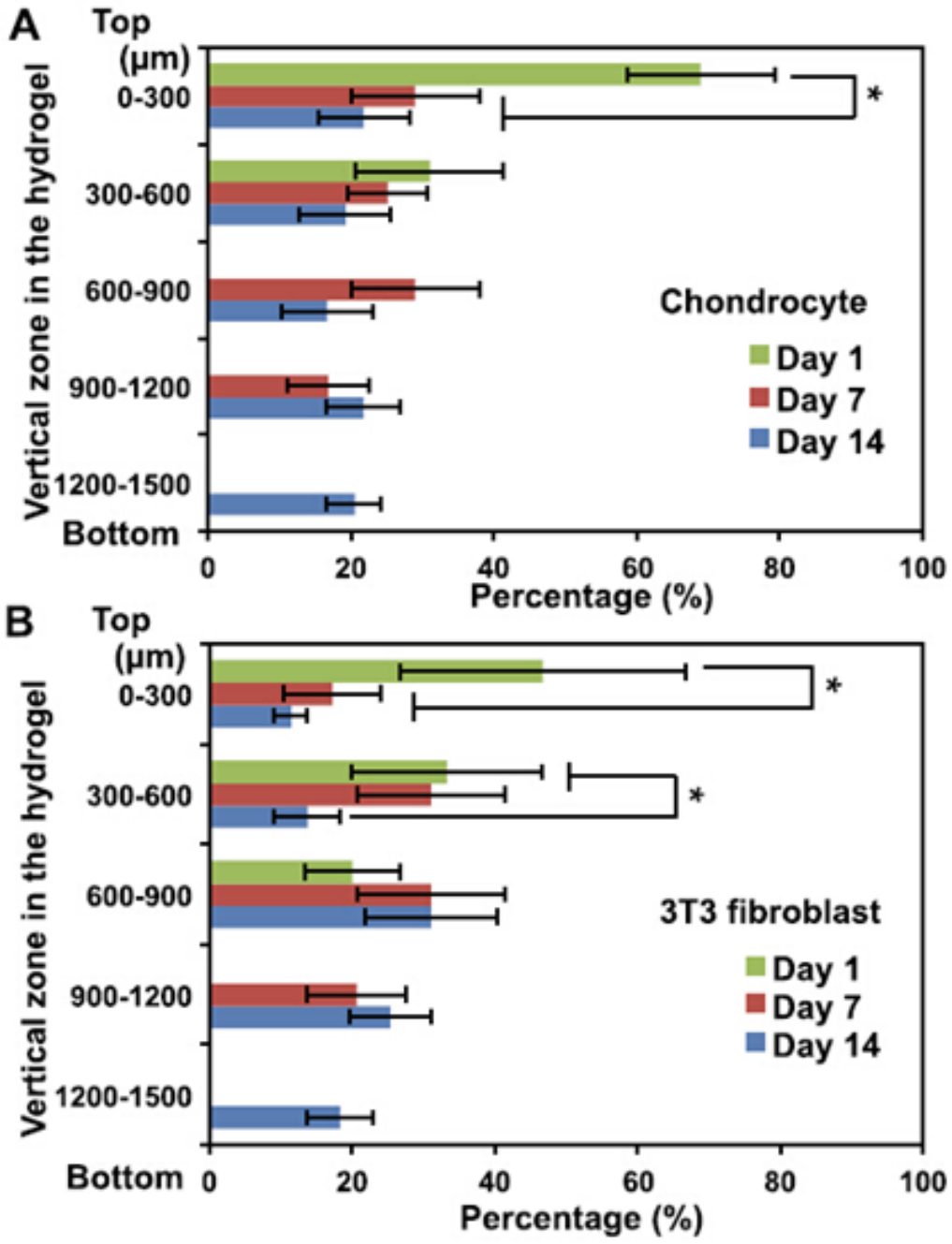

Figure 2. 8 Cellular infiltration behaviors of the chondrocytes (A) and the 3T3 fibroblasts (B) were evaluated by infiltrated cell percentages at various zones inside the meniscus-derived hydrogels up to 14 days.

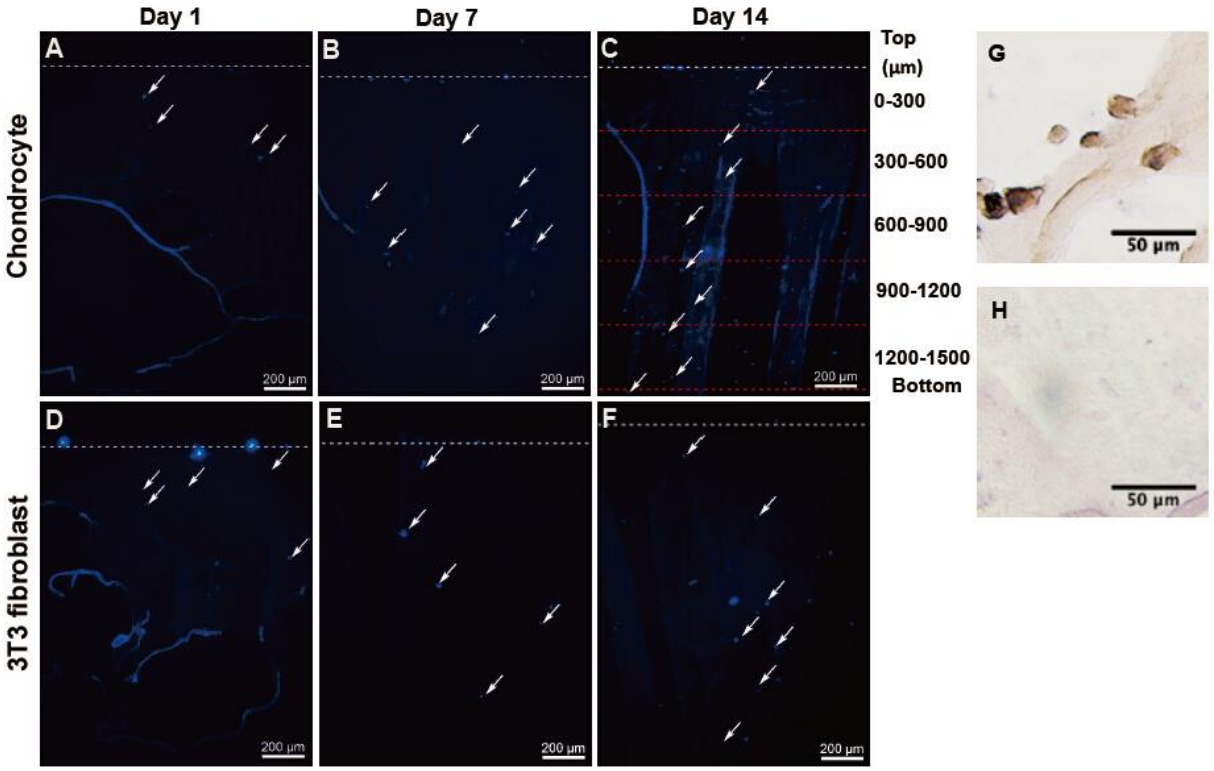

Figure 2. 9 DAPI stained images of chondrocyte (A, B, and C) and 3T3 fibroblast (D, E, and F) infiltrated into the meniscus-derived hydrogel. Dashed lines show the divided vertical zones inside the hydrogel to quantify the percentage of infiltrated cells. (G) An immunohistochemical image shows that positive SOX9 stained chondrocytes infiltrated into the hydrogel at day 14, indicating that the cells retained their chondrocyte morphology and phenotype. (H) An immunohistochemical image shows negative SOX9 staining in the cell-free hydrogel.

The infiltration behavior of the fibroblasts was similar to that of the chondrocytes. The fibroblasts were only found in 0-300 μm zone (47 ± 20%), 300-600 μm zone (33 ± 13%) and 600-900 μm zone (20 ± 7%) at day 1 (Figure 2.8B and 2.9D). They were observed in the deeper zone of 900-1200 μm (21 ± 7%) at day 7 (Figure 2.8B and 2.9E) and then the deepest zone of 1200 -1500 μm (18 ± 5%) at day 14 (Figure 2.8B and

2.9F). Compared to the cell distribution at day 1, the percentages in the top two zones (0 – 300 and 300 – 600 μm) decreased at day 14 ($p < 0.05$).

2.3.6 *In vivo* biocompatibility

The meniscus-derived hydrogel (ECM concentration: 10 mg/mL) was subcutaneously injected into mouse dorsal regions to evaluate *in vivo* hydrogel formation and tissue compatibility. The pre-gel solution was smoothly injected into the mouse dorsal through a 26-gauge needle and formed a bolus in the injection site (Figure 2.10A). After 30 min, the subcutaneous bolus solidified into a stable opaque hydrogel that was capable of maintaining its shape when it was explanted (Figure 2.10B). The formed hydrogel had a visible decrease in volume from 30 min (Figure. 2.10B) to 3 days (Figure 2.10C) and continuous volume reduction with thinning from day 3 to day 7 (Figure 2.10D). No obvious angiogenesis was observed up to day 7.

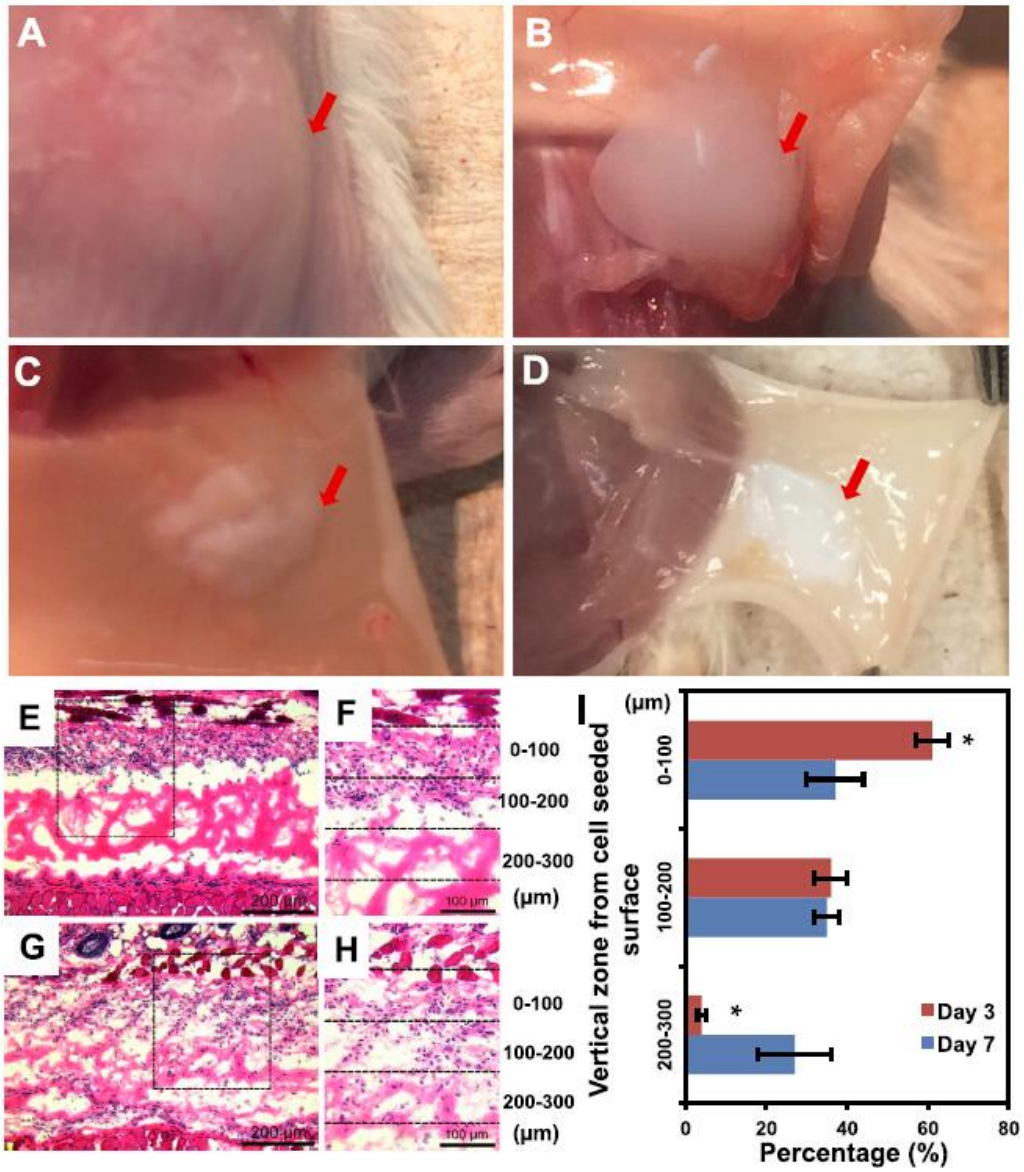

Figure 2. 10 The meniscal ECM pre-gel solution (100 μL each injection) was injected into a mouse subcutaneous tissue through a syringe with a 26G needle and formed a bolus (A). The formed opaque hydrogel was seen between muscle and skin tissues after 30 min (B). After 3 day implantation, the hydrogel volume obviously decreased (C). At day 7 post-implantation, the hydrogel volume continued to decrease with thinning (D). The red arrows point at the hydrogel implants. (E) with a magnified image (F) and (G) with a magnified image (H) are H&E stained images for the explants at

days 3 and 7, respectively. S, I, and M represent skin tissue, implant, and muscle tissue, respectively. The blank frame pointed to the area for the magnified image. Dashed lines show the three zones divided in the implanted material area to quantify the percentage of infiltrated cells. (I) show the percentages of the infiltrated inflammatory cells in the three zones of the implanted hydrogel at days 3 and 7.

H&E stained images showed that the hydrogel was located between skin and muscle (Figure 2.10E-H). At day 3 (Figure 2.10E and F), small numbers of granulocytes (purple dots) were found in the loose tissue surrounding the hydrogel with limited cell infiltration. However, at day 7 (Figure 2.10G and H), a large number of macrophages infiltrated the hydrogel and were even seen at the center area of the hydrogel. The material appeared to be partially degraded at day 7 (Figure 2.10G). We found no apparent angiogenesis in the surrounding tissue of the implant at days 3 and 7. For *in vivo* cell infiltration into the hydrogel (Figure 2.10I), the granulocytes were mainly found in 0 -100 μm zone (61 ± 4%) and 100 – 200 μm zone (36 ± 4%), and a low percentage (4 ± 1%) of cells was seen in 200-300 μm zone at day 3. At day 7, the cells were evenly distributed in the 3 zones inside the implant. Compared to the cell distribution at day 3, the cell percentage in the 0-100 μm zone decreased to 37 ± 7% while the cell percentage in the 200-300 μm zone increased to 27 ± 9%.

2.4 Discussion

To accommodate tissue specificity, many tissues and whole organs have been used to produce decellularized scaffolds [68, 155]. The meniscal tissues from rats, ovine, porcine, and even human have been decellularized using a variety of methods,

including detergent rinsing (e.g., SDS, peracetic acid, Triton X-100, EDTA, and guanidine hydrochloride/ H_2O_2), enzyme digestion, gamma irradiation, sonication and their combinations [79-82, 84, 86, 88-91]. The resulting decellularized meniscal scaffolds had no cytotoxicity, and it supported chondrocyte growth and promoted MSC differentiation into the chondrocyte-like cells *in vitro* [79, 84, 89]. The rMSC-seeded decellularized meniscal scaffolds exhibited great chondroprotective ability at 8-week implantation in a rat knee meniscal defect model [80]. These works showed the decellularized meniscal scaffold is very promising for meniscal regeneration, but the implantation of these scaffolds requires a traumatic surgical procedure.

To reduce surgical trauma caused by scaffold implantation, the decellularized scaffolds were further processed into injectable hydrogel materials through enzymatic digestion. Varieties of decellularized tissue matrixes including heart [152, 158, 162], liver [74], bone [163], central nerve system [165], brain [168], skin [160], and urinary bladder [164] have been digested into flowable solutions that are suitable for injection and can form solid hydrogels *in situ* under a physiological condition. For example, the porcine heart-derived ECM hydrogel was injected into a rat myocardial infarction model, and it was even delivered into a porcine heart through a catheter [158, 159]. In this study, we processed the porcine meniscus into an injectable hydrogel that is capable of being used for minimally invasive surgery for the treatment of meniscus injuries and diseases.

The major challenge for decellularization is to eliminate cellular components to reduce the immune response while retaining the maximum amounts of bioactive molecules. The meniscus has a thick and dense fibrous structure, and the cells are

embedded in densely compacted ECM [174], which limits the decellularization of the whole meniscal tissue [86]. Substantial improvement was made when Azhim *et al* sliced the meniscal tissue into thin slices (3 mm thickness) [88]. Grinding the meniscus into powder (Figure 2.1C) allowed maximum exposure of the tissue to the detergent, facilitating the elimination of the cellular components. More than 98% of DNA in the native meniscal tissue was removed. The DNA content (1.3 ± 0.3 ng/mg dry weight) in the decellularized scaffold is much lower than 50 ng/mg dry weight, which is the minimal criterion to satisfy the intent of complete decellularization [68, 170]. It should be noted that a similar approach of using ground tissue to ECM gel has been used to prepare myocardial injectable scaffolds [152].

The retention of bioactive molecules is vital for the bioactivity of the biological matrix. The decellularization procedure and the SDS detergent do not cause a problem on the collagen retention because the native collagen is generally not water soluble, so the collagen content was found to be well preserved in the decellularized matrix [89]. The high retention of collagen and the loss of other components during decellularization resulted in a significantly higher collagen percentage in the decellularized matrix than that in the native tissue (Figure 2.2F) [166]. On the other hand, the GAG content in the decellularized matrix was much lower than that in the native meniscus, which is consistent with previous reports [86, 89]. Because the GAG is highly water soluble and the decellularization procedure is carried out in aqueous solution, it is likely that most GAG is washed away during the decellularization procedure. In addition, SDS also can separate GAG from the proteins in the ECM, which may lead to the further loss of GAG [68].

The gelation mechanism of the ECM hydrogels was not yet fully understood [74, 152, 160, 163, 164, 167]. It is generally believed that the presence of some proteins, such as collagen, laminin, elastin, and proteoglycan, contributes to molecular self-assembling for the gelation [175, 176]. Collagen, the major component in the hydrogel, is considered as a major self-assembling protein responsible for the gelation [163-165]. The turbidimetric kinetics for the meniscus-derived hydrogel is similar to pure type I collagen hydrogel [164, 177, 178] and other ECM hydrogels derived from urinary bladder [164], central nervous system [165], bone [163] and skin [160]. Interestingly, the meniscus-derived hydrogels with different collagen concentrations had the same gelation time, while the gelation time of pure type I collagen hydrogel decreased with increasing collagen concentration [175]. The gelation time of GAG/collagen mixture was independent on collagen concentration [177]; thus, the occurrence of the same gelation time may be caused by the presence of GAG, which can electrostatically interact with collagen to affect the gelation behavior [165, 177]. Additionally, other self-assembling molecules such as laminin may contribute to the gelation [164].

The mechanical environment has profound effects on cellular behaviors such as cell adhesion, cell tension, and cytoskeleton organization [160, 179-181]. Therefore, the mechanical properties of hydrogels are desired to be tunable for modulating cell response *in vitro* [182, 183] and *in vivo* [184]. Varying ECM concentrations of the meniscus-derived hydrogel was able to modulate its mechanical properties, which are comparable to the mechanical properties of the collagen hydrogel (3 mg/mL, approximately 280 Pa in peak compressive strengths and 1 kPa in initial modulus) [185]. It is notable that the mechanical properties of the hydrogels are much lower than those

of the native meniscus (100 ~ 400 kPa in modulus [28, 105] and 100 ~ 300 MPa in tensile strength [11]). Therefore, the meniscus-derived hydrogel in this study is not suitable to be used directly as a whole meniscus replacement. However, it is suitable to be applied as an *in vitro* 3D matrix for tissue engineered meniscus, and as an injectable material to repair and regenerate partially defective/diseased meniscus, which is popularly seen in meniscal injuries and diseases [28, 186].

The concept on cellular biology of meniscus denotes that it contains two types of cells, fibroblast-like cells in the outer vascularized meniscal zone and chondrocyte-like cells in the middle and inner avascular meniscal zones [4, 28, 187]. Chondrocytes [63, 188, 189], fibroblasts [82, 84], or both [86, 89] have been utilized extensively to evaluate the cellular compatibility of scaffolds and their potential applications for meniscus repair and regeneration. Thus, both the chondrocytes and the 3T3 fibroblasts were selected for *in vitro* biological evaluation of the hydrogel in this study. The meniscus-derived hydrogel exhibited a good cellular compatibility without apparent toxicity (Figures 2.5, 2.6, 2.7, 2.8, and 2.10). Its uniform cellularization was easily achieved by blending the pre-gel solution and the cells. In addition, robust cell growth was found both on the 2D ECM-coated surface and inside the 3D hydrogel. Compared to the TCPS, the meniscal ECM coated surface maintained the chondrocyte morphology better. Some bioactive components in the meniscus-derived hydrogel may favor the maintenance of the chondrocyte morphology. However, some chondrocytes inside the hydrogel exhibited differentiated morphology, which may be attributed to the part of ECM components in the hydrogel derived from the outer area of the native meniscus that supports fibroblast-like cell growth.

The cell infiltration into the scaffolds is especially useful for tissue remodeling and regeneration [160, 190, 191]. The rapid cellular infiltration was obviously observed during *in vitro* 14 day cell culture and *in vivo* 7 day subcutaneous implantation of the meniscus-derived hydrogel, which is different from the decellularized meniscal scaffolds [83, 84]. This may be the result of the fast degradation and the loose structure of the hydrogel. On the other hand, the *in vitro* chondrocyte infiltration into the hydrogel suggests that the chondrocyte-like cells from the native meniscus might migrate into the hydrogel *in vivo*, which would lead to tissue regeneration. The infiltrated cells maintained their chondrocyte morphology and phenotype during the 14-day culture *in vitro* (Figure 2.9G). It was reported that the chondrocytes could migrate from native cartilage to implanted adjacent scaffolds *in vivo* and maintain typical chondrocyte-like morphology [192, 193].

The good injectability of the meniscus-derived hydrogel was verified by injecting the pre-gel solution into the mouse subcutaneous tissue. The *in vivo* environment has no obvious effect on the gelation. It indicated that the hydrogel is suitable as an injectable material for minimally invasive surgery, which has no conflict with current meniscus surgery [28]. Furthermore, the meniscus-derived hydrogel has good *in vivo* biocompatibility with minor inflammation and without severe immune response during 7 day implantation. The *in vivo* degradation of the hydrogel was obviously observed. The degradation of the hydrogel would release many bioactive components, such as peptides, which are useful for cell recruiting [194] and tissue remodeling [195], although many components still are unknown. For example, the degradation products from digested decellularized porcine urinary bladder matrix quickly expanded the

perivascular stem cells (PSCs) and still maintained their undifferentiated multipotent state, which was important for PSC accumulation at the injury site [196]. On the other hand, the degradation of the ECM hydrogel may be too fast to provide mechanical support and to promote tissue regeneration *in vivo*. Such drawbacks could be overcome by combining the ECM hydrogel with synthetic polymers as shown in previous works [53, 197].

Some limitations must be mentioned. First, the SDS treatment resulted in a lower GAG content of the decellularized meniscal matrix. The potential SDS residue may have adverse effects on cell growth and tissue formation, although it was not found in our study. A mild detergent may be used for meniscal decellularization to improve GAG retention. Second, we quantified only two major components among the complex components of the meniscus-derived hydrogel. The mass spectrometer (MS) was used to analyze the multiple components in the decellularized matrix [55]. But some components are very difficult to be solubilized, which limited our analysis of the components using an MS. Besides MS, methods such as ELISA [198] and immunohistochemical staining [199] are feasible to quantitatively and qualitatively determine other components in the decellularized matrix. Third, chondrocyte-like cells and fibroblast-like cells isolated from the meniscus might be more appropriate for material evaluation for meniscus regeneration application, although the primary chondrocytes and the fibroblasts were commonly used for the same purpose [4, 63, 84]. Combining two kinds of cells isolated from the fresh meniscus with the meniscus-derived hydrogel will be our future focus. Last, the *in vivo* study was conducted over a relatively short term. The *in vivo* mechanical and structural change of the hydrogel with

time has not been assessed. Long-term *in vivo* study will be conducted to further investigate biocompatibility, bioactivity, and property change of the hydrogel.

2.5 Summary

An injectable hydrogel derived from the native porcine meniscus was developed through modified decellularization and pepsin digestion. The hydrogel exhibited a fibrous morphology. Its mechanical properties were tunable by altering ECM concentration. It had good cytocompatibility without toxicity. The chondrocyte and the fibroblast were easily encapsulated into the hydrogel and grew well inside. The hydrogel allowed a rapid cell infiltration *in vitro* and *in vivo*. It was smoothly implanted into a mouse subcutaneous model by syringe injection and showed a minor inflammation without specific immune responses within 7-day implantation. The injectable meniscus-derived hydrogel would be promising for applications in meniscus repair and regeneration.

CHAPTER 3

OPTIMIZING INJECTABLE MENISCAL ECM BY ALTERING CHEMICAL DETERGENTS

3.1 Introduction

The native extracellular matrix (ECM), composed of the secreted products of the resident cells of tissues [200], reciprocally interacts with its surrounding microenvironment and provides structural and chemical cues for cell proliferation, migration, and differentiation [201, 202]. The use of ECM materials as biological scaffolds for clinical applications involves the decellularization of tissues and/or organs through a variety of methods, including enzymatic, physical and chemical treatments. The purpose of decellularization is to eliminate antigens within the tissues and/or organs to avoid immune reactions, meanwhile preserving the bioactive components of ECM. Striking a balance between the elimination of antigens and minimized loss of bioactive ECM components is essential for successful tissue/organ decellularization, as the decellularization process should be aggressive enough to remove antigens and it unavoidable denatures some proteins and other bioactive components [203]. In addition, for a certain type of tissue, the composition, density, and architecture of ECM are closely related to the physiological function [204, 205] and differ from the other tissues to some extent. Therefore, numerous efforts have been drawn in the optimization of decellularization process for decellularized ECM materials [206-212].

Among the current well-established decellularization approaches, enzymatic digestion is of high efficiency to cleave and break down the proteins and

macromolecules that elicit immune reactions and therefore be commonly employed to prepare decellularized ECM materials [213]. However, a complete elimination of cellular components by enzymatic treatment alone is difficult and prolonged exposure to enzymes is disruptive to ECM ultrastructure [68]. For example, trypsin, the most widely used biological agent for decellularization, is reported to be more disruptive to collagen and elastin compared to chemical detergents [214, 215]. Therefore, a short time exposure to trypsin is always used in the initial step of a combined decellularization process to slightly disrupt the ultrastructure of ECM, improving the penetration of subsequent agents for complete decellularization of dense tissues, such as cartilage [216], dermis [160], and meniscus [82]. The second option for decellularization, physical treatment, including sonication, freeze-thaw cycles, and irradiation are generally believed as the gentle process to decellularize tissues and preserve ECM integrity, while these approaches are not capable of working alone to eliminate antigens. A subsequent enzymatic or chemical treatment is always required after physical treatment to allow the maximal removal of antigens. In comparison to the enzymatic and physical methods, chemical treatments provide a flexible platform to specifically decellularize each type of tissue and/or organ regarding the cellularity, density and thickness, by altering agents (e.g. detergents, acids/bases, and hypotonic/hypertonic solutions) [215], concentrations [217], and exposure time [169]. This is advantageous for the optimization of decellularization protocol, especially for several thick and dense tissues.

Meniscus represents one of the thick and dense tissues that are difficult to be decellularized because the densely compacted ECM not only confines the embedded

cells but also hurdles detergent penetration and cellular removal [86, 174]. Previous reports on meniscus decellularization involved the physical treatments of freezing-thawing cycles [80] and sonication [88], as well as chemical and/or enzymatic treatments of SDS/PAA [84], SDS/H_2O_2/NaOH [89], trypsin/TX/PAA [82] and TX/PAA [129]. The DM-ECM scaffolds facilitated the proliferation of human chondrocytes [89] and human dermal fibroblasts [84] and induced the differentiation of rat mesenchymal stem cells into chondrocyte-like cells [79]. However, the DM-ECM scaffolds in the solid form exhibited a relatively denser structure that could substantially limit the cell infiltration. Besides, the filling of an irregularly shaped defect of menisci with a solid DM-ECM scaffold is not easily achievable.

We proposed a meniscus decellularization process by grinding menisci into powders and then treating with SDS, attaining an efficient antigen elimination and enriched collagen in DM-ECM which can be processed into an injectable hydrogel [218]. However, SDS treatment had a depletive effect on glycosaminoglycans (GAGs) of DM-ECM. Toward this end, we aimed to explore the optimal decellularization method by comparing three different chemicals, ionic detergent SDS, nonionic detergent TX and acidic solution PAA for meniscal decellularization. All the chemicals were reported to be effective in thick and dense tissue decellularization, while the outcomes varied more or less [208, 212, 218-220]. We compared the DNA removal, collagen and GAG contents of the obtained DM-ECMs and then processed the DM-ECMs to hydrogels. The hydrogels were characterized in terms of fibrous structures, gelation behaviors, and mechanical properties and then encapsulated with bovine meniscal

fibrochondrocytes. The cell proliferation and GAG accumulation inside the hydrogels were measured to determine the optimal protocol for DM-ECM hydrogel preparation.

3.2 Experimental section

3.2.1 Materials

SDS, Triton X-100, peracetic acid, EDTA, pepsin, HCl, NaOH, 1,9-dimethyl methylene blue (DMMB), propan-1-ol, sodium acetate, Guanidine hydrochloride (GuHCl), FBS, and DMEM were supplied by Sigma. Penicillin–streptomycin–fungizone (PSF) and 4′,6-diamidino-2-phenylindole (DAPI) were obtained from Life Technologies, Inc.

3.2.2 Decellularization of menisci using different detergents

Fresh porcine knee joints were collected from a slaughterhouse within 24 h after slaughter. The menisci were harvested immediately and stored at -80 ^{o}C. The menisci were decellularized by three different chemicals, including SDS, TX and PAA (Figure. 3.1). Briefly, the menisci were sliced into thin pieces and then frozen at -80 ^{o}C for grinding. The ground sample was re-frozen and re-ground. This step was repeated at least 5 times until the menisci became a coarse powder. Then the meniscal powder was separately decellularized by the three chemicals with stirring for 72 h. 1% SDS/PBS solution, 1% TX solution, and 0.1% PAA/4% ethanol solution were used at this step and the resulted DM-ECMs were designated as SDS-ECM, TX-ECM, and PAA-ECM, respectively. Then the meniscal powder was agitated in 0.1% EDTA for 24 h, followed by washing with a large amount of DI water to remove residual chemicals.

Finally, the obtained DM-ECM powders were freeze-dried and stored at -20 ºC for further use.

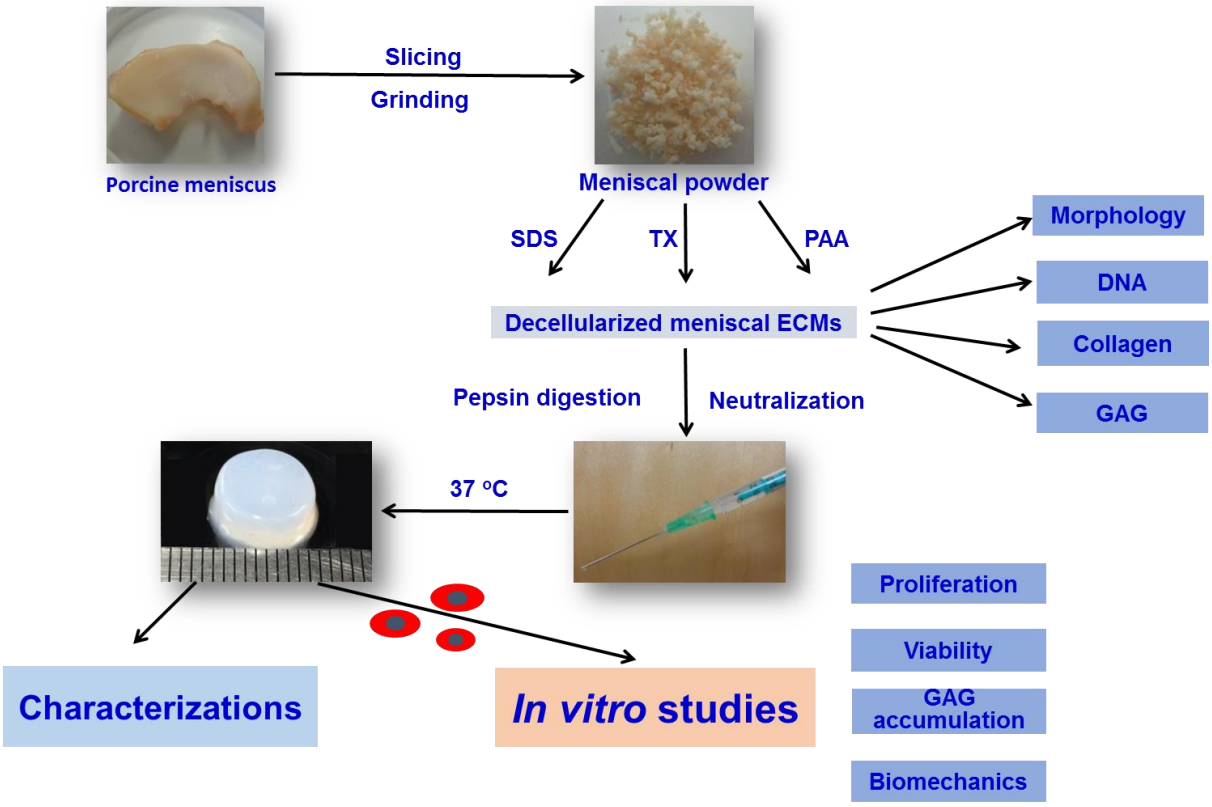

Figure 3. 1 Schematic of the experimental design.

3.2.3 Characterizations of decellularized meniscal ECMs

The DM-ECMs and freeze-dried native tissue were sputter coated with silver, and then their morphologies were observed under a scanning electron microscope (SEM, S-3000N, Hitachi).

The DNA and GAG contents of the DM-ECMs and native meniscus were determined using digested DM-ECM solutions. Briefly, the DM-ECMs were solubilized by pepsin in 0.01 M HCl at room temperature until no visible particle was shown. The DNA was extracted as a previous protocol and quantified by a PicoGreen DNA assay

(Life Technologies, Inc). The GAG content was determined through a DMMB method as ref [221]. Briefly, a DMMB working solution was prepared by dissolving 16 mg in 1 liter buffer solution containing 50 mL ethanol, 400 mL of 1 M GuHCl, 2 g sodium formate, and 2 mL formic acid and store at 4 ^{o}C in the darkness. A 4 M GuHCl buffered in 50 mM sodium acetate (pH =6.8) solution containing 10% propan-1-ol was prepared and used as a decomplexation solution. For the DMMB test, 1 mL DMMB working solution was added to 0.1 mL digested sample and vigorously vortexed to allow GAG-DMMB complex formation. The pellet of GAG-DMMB complex was then obtained by centrifuging the sample at 11,000 rpm for 10 min and discarding the supernatant. Then 1 mL decomplexation solution was added to solubilize the GAG-DMMB complex. Absorbance was read at 650 nm and the GAG content was determined by comparing with a standard curve of known shark chondroitin sulfate (Sigma). The collagen content was determined using a hydroxyproline assay (Sigma) and converted by the relationship that the hydroxyproline composes 14.3% of the collagen [163].

3.2.4 ECM solubilization and gel electrophoresis

The DM-ECMs were enzymatically digested with pepsin/0.01 M HCl solution at the ECM concentration of 15 mg/mL under stirring at room temperature. The pepsin was used at the ECM/pepsin ratio of 10:1 for the digestion. After 48 h, the DM-ECMs were fully digested and formed a viscous solution without any visible particles.

Solubilized DM-ECMs were analyzed with sodium dodecyl sulfate polyacrylamide gel electrophoresis (SDS-PAGE) and compared with collagen type I. DM-ECM solutions were run on a Tris/glycine/SDS buffered Mini-PROTEAN TGX 4-20%

polyacrylamide gel (Bio-Rad). SDS-PAGE was performed on a Mini-PROTEAN Tetra Cell (Bio-Rad) at 200 V and stained with Coomassie Brilliant Blue R-250 (Bio-Rad) for imaging.

3.2.5 Hydrogel characterization

The digested DM-ECM solutions were neutralized to form pre-gel solutions using 0.1 M NaOH and 10X PBS and then diluted to desirable ECM concentrations with 1X PBS in an ice bath. Finally, the pre-gel solutions were induced to solid hydrogels by warming in a 37 ^{o}C incubator for 30 min.

The DM-ECM hydrogels were characterized in terms of gelation behaviors, morphologies, and mechanical properties. The gelation behaviors were evaluated by a turbidimetric absorbance test as previously reported [160]. Briefly, the DM-ECM pre-gel solutions at ECM concentrations of 4, 6, 8 10, and 12 mg/mL were injected to a 96-well plate at 100 µL per well and read at 405 nm every 3 min up to 1 h at 37 ^{o}C using a spectrophotometrically plate reader (Infinite M200, UK) (n=4). The obtained readings were then plotted from 0 to 1 (initial absorbance to the maximal absorbance) using the following equation, normalized absorbance = $(A-A_0)/(A_m-A_0)$, where A indicates the absorbance at each time point, and A_0 represents the initial absorbance and the A_m stands for the maximal absorbance.

To examine the morphologies, the DM-ECM hydrogels with ECM concentration of 10 mg/mL were formed and frozen in liquid nitrogen, freeze-dried and sputter coated with silver, finally observed under SEM. The fiber diameters of the hydrogels were calculated using the ImageJ software.

The compressive behaviors of the DM-ECM hydrogels with ECM concentrations of 6, 8, 10, and 12 mg/mL were determined as previously reported [218]. The hydrogels (5 mm in height and 10 mm in diameter) were form in cylinder molds (10 mm in diameter) by incubating the pre-gels solutions at 37 ^{o}C for 30 mins. The cylinder hydrogels were then tested using an MTS Insight machine with a 10 N load cell under a crosshead speed of 1 mm/min and the test was stopped until failure (n=4).

3.2.6 Cell isolation

Knee joints of calves were freshly harvested from a local slaughterhouse and transferred under aseptic condition at in 4 ^{o}C container. Bovine fibrochondrocytes were isolated from the inner zone of the menisci as refs [125]. Briefly, the menisci were carefully dissected from the knee joints, briefly disinfected with 70% ethanol and transferred into a cell culture hood and then washed with PBS containing 1% PSF. The disinfected menisci were separated to outer 1/3 zone and inner 2/3 zone. The outer zone was discarded and the inner zone was minced into 1-2 mm^3 particles. The minced meniscal particles were digested with 2 mg/mL collagenase type II (Worthington Biochemical Corporation, Lakewood, NJ) in DMEM containing 1% PSF at 37 ^{o}C for 10 h. Upon the completion of digestion, the cell solution was filtered through a 70 μm nylon cell strainer, centrifuged at 1200 rpm for 10 min and washed twice with PBS containing 1% PSF to remove the residual collagenase. Then the cells were maintained in DMEM supplemented with 10% FBS and 1% PSF in a humidified incubator with 5% CO_2 at 37 ^{o}C. The medium was refreshed after 4 days for the first time medium change and then

every 2 days subsequently. The cells were subcultured at 80% confluence to the passage 2 (P_2) for future use.

3.2.7 Cell encapsulation into hydrogels

Generally, the fibrochondrocytes easily lost their typical polygonal morphology and function during monolayer culture [125]. Therefore, we processed the DM-ECMs to hydrogels to reconstitute the three-dimensional (3D) meniscal ECM microenvironment for fibrochondrocyte growth. The P_2 fibrochondrocytes were mixed with DM-ECM pre-gel solutions to yield cell encapsulated solutions with the ECM concentration of 10 mg/mL and the cell density of 5×10^6 cells/mL. Then 150 μL cell encapsulated solution was injected into a stainless-steel ring (10 mm in diameter) placed in a well of 24-well plate and incubated at 37 ^oC for 30 min to allow hydrogel formation. Subsequently, additional complete medium was added to each well and the medium was changed every two days up to 28 days of culture. The DM-ECM hydrogels without cells were prepared and cultured under the same conditions as the cell-encapsulated hydrogels.

3.2.8 Cell growth and GAG accumulation within the hydrogels

The viability of fibrochondrocytes inside the DM-ECM hydrogels was evaluated via a live/dead staining. At pre-designed time points of 14 and 28 days, live/dead staining was performed as ref [218]. The cell proliferation was determined by quantifying DNA content and the GAG accumulation was quantified using the DMMB method. Briefly, the samples (cell-encapsulated and non-encapsulated hydrogels)

were harvested and stored at -80 ^{o}C until the DNA and GAG quantifications. The frozen samples were freeze-dried and digested with papain at 60 ^{o}C for 2 h. The DNA and GAG contents were then determined using the PicoGreen DNA assay and DMMB test, respectively.

3.2.9 Biomechanical analysis

The biomechanical properties of the fibrochondrocyte-encapsulated hydrogels were assessed to illustrate cell-matrix interactions. After 4 weeks of culture, the samples were harvested and the top view and side view images were recorded using a digital camera. The sample diameter and height were measured by a caliper. Then the compressive stresses and strains of the samples were measured using an MTS Insight machine (MTS, Eden Prairie, MN) with a 10 N load cell under a crosshead speed of 1 mm/min until failure (n=3). Hydrogels without cells were formed and cultured up to 4 weeks and tested as controls.

3.2.10 Statistical analysis

Results were expressed as means ± standard deviations. Significant differences were assessed by one-way ANOVA followed by a Tukey post hoc test. *P*-value less than 0.05 was considered as significantly different.

3.3 Results

3.3.1 Decellularization of the meniscus

The residual DNA is the major evidence to evaluate cellular removal of decellularized ECMs. H&E histology demonstrated that decellularized meniscus ECMs absent of nuclei and showed disruptive structures (Figure 3.2 A, B, and C). The PAA-ECM (Figure 3.2 A) exhibited relatively denser fibrous structure over the SDS-ECM (Figure 3.2 B) and TX-ECM (Figure 3.2 C). Elimination of cellular DNA was also illustrated by the DAPI staining, as no positive nuclear staining was found (Figure. 3.2 D, E, and F).

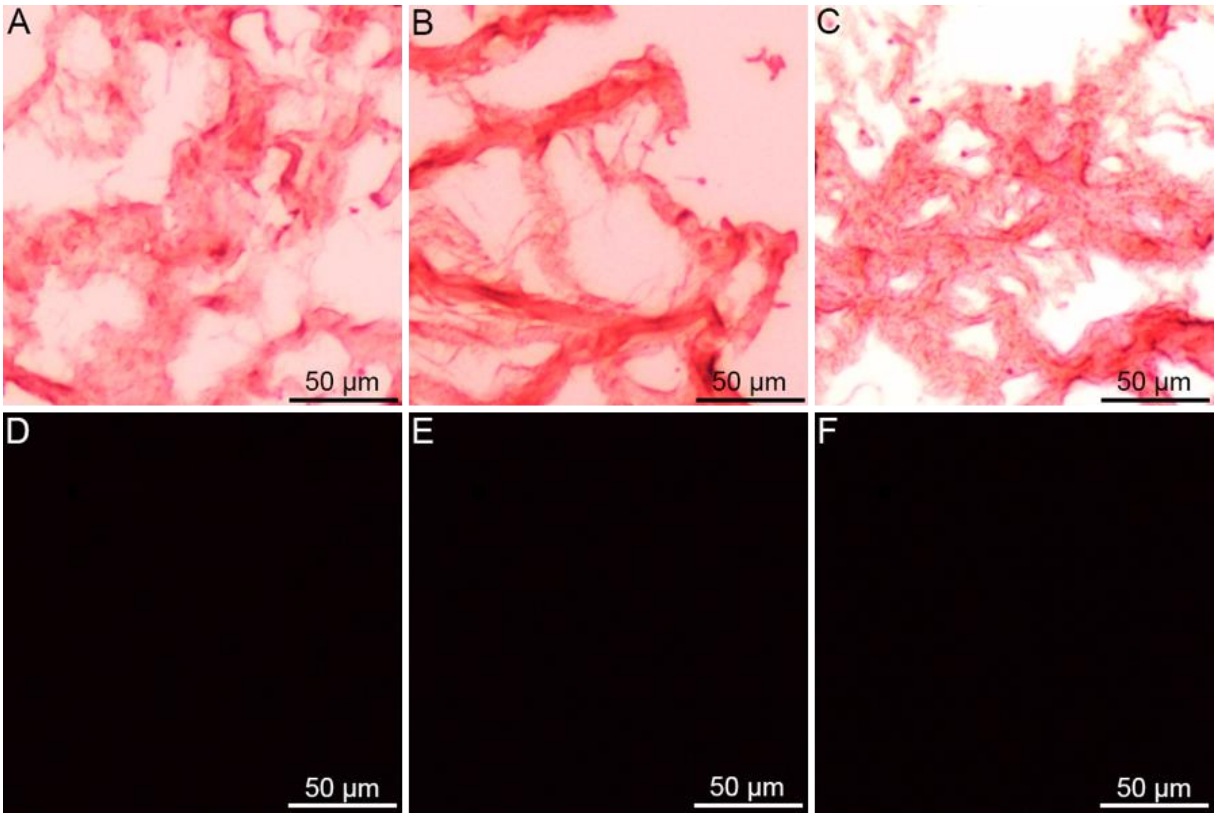

Figure 3. 2 H&E (A, B, and C) and DAPI (D, E, and F) staining of the SDS-ECM (A and D), TX-ECM (B and E), and PAA-ECM (C and F).

The DNA residual was quantitatively determined using the PicoGreen assay to verify the efficiency of the decellularization processes. All the DM-ECMs had a striking decrease in DNA content compared with the native meniscal tissue (Figure 3.3). Especially, the PAA treatment exhibited an extremely depletive effect on DNA, as more than 99.9% DNA was eliminated.

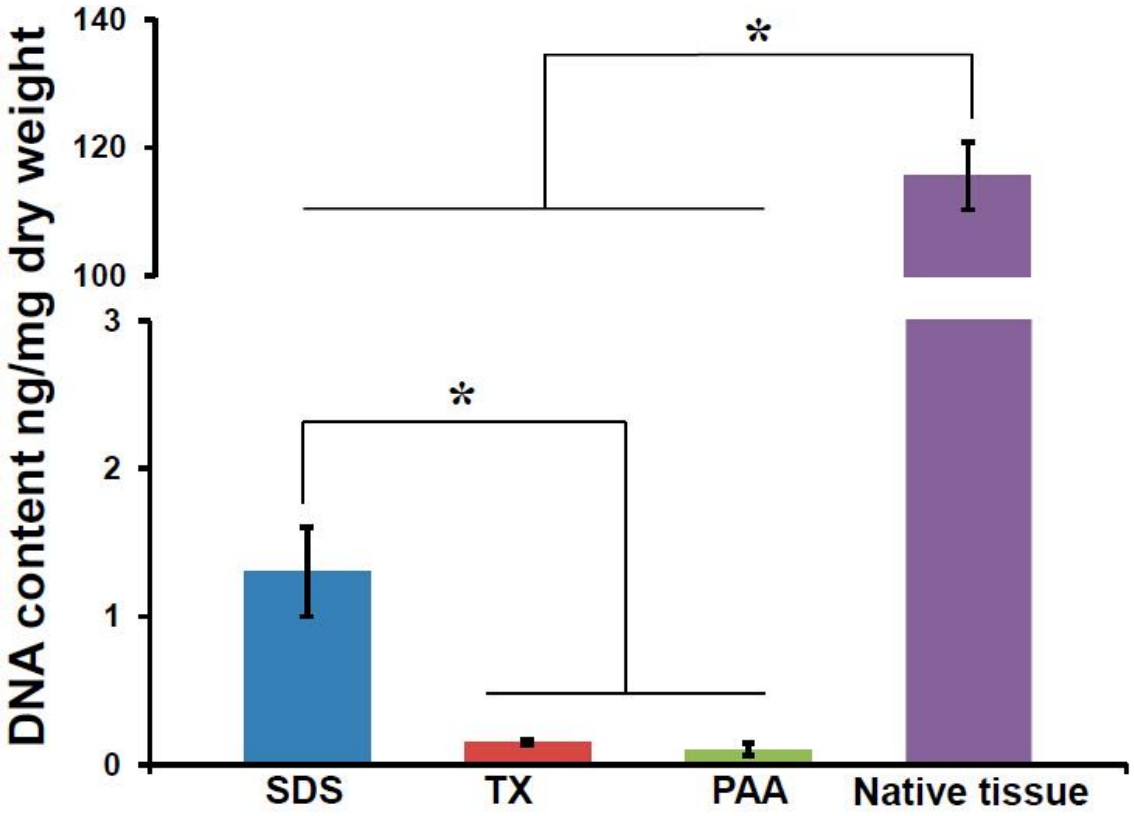

Figure 3. 3 The contents of residual DNA in the SDS, TX and PAA-treated meniscus ECMs, which are significantly lower than that of the native meniscus tissue.

3.3.2 Structures and compositions of the DM-ECMs

The SDS-ECM (Figure 3.4 A and B) lost structural integrity and exhibited a disorganized structure as disruptions among the ECM pieces were observed. The structure of the TX-ECM (Figure 3.4 C and D) was destroyed partially during the

decellularization process. The SDS-ECM and TX-ECM partially broke down to fibrils. Compared to the SDS-ECM and TX-ECM, the PAA-ECM (Figure 3.4 E and F) remained a relatively well-preserved architecture without fibrils that similar to the native meniscal ECM (Figure 3.4 G and H).

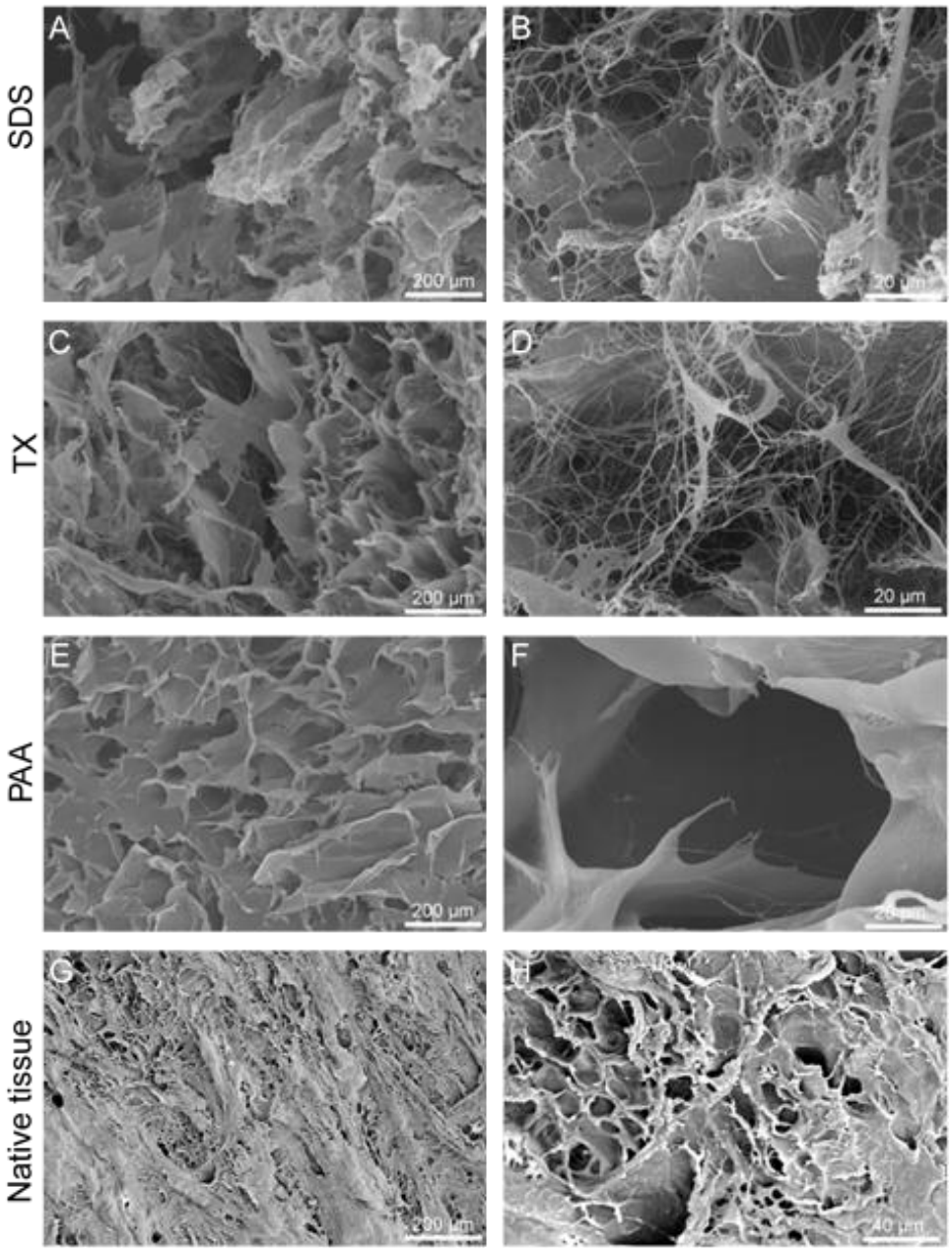

Figure 3. 4 SEM images revealed the SDS (A and B), TX (C and D) and PAA-treated (E and F) meniscus ECMs and the native meniscus tissue (G and H).

The collagen contents (Figure 3.5A) of the SDS-ECM, TX-ECM, and PAA-ECM were 78 ± 22%, 77 ± 10% and 76 ± 9%, respectively, which were higher than that of the native meniscal tissue (65 ± 12%). The SDS-ECM and TX-ECM had GAG contents of 0.6 ± 0.1 µg/mg and 0.8 ± 0.4 µg/mg (Figure 3.5B), respectively. The PAA-ECM had a significantly higher GAG content of 6.2 ± 0.5 µg/mg compared to the SD-ECM and TX-ECM. The GAG contents of all the DM-ECMs were significantly lower than the native meniscal tissue (15.0 ± 5.6 µg/mg).

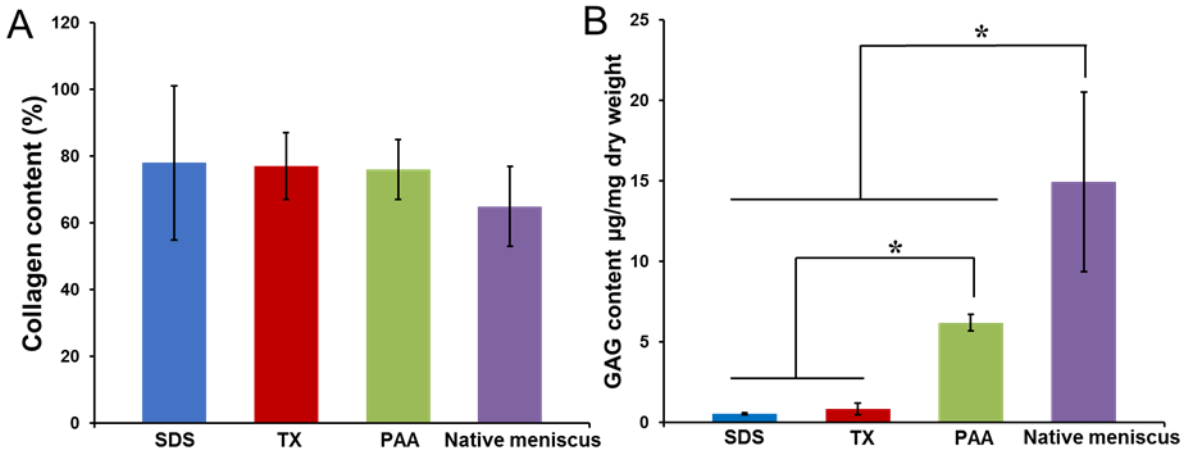

Figure 3. 5 Collagen (A) and GAG (B) contents of the SDS, TX and PAA-treated meniscus ECM.

Gel electrophoresis analysis was used to demonstrated the DM-ECM compositions. Figure 3. 6 showed that the solubilized DM-ECMs had the identical protein band pattern, and contained the corresponding bands to collagen and lower molecular weight bands, indicating that the DM-ECMs retained compositional complexity.

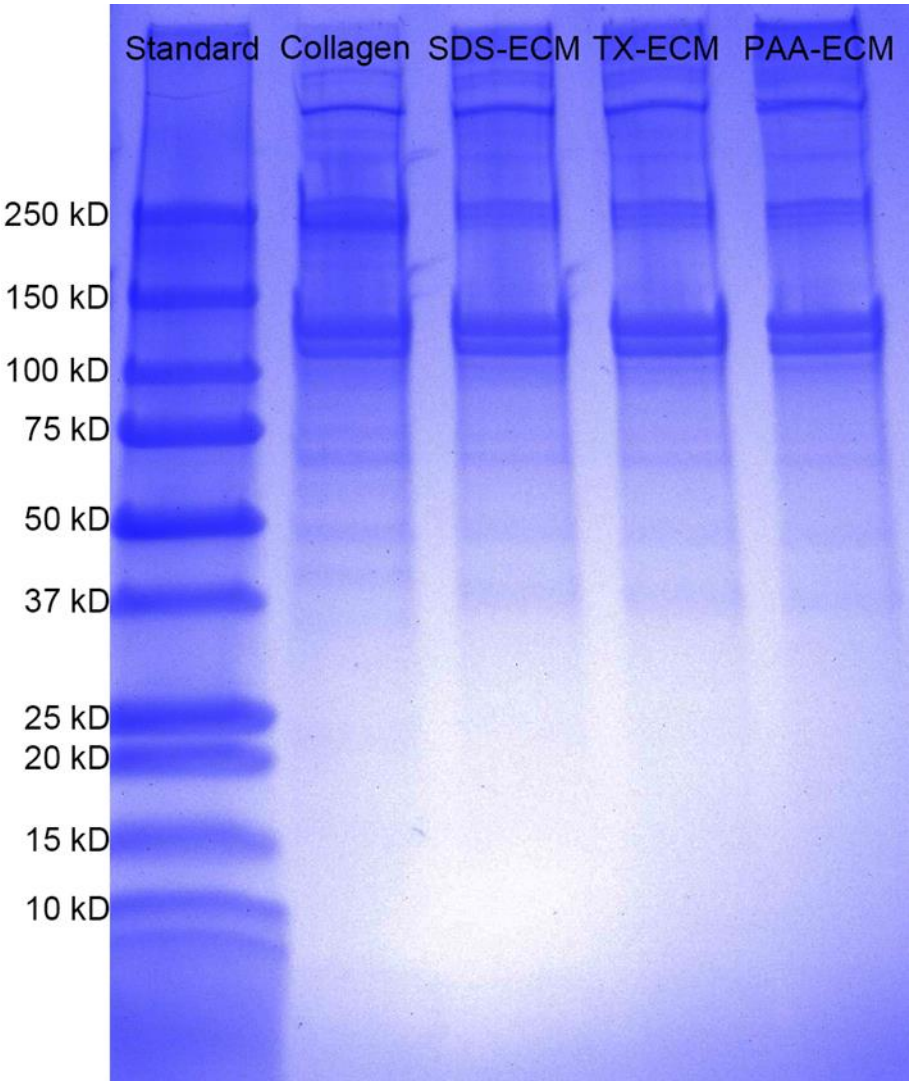

Figure 3. 6 Gel electrophoresis analysis of the DM-ECMs.

3.3.3 Hydrogel properties

The hydrogels of had a porous structure composed of nanofibers and sheets (Figure 3.7A, B, and C). A higher content of sheets and a lower content of nanofibers were observed in the PAA-ECM hydrogel (Figure 3.7C) compared to the SDS-ECM (Figure 3.7A) and TX-ECM (Figure 3.7B) hydrogels. The average fiber diameters of the three hydrogels had no significant difference (around 400 nm) (Figure 3.7D).

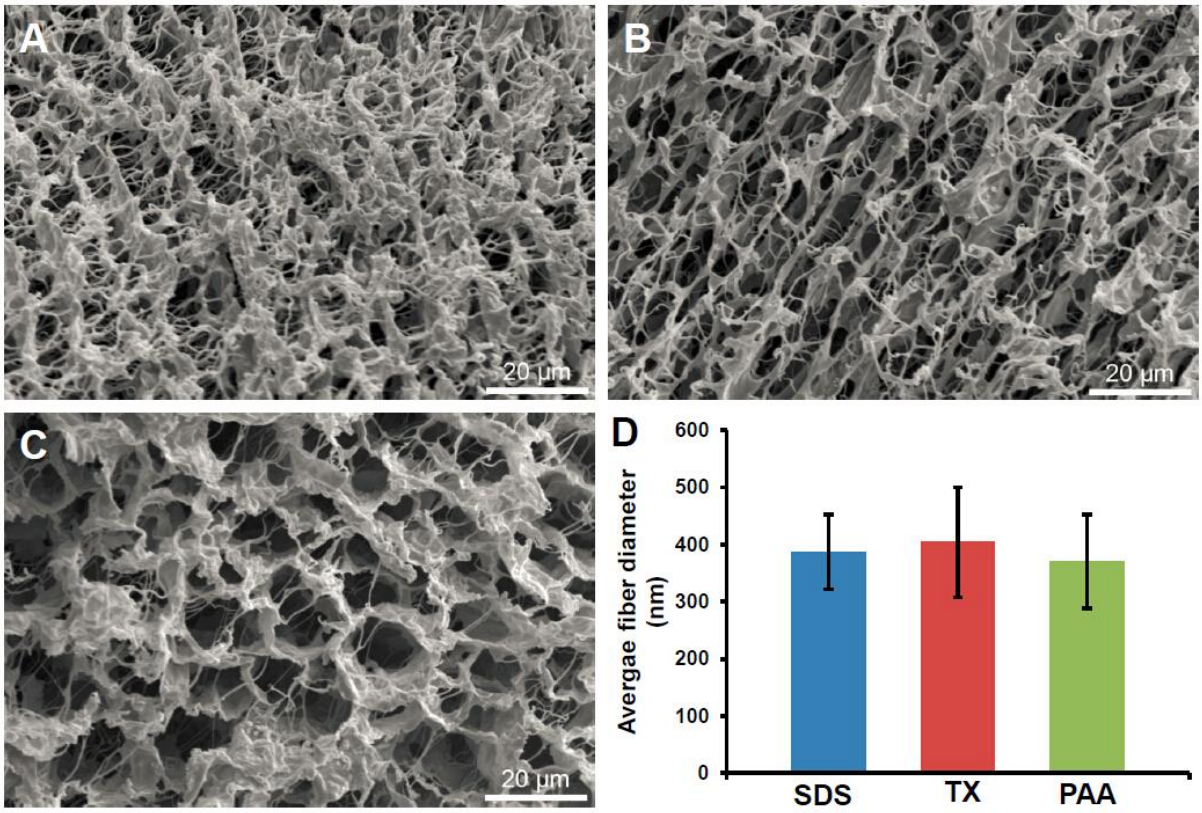

Figure 3. 7 SEM images of the SDS (A), TX (B) and PAA-treated (C) meniscus ECM hydrogels and their average fiber diameters (D).

The DM-ECMs were readily solubilized by pepsin and were capable of forming solid hydrogels within 30 min at physiological temperature. No significant difference was found in the gelation behaviors and fiber diameters of the hydrogels prepared from different DM-ECMs (Figure 3.8), indicating that the collagen was majorly contributed to the hydrogel formation.

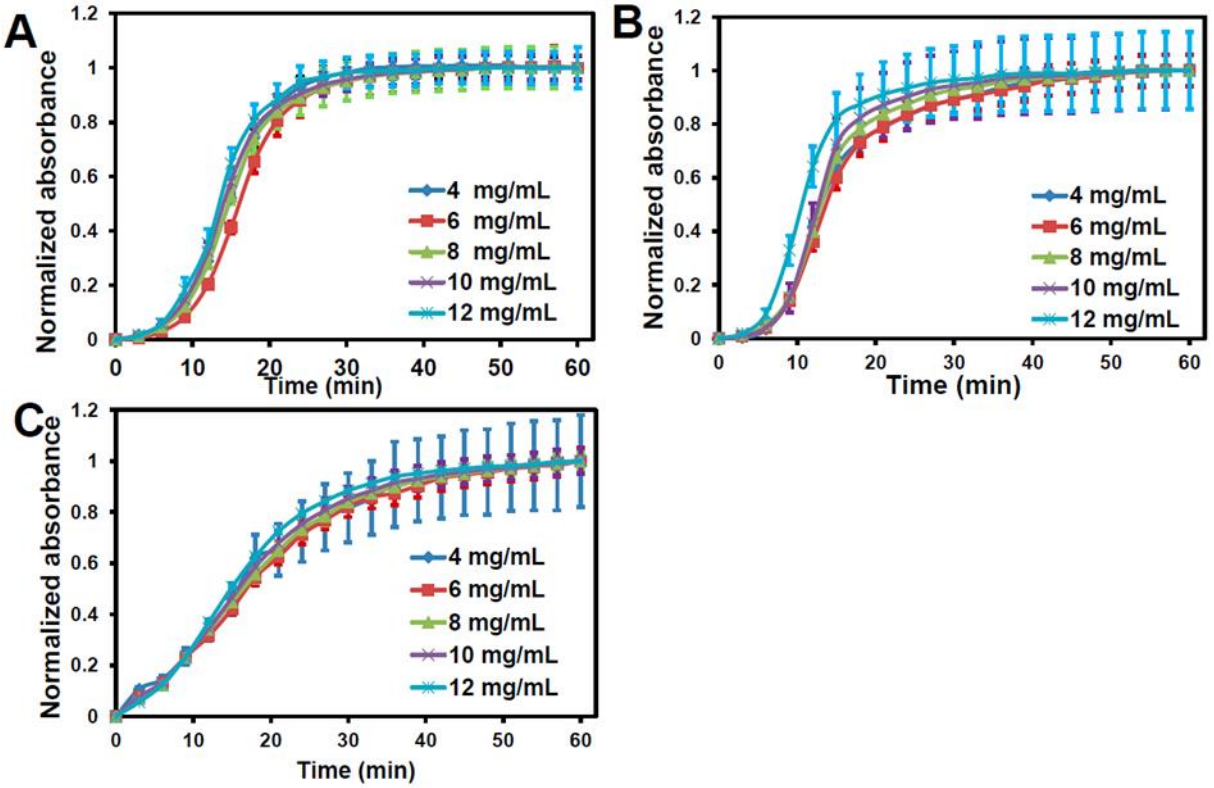

Figure 3. 8 Turbidimetric gelation curves of the SDS (A), TX (B) and PAA-treated (C) meniscus ECM hydrogels at varying concentrations.

All the hydrogels exhibited tunable peak compressive strengths and initial moduli by varying the ECM concentrations. The PAA-ECM hydrogels had peak compressive strengths ranged from 927 ± 123 to 2149 ± 182 Pa with the ECM concentrations increased from 6 to 12 mg/mL, which was significantly higher than that of the SDS-ECM and TX-ECM hydrogels (Figure 3.9A). The initial moduli of the PAA-ECM hydrogel with ECM concentrations from 6 to 12 mg/mL increased from 715 ± 307 to 2216 ± 786 Pa, which were significantly higher than that of the hydrogels prepared from TX-treated DM-ECM at high ECM concentrations (10 and 12 mg/mL) while there was no significant difference between the PAA-ECM hydrogel and SDS-ECM hydrogel in initial moduli (Figure 3.8B).

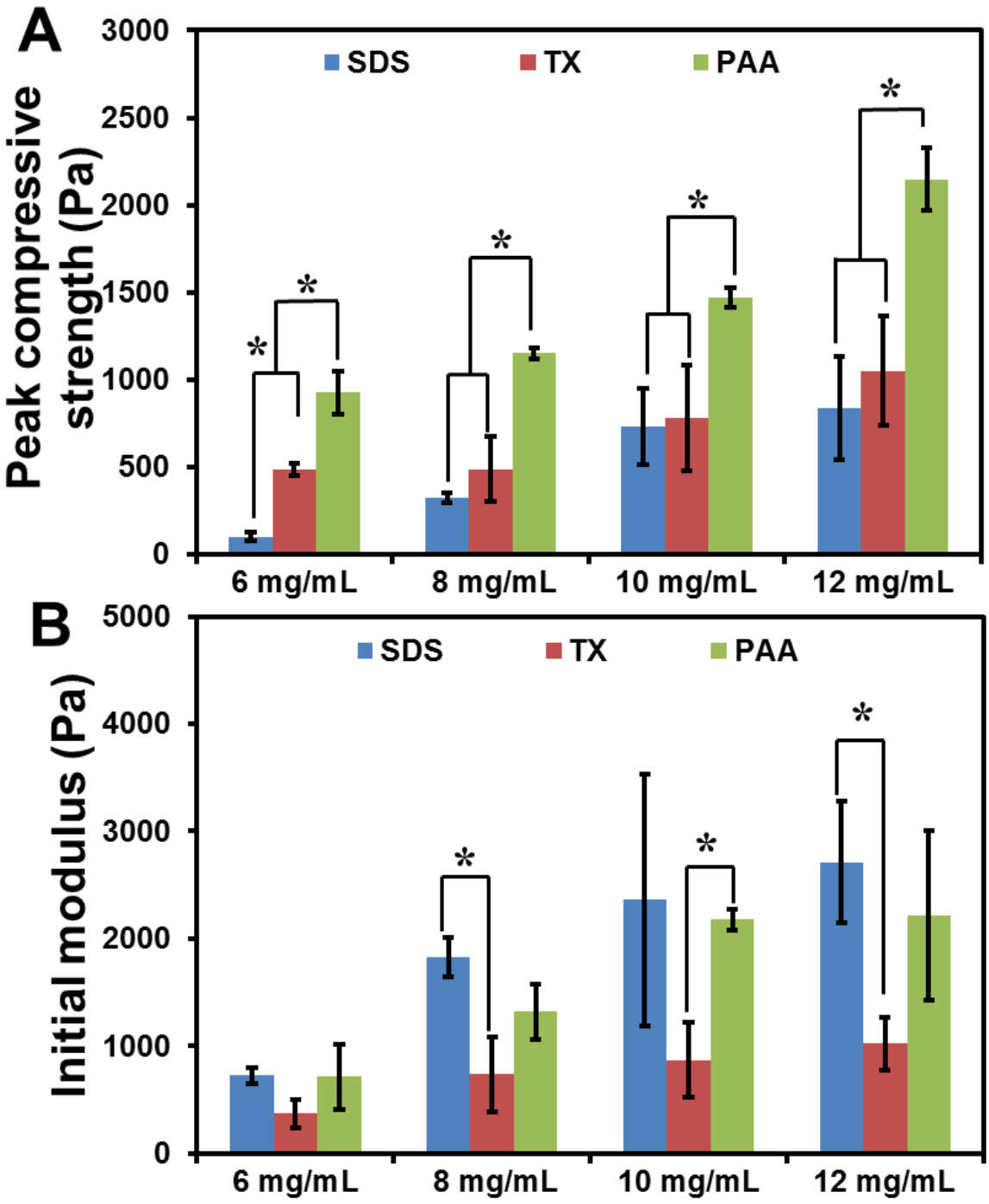

Figure 3. 9 The peak compressive strengths and initial moduli of the SDS, TX and PAA-treated meniscus ECM hydrogels.

3.3.4 Cell growth and GAG accumulation

Live/dead staining images demonstrated that all the hydrogels supported high cell viability, as predominate cells were found to be living (green) with a small portion of dead cells (red dots) during a 28 day *in vitro* culture period (Figure 3.10). Fibrochondrocytes had a uniform distribution within the hydrogels. Most of the cells exhibited a round shape with a few cells showing a spindle shape, similar to the fibroblast-like cell, at day 14 (Figure 3.10A, B, and C). At day 28, all the fibrochondrocytes showed a round shape in the hydrogels and no spindle-shaped cells were observed (Figure 3.10A, B, and C).

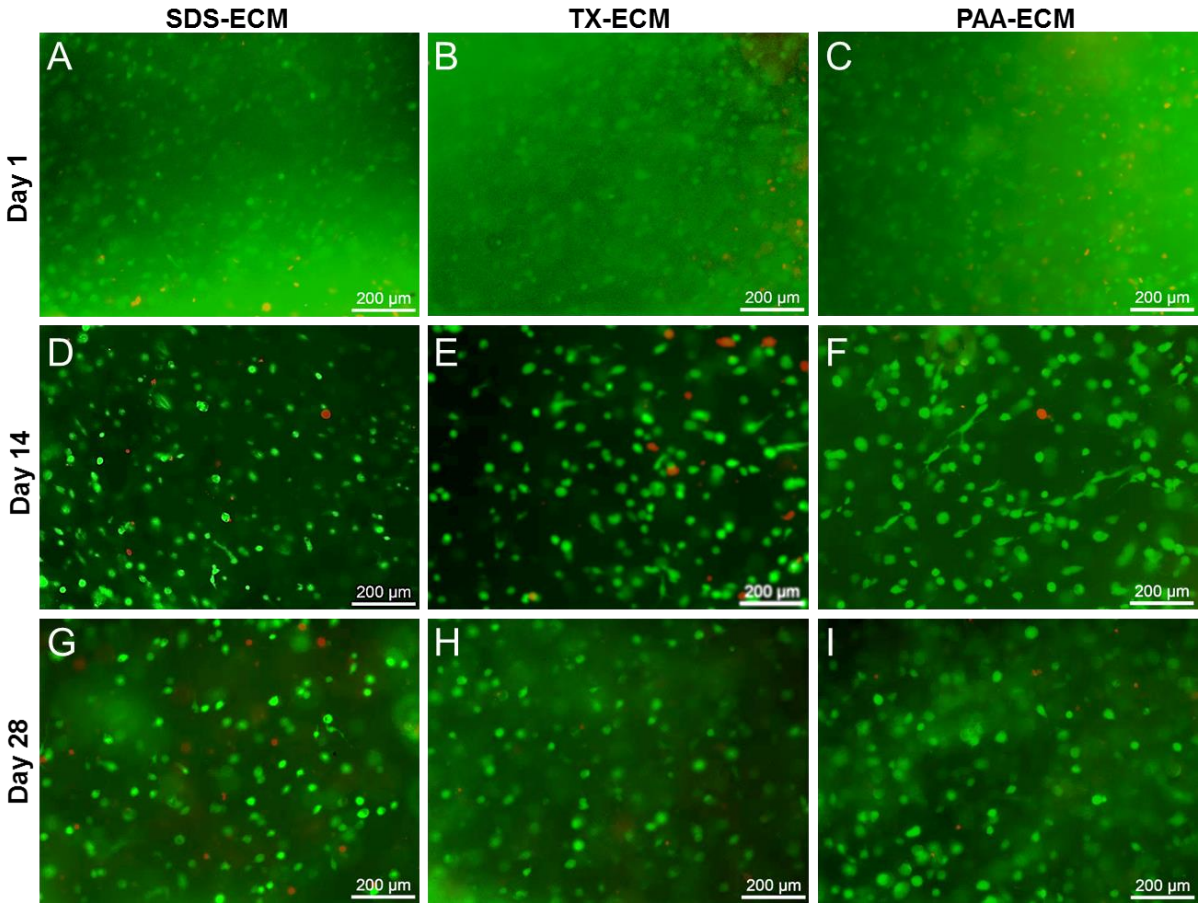

Figure 3. 10 Live/dead staining of fibrochondrocyte-seeded hydrogels at day 1 (A-C), 14 (D-F), and 28 (G-I).

The non-encapsulated DM-ECM hydrogels had negligible DNA and GAG contents (data not shown) compared to that of the cell-encapsulated hydrogels. Therefore, all the following reported DNA content was considered as cellular DNA and present GAG contents were attributed to the fibrochondrocyte-generated GAG during the culture. The total DNA and accumulated GAG were reported based on the per cell-seeded hydrogel level to determine their variations over time, which was previously reported in [92]. The cell-seeded hydrogels had slightly higher total DNA contents over the culture, but there was no significant difference, indicating that the fibrochondrocytes maintained a high level of viability throughout the entire culture period (Figure 3.11A). The fibrochondrocytes were found to produce GAG in the hydrogels from the early stage of the culture though the amount of the accumulated GAG was low at day 1 (Figure 3.11B). Interestingly, the accumulated GAG was observed to increase to ~ 4 folds and ~ 9 folds (compare to day 1) at day 14 and 28, respectively. In addition, the fibrochondrocytes in the PAA-ECM hydrogels secreted significantly higher GAG than that of the SDS-ECM and TX-ECM hydrogels at day 28. The fibrochondrocytes produced significantly higher GAG/DNA in the PAA-treated DM-ECM hydrogel compared to the SDS-treated DM-ECM hydrogel at day 28 (Figure 3.11C).

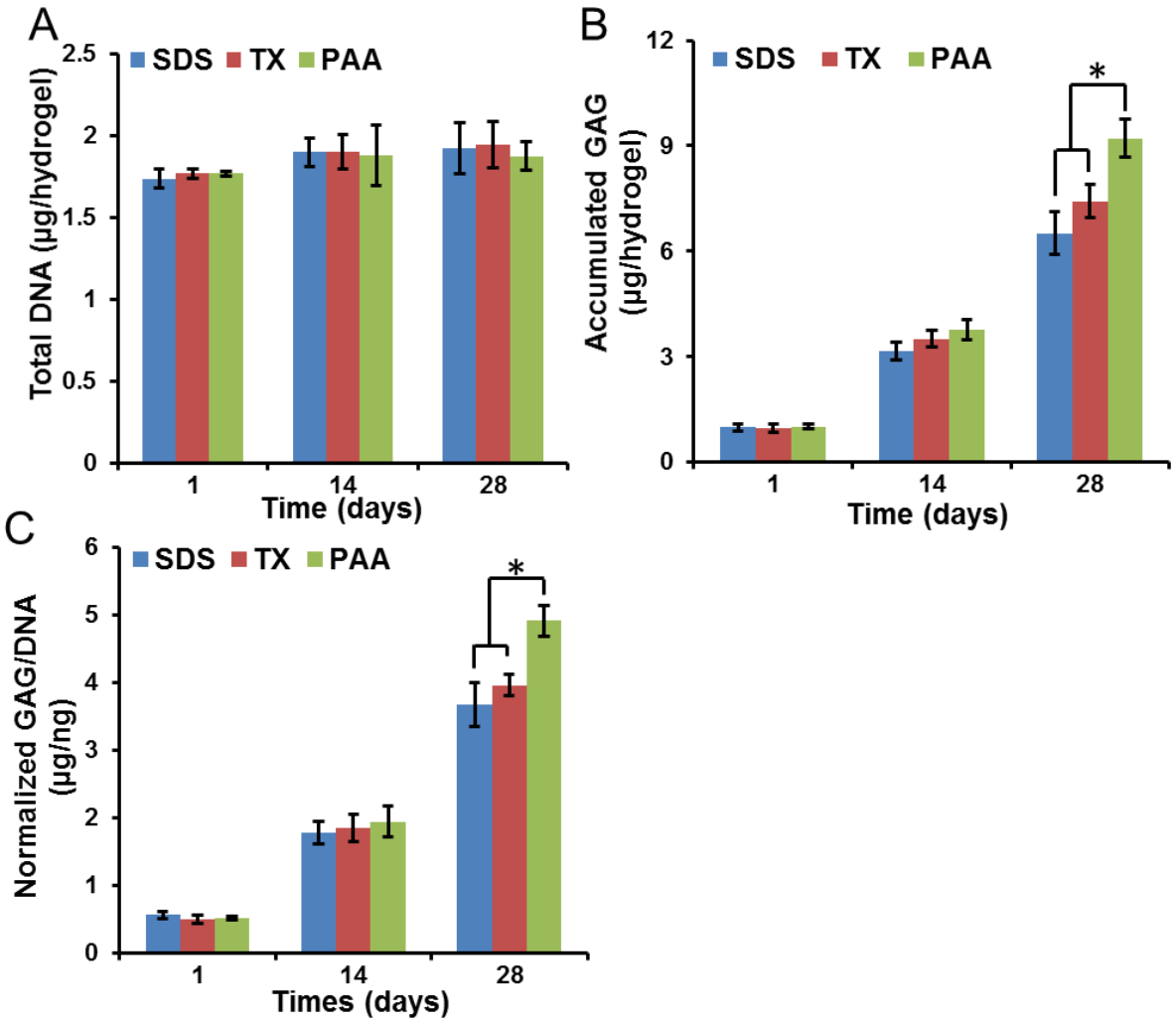

Figure 3. 11 Total DNA (A), accumulated GAG (B) and GAG/DNA ratio (C) of the fibrochondrocyte-seed hydrogels up to 28 days.

3.3.5 Histological analysis

H&E staining was performed at 28 days to visualize the cell morphology inside the ECM hydrogels (Figure 3.12). Our results showed that the fibrochondrocytes were oval to round in shape and evenly distributed in the hydrogel, which confirmed that observation of the live/dead staining (Figure 3.10).

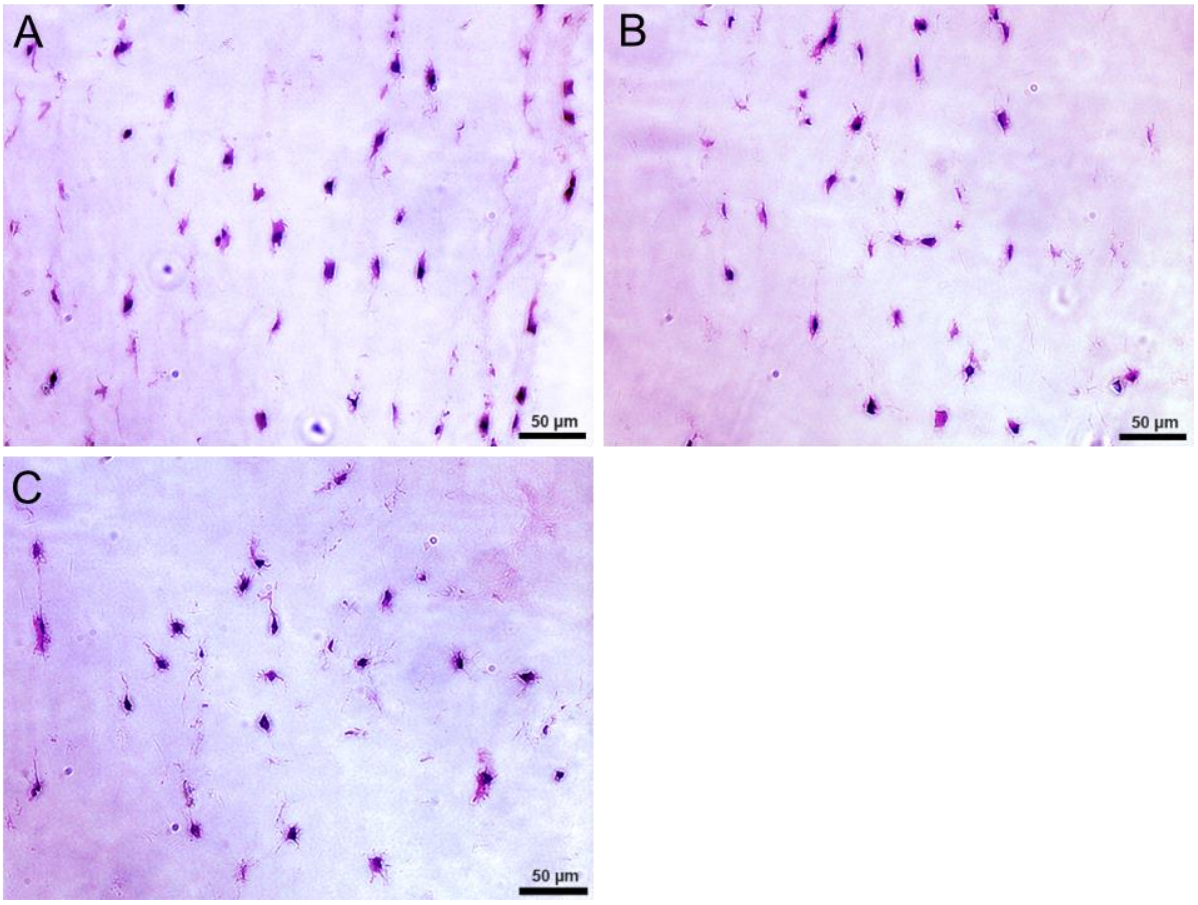

Figure 3. 12 H&E staining of the fibrochondrocyte-seed SDS-ECM (A), TX-ECM (B), and PAA-ECM (C) hydrogels up to 28 days.

3.3.6 Biomechanical properties

After 4 weeks of culture, all the fibrochondrocyte-seeded hydrogels maintained their cylinder shape (Figure 3.13). The SDS-ECM (Figure 3.13A and D) and TX-ECM (Figure 3.13B and E) hydrogels appeared to be weaker and softer compared with the PAA-ECM hydrogel (Figure 3.13C and F).

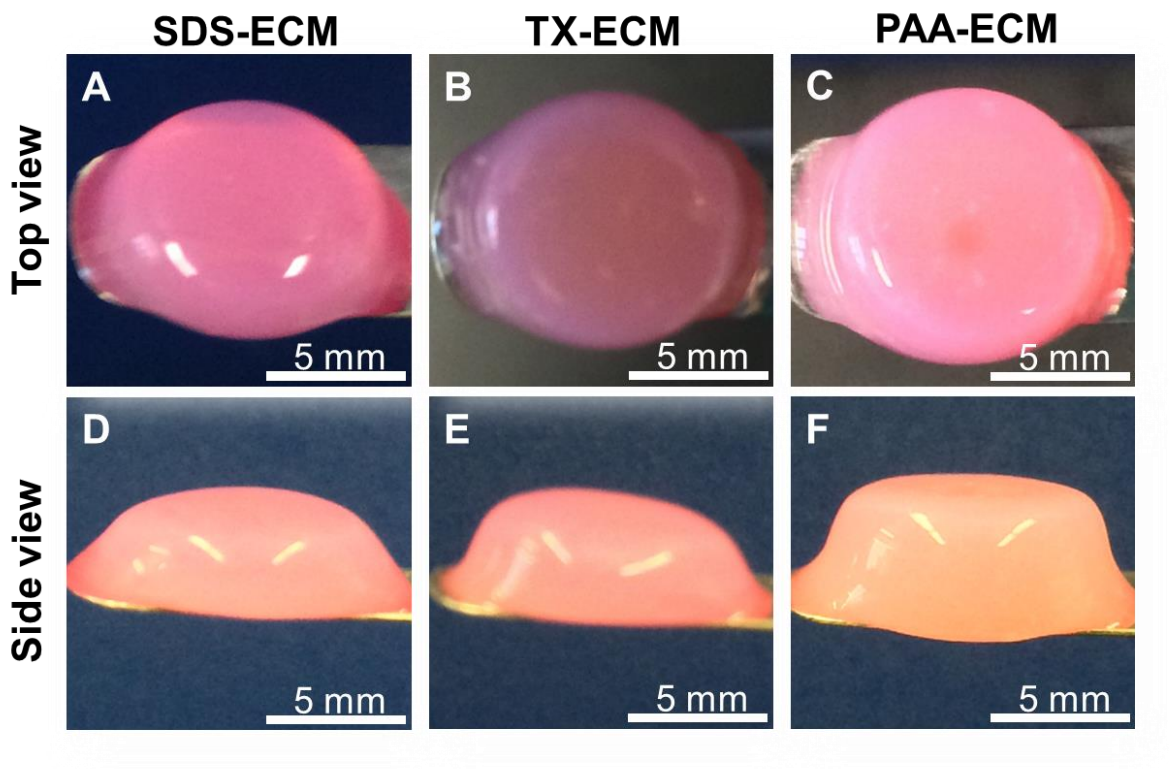

Figure 3. 13 Macroscopic images of the fibrochondrocyte-seeded hydrogels after 28-day culture. SDS (A and D), TX (B and E) and PAA (C and F)-treated meniscus ECM hydrogels.

As shown in Figure 3.14A, the typical compressive curves revealed that the PAA-ECM hydrogel was much stronger than the SDS-ECM and TX-ECM hydrogels. Quantitatively, the PAA-ECM hydrogel had the greatest peak compressive strengths of 14.6 ± 1.8 kPa, which is significantly higher than that of the TX-ECM (9.6 ± 1.8 kPa) and SDS-ECM (4.0 ± 0.6 kPa) hydrogels (Figure 3.14A). More importantly, all the fibrochondrocyte-encapsulated hydrogels had significantly greater compressive strengths compared to their respective hydrogels (Figure 3.9A and Figure 3.14B) (SDS-ECM: 4.0 ± 0.6 kPa vs 0.7 ± 0.2 kPa; TX-ECM: 9.6 ± 1.8 kPa vs 0.8 ± 0.3 kPa; PAA-ECM: 14.6 ± 1.8 kPa vs 2 ± 0.2 kPa). Control groups of hydrogels without cells

were found to retain their original shape, however, they were too weak to be handled for the test (data not shown). No significant difference in the initial modulus was found among the fibrochondrocyte-encapsulated hydrogels (Figure 3.14C).

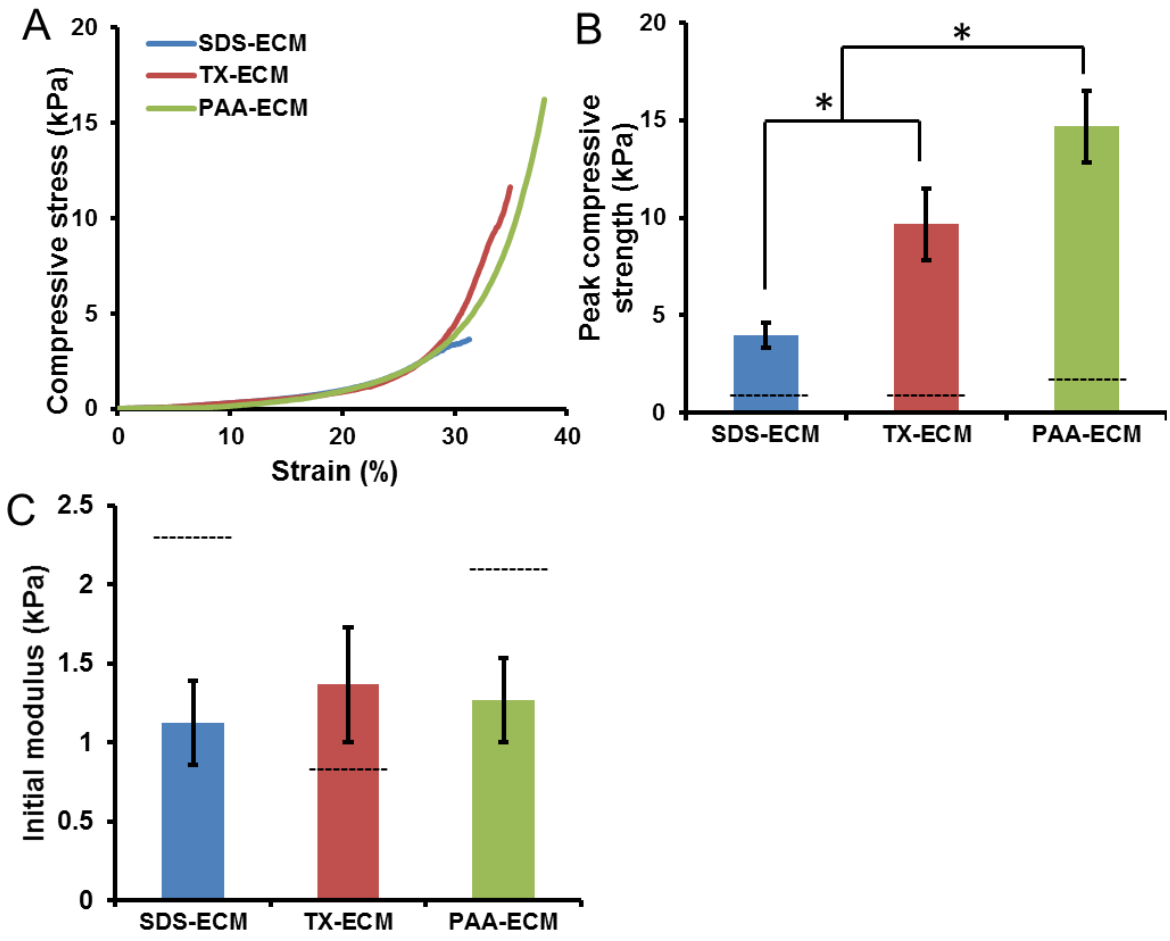

Figure 3. 14 (A) Typical curves of fibrochondrocyte-seeded hydrogel compressive stresses with the peak compressive strengths (B) and initial moduli (C) at 28 days. Dash lines indicate the peak compressive strengths (B) and initial moduli (C) of the non-seeded hydrogels at day 0.

3.4 Discussion

Previously, we have developed an injectable hydrogel derived from DM-ECM which represented an advantageous means that could be delivered through a minimally invasive surgery [218]. However, we were found a huge loss in GAG content during the decellularization process. The objective of this study was to determine the procedure which is the most effective on antigen removal and least detrimental in bioactive components for meniscus decellularization among three chemical-based protocols and assess the biological performance of the DM-ECM hydrogels. Three detergents with appropriate concentrations (1% SDS, 1% TX, and 0.1% PAA) commonly used for tissue decellularization were selected according to previous studies [129, 222] to decellularize porcine menisci. The comparison was based on the completion of cellular removal, preservation of the structure and bioactive compositions of the DM-ECMs, as well as the mechanical properties and biological effects on the fibrochondrocyte of the DM-ECM hydrogels.

A more recent study utilized a serial of acids for meniscal decellularization and found that formic acid is the most effective for cellular removal but substantially cause the loss of collagen [87]. They also indicated that a low concentration (0.15%) of PAA was more compatible with collagen and a prolonged 0.15% PAA treatment from 2 h to 12 h could significantly improve the cell removal from ~10% to ~70%. In our study, 0.1% PAA was used to decellularize the meniscal particulates, and this treatment resulted in a negligible DNA residual and was more efficient than SDS and TX. The PAA-based process was reported to be highly efficient for cellular nucleic acid removal at low concentration of 0.1%~0.15% [87]. It might attribute to the grinding process and the

prolonged treatment time that softened the menisci and allowed substantial PAA permeability into the dense ECM, finally expelled the meniscal cells.

Besides a thorough removal of cellular components, an optimal protocol for tissue decellularization should have minimal adverse effect on ECM architecture preservation and bioactive component retention [155]. The native meniscus comprises sparsely distributed cells embedded in the densely compacted and well-organized ECM (Figure 3.4G and H). The SDS-based decellularization process severely disrupted and damaged the ECM (Figure 3.4A and B) and caused a depletive effect on GAG content (Figure 3.5B). This is because the negatively charged hydrophilic head group of SDS can lysis cells, denature proteins and disrupt the ECM structure and cause the loss of ECM compositions [223]. The DM-ECM treated by TX showed a less disrupted and slightly damaged ECM structure (Figure 3.4C and D) compared with the SDS group. As a non-ionic detergent, TX was considered as a less strong chemical for tissue decellularization which was non-denaturant to proteins [223], while resulted in a considerable loss in GAG in consistent with previous studies [212]. The PAA-treated DM-ECM exhibited a better acid tolerance by showing a well-preserved architecture of ECM with the highest GAG retention. PAA was superior to the SDS and TX in maintaining ECM structure and retaining GAG. As an acidic solutions, PAA was less disruptive to the interactions between the matrix proteins, therefore, it had minimal effect on ECM compositions [87]. In addition to the collagen and GAG retention, several lower molecular bands were observed by gel electrophoresis. These findings demonstrate that the DM-ECMs retained their biochemical components, including

meniscus tissue-specific cues that could be essential for cell-matrix interaction and tissue remolding.

The predominant component of the decellularized ECM that determinates gelation behaviors and hydrogel formation is collagen [163]. Therefore, the hydrogels of DM-ECMs treated by different chemicals had similar gelation kinetics as there was no significant difference in collagen content among the DM-ECMs. The gelation behaviors indicated that the DM-ECM materials could be delivered to the targets by injecting, which substantially benefited a minimally-invasive surgery for meniscus repair. The excellent injectability of ECM hydrogels was proved using various types of ECMs *in vitro* and *in vivo* [158, 163, 218, 224], which enables the ECM hydrogel as an advantageous means to deliver cells and growth factors.

Biological hydrogels with tunable mechanical properties were capable of modulating cell-matrix interactions which are highly expected for tissue repair and functional tissue regeneration [225]. The mechanical properties of the DM-ECM hydrogels could be readily tuned by alternating the ECM concentration, as they showed increased peak compressive strengths and initial moduli with the increase of ECM concentration. It should be noted that the PAA-ECM hydrogel had significantly higher peak compressive strengths at the same ECM concentration compared with the SDS-ECM and TX-ECM hydrogels. This could be attributed to the higher content of GAG, as GAG was able to modulate collagen self-assembly and fiber crosslinking which results in improved mechanical properties [163].

The cellular nature of meniscus was sophisticated and largely unknown to date. It was generally believed that the outer zone majorly contained fibroblast-like meniscal

cells and was vascularized with blood supply from the synovial fluid [226]. Increasing evidence showed that the injured outer zone of the meniscus was capable of self-healing with simple surgery [4]. The meniscal inner zone predominantly composed of fibrochondrocytes with limited capability for spontaneous healing due to the avascular nature of the inner zone, and most injuries occur in the avascular part [227]. Therefore, the fibrochondrocyte was considered as the ideal cell source and the most frequently utilized to regenerate and repair meniscal tissue [228, 229]. Fibrochondrocytes experience rapid growth rates and higher metabolic activities on the surface of eletrospun nanofibrous mats or within 3D porous scaffolds [106, 117, 230], while they proliferate slowly when cultured within hydrogels [92, 231]. In this study, the bovine fibrochondrocytes had uniform distribution inside the hydrogels and maintained unchanged total numbers of cells at day 28 by quantifying the cellular DNA content, which is line with a previous report that fibrochondrocytes maintained stable levels of total DNA cultured collagen type I hydrogels at 28 days [92]. Fibrochondrocyte-encapsulated hydrogel constructs maximally resemble the cell-embedded matrix of the native meniscus, which allows minimal nutrient exchange and metabolic waste diffusion and supports limited cell proliferation [92, 93]. While the DM-ECM hydrogels maintain good cell viability, future study should focus on the determination of phenotype of the encapsulated cells via PCR and immunohistochemical analysis.

Three-dimensional culture of fibrochondrocytes in hydrogels is favorable for the accumulation of the cell-secreted GAG [92, 93, 95]. The fibrochondrocyte-encapsulated PAA-ECM hydrogel construct held a relatively higher GAG accumulation than the SD-ECM and TX-ECM hydrogel constructs at the end of culture. The higher

GAG content of the PAA-ECM hydrogel was attributed to the greater GAG accumulation within the cell-seeded hydrogel construct. The PAA-ECM hydrogel has an 8 to 10-fold higher GAG content than the SDS-ECM and TX-ECM hydrogels, which might substantially modulate cellular growth and GAG accumulation. This is because GAG dynamically reacts with meniscus cells to help the cells maintaining a high level of chondrogenesis and producing more proteoglycans including GAG [232]. Calamia et al demonstrated that GAG could affect chondrocyte growth and modify cartilage ECM metabolism by promoting chondrocyte-secreted protein products of aggrecan, biglycan, and cartilage oligomeric matrix protein [233]. Another important finding is the increasing accumulation of GAG produced by the fibrochondrocytes in the three DM-ECM hydrogels, which almost attained 30% of the GAG content of the native meniscus. It indicated that the bovine fibrochondrocytes maintained the chondrogenic characteristics and could generate extracellular matrix components in the 3D culture. A similar work conducted by Puetzer et al showed that a high-density type I collagen hydrogel was suitable for fibrochondrocyte proliferation and GAG accumulation [92]. As a water-soluble compound, GAG is easily lost during monolayer cell culture. The DM-ECM hydrogels provided a 3D microenvironment resembling the native meniscal ECM for fibrochondrocytes, which contributed to the GAG producing. Furthermore, the DM-ECM hydrogels were desirable for GAG retention as collagen fibrous network could prevent the GAG from washing out during the refreshing of cell culture medium.

A significantly higher GAG/DNA ratio was found in the PAA-ECM hydrogels compared to the SDS-ECM and TX-ECM hydrogels. One possible reason is that the PAA treatment resulted in a higher GAG retention that could modulate the collagen to

form a denser fibrous network. Another plausible explanation is related to some other bioactive ECM molecules such as elastin and growth factors within the hydrogels. PAA was relatively milder for meniscus decellularization, it probably allowed higher retentions of elastin and growth factors, which stimulated fibrochondrocytes to produce GAG. Future work is needed to address the quantification of other important ECM components in the DM-ECM.

One important finding is the strikingly improved compressive strength of the fibrochondrocyte-encapsulated hydrogels. It was found that all the fibrochondrocyte-encapsulated hydrogels maintained their original shape and showed much higher compressive strength after 4 weeks of culture. However, the hydrogels without cells could keep their cylinder shape, but they were not capable of being mechanically tested. The loss of structural integrity might be resulted from the progressive hydrolysis during the *in vitro* culture. All results evidenced the critical roles of cell-matrix interactions in improving the structural stability and enhancing the mechanical properties of the fibrochondrocyte-encapsulated hydrogels. When cultured with scaffolds, fibrochondrocytes produced ECM including collagen and GAGs that contribute to the increased mechanical strength [124, 232]. The fibrochondrocyte-encapsulated PAA-ECM hydrogel had the greatest compressive strength since the mechanical strength is highly relevant to the highest amount of accumulated GAG within the hydrogel.

3.5 Summary

By comparing the different chemicals that applied to meniscus decellularization, we found PAA is more efficient for meniscus decellularization than SDS and TX. The

PAA-ECM had the greatest DNA removal and GAG retention, with comparable collagen content to the SDS-ECM and TX-ECM. The PAA-ECM hydrogels had the highest compressive strength due to its greater content of GAG that is capable of modulating collagen self-assembly. We found the bovine fibrochondrocyte-encapsulated PAA-ECM hydrogel exhibited strongest mechanical strength, which might attribute to the greatest amount of accumulated GAG. Although the underlying mechanism of the significantly elevated GAG accumulation within the PAA-ECM hydrogel is largely unknown, PAA-based treatment is believed to the optimal for meniscus decellularization and ECM hydrogel preparation.

CHAPTER 4

PREPARATION AND CHARACTERIZATIONS OF REGIONALLY DECELLULARIZED MENISCAL ECM HYDROGELS

4.1 Introduction

The menisci are semilunar fibro-cartilaginous tissues located in the lateral and medial sides of tibial plateau of the knee joints. With a concave superior surface and a flat inferior surface, a single piece of meniscus is well-fitted the femoral condyle and the tibial plateau, making it an ideal cushion in the knee joint [3]. The main function of menisci is to provide shock absorption, lubrication, and stability to ensure the knee joint function properly by dispersing and partly absorbing the compressive pressure between the femur and tibia. However, the menisci are vulnerable due to sports activity-caused traumas and degenerative diseases, especially among aged people [4]. Meniscal tears are the most frequent causes of orthopedic surgical procedures and present a significant risk of the initiation of osteoarthritis [234].

A comprehensive understanding of the biochemical and biomechanical properties of menisci could substantially benefit the meniscal repair and regeneration in the clinic [121, 174]. Macroscopically, the meniscus has a complicated shape with decreasing thickness from the out portion to the inner portion to increase the congruence with the tibia and femur. The ECM compositions and cell types define the function: the collagen and proteoglycans secreted by the local cells closely correspond to the tensile and compressive properties. Specifically, the outer meniscal cells have a fibroblast-like phenotype and mainly produce type I collagen associated with fibrous tissue [19]. In

contrast, the inner meniscal cells have a phenotype and a gene expression profile more similar to chondrocytes which generate more type II collagen and GAGs [235]. The meniscal outer zone is generally vascular and mainly composes type I collagen with a lower GAG content and exhibits a stronger tensile stress in the circumferential direction, whereas, the meniscal inner zone is avascular with higher contents of type II collagen and GAG, but a decreased content of type I collagen and shows a greater compressive stiffness [17]. To this end, regional variations of the meniscal ECM compositions should be highlighted in meniscal repair and regeneration.

Recent advances in tissue engineering present great potential to repair the injured menisci and regenerate the whole menisci to attain the ultimate goal of allowing functional tissue restoration and reducing the risk of osteoarthritis (OA) [236]. Current approaches of meniscus tissue engineering have focused on the development of scaffolds using either synthetic materials or natural materials, and incorporating of the scaffolds with appropriate cell sources to reconstruct engineered meniscal tissues [187]. These meniscal scaffolds replicated the complex geometry of the native menisci and maintained cell viability *in vitro* and *in vivo* [48, 92, 94]. And the efforts showed some encouraging signs that macroscopically repaired the injured menisci in preclinical studies. However, the implants were found to be inferior to the native meniscal tissue as they had abnormal matrix depositions and decreased mechanical properties [237]. Therefore, creating a regenerated meniscus that biochemically and biomechanically resembles the native meniscal tissue is still a huge challenge [231].

Biological scaffolds prepared from native tissues/organs through decellularization process have gained increasing attentions and are widely utilized for tissue-specific

regenerative and therapeutic applications [68, 238]. Decellularized meniscal ECM (DM-ECM) was demonstrated to be biochemically similar to the native meniscus because considerable bioactive components such as collagens and proteoglycans could be identified in the DM-ECM. Previously, we reported an injectable DM-ECM hydrogel that could induce bovine fibrochondrocytes producing meniscal specific matrix. Given that the meniscus is various in cell populations and biochemical compositions in its three distinct zones, the regionally specific meniscal ECMs could affect the cell-matrix interactions of fibrochondrocytes. Furthermore, it is unknown which regional DM-ECM is the best for inner meniscus regeneration. In the current study, we aim to investigate and compare the effects of regionally specific DM-ECM on the growth and ECM product accumulation of fibrochondrocytes for inner meniscus repair and regeneration. Specifically, porcine menisci were regionally divided into three zones (outer, middle, and inner zones), separately decellularized and processed into regionally specific DM-ECM hydrogels. Bovine fibrochondrocytes were encapsulated with the DM-ECM hydrogels to compare the regional-specific effects on the three-dimensional constructs and the cell-matrix interactions. The cell morphology, proliferation, cell-secreted matrix, and biomechanical properties of the cell-seeded hydrogels were determined to verify the regionally specific effects.

4.2 Experimental section

4.2.1 Materials

PAA, EDTA, pepsin, HCl, NaOH, 1,9-dimethyl methylene blue (DMMB), propan-1-ol, sodium acetate, GuHCl, FBS, and high glucose DMEM were supplied by Sigma. PSF and DAPI were obtained from Life Technologies, Inc.

4.2.2 Regional meniscal tissue decellularization

Porcine menisci were dissected from the knee joints of adult pigs (weighing 80-100 kg) that were freshly harvested from a slaughterhouse. The fats and connective tissue were carefully removed with a scalpel to obtain menisci with only fibrocartilaginous tissue. The menisci were radially separated into outer, middle and inner regions (Figure 4.1), separately sliced to thin pieces and then frozen at -80 ^{o}C. The regional menisci were separately decellularized using PAA. Briefly, the frozen samples were pulverized into coarse powders and treated with 0.1% peracetic acid (PAA)/4% ethanol solution for 3 days. The PAA solution was refreshed every 24 h. Then the samples were stirred in 0.1% EDTA overnight followed by thorough washing with deionized water to remove the residual chemicals. Finally, the decellularized samples were lyophilized and stored at -20 ^{o}C for further use. The decellularized outer, middle, and inner meniscal ECMs were designated as OM-ECM, MM-ECM, and IM-ECM, respectively.

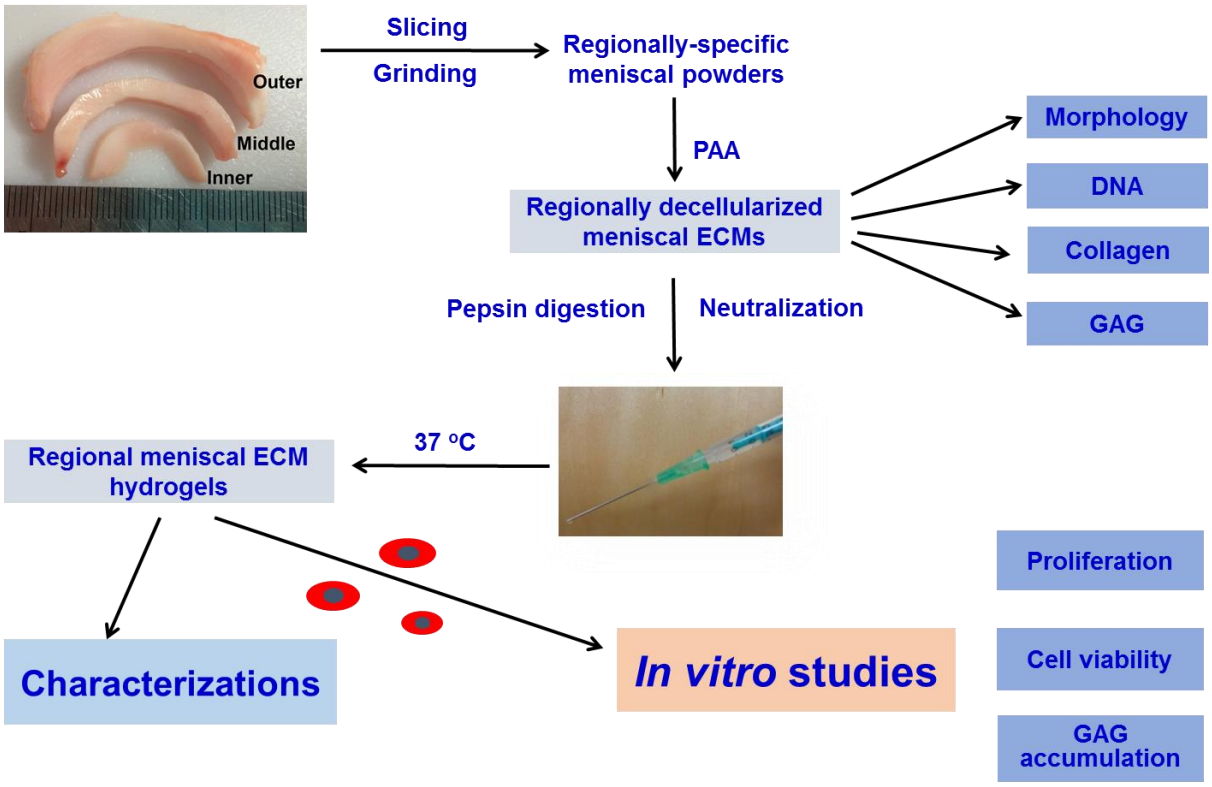

Figure 4. 1 Schematic of the preparation and characterization of regionally specific meniscus ECM hydrogels.

4.2.3 Characterizations of the regionally decellularized menisci

To evaluate the efficiency of decellularization on cellular removal and determine the retentions of the biochemical components, we utilized SEM, histological staining and quantitative analysis of DNA, collagen and GAG contents to characterize the regionally decellularized ECMs. Native meniscal samples of the outer, middle, and inner regions were used as controls for all the tests.

The samples were fixed with 4% paraformaldehyde (Sigma) and lyophilized for morphological study. After sputter coating with silver, the morphologies of samples were visualized using a SEM (S-3000N, Hitachi).

The DNA and GAG contents of the DM-ECMs were determined using enzymatically digested samples as Ref [218]. Briefly, the samples were solubilized with 1 mg/mL pepsin/0.01 M HCl at an ECM concentration of 15 mg/mL at room temperature until no visible particle remained. The DNA and GAG were then quantitatively analyzed using the PicoGreen DNA assay (Life Technologies, Inc.) and DMMB method (n = 3), respectively. Collagen content was determined by quantifying the hydroxyproline with a hydroxyproline assay kit (Sigma) according to the manufacturer's instruction and calculating the collagen with a converting factor of 14.3%.

4.2.4 Preparation and characterizations of the regional DM-ECM hydrogels

The DM-ECMs were enzymatically digested at the ECM concentration of 15 mg/mL using 1 mg/mL pepsin in 0.01 M HCl at room temperature for 48 h. The DM-ECM digests were neutralized with 0.1 M NaOH and 10X PBS and then diluted to pre-determined ECM concentrations to form pre-gels in an ice bath. To induce gelation and form solidified hydrogels, the pre-gels were loaded in a syringe, injected into cylinder molds and warmed in a 37 ^{o}C incubator for 30 min.

Composition analysis of the solubilized DM-ECMs was carried out SDS-PAGE, with collagen type I as a control. Briefly, digested DM-ECM solutions were run on a Mini-PROTEAN TGX, 4−20% polyacrylamide gel in Tris/glycine/SDS buffer (Bio-Rad). A voltage of 200 V was applied for the gel electrophoresis that was performed in a Mini-PROTEAN Tetra Cell (Bio-Rad). The gel was then stained with Coomassie Brilliant Blue R-250 (Bio-Rad).

The gelation behaviors of the hydrogels were turbidimetrically determined as previous protocol [165]. The pre-gels with ECM concentrations of 10 mg/mL were prepared and transferred to a 96-well plate (100 µL per well, n = 4), and then the absorbance was read spectrophotometrically at 490 nm at 37 ^{o}C on a pre-warmed Infinite M200 plate reader every 2 min for 1 h. The results were normalized from the initial absorbance (A_0) to the maximal absorbance (A_m) at each time point (A) and determined by the following equation: normalized absorbance = $(A-A_0)/(A_m-A_0)$. The time of half gelation ($t_{1/2}$) was defined as the time reaches 50% absorbance; the lag time (t_{lag}) was determined by extrapolating the linear portion of the gelation curve to 0% absorbance; and the gelation rate (S) was defined as the slope of the linear portion of the curve [160, 218].

The morphologies of the hydrogels were examined using SEM. The DM-ECM hydrogels with ECM concentration of 10 mg/mL frozen in liquid nitrogen, lyophilized and mounted for sputter coating of silver. The samples were then imaged with a SEM (S-3000N, Hitachi).

The compressive properties of the hydrogels were examined as our previous report [218]. Briefly, pre-gels with ECM concentrations of 6, 8 10, and 12 mg/mL were transferred to plastic cylinder molds (10 mm in inner diameter) and warmed at 37 ^{o}C for 30 min to form solidified hydrogels. The samples were then tested using an MTS Insight machine (MTS, Eden Prairie, MN) with a 10 N load cell at a crosshead speed of 1 mm/min until failure (n = 4).

4.2.5 Cell isolation and maintenance

The knee joints of calves were obtained from a local abattoir within 36 hours of slaughter. The cells were isolated according to the previous protocols [16, 115]. Briefly, the knee joints dissected to allow the access of menisci under aseptic condition. The horns and connective tissues were resected and the remaining menisci were divided into outer two-third and inner one-third parts. The inner portion was minced into 1-2 mm^3 cubes and incubated with 0.2% type II collagenase in Dulbecco's modified Eagle medium (DMEM) with 1% penicillin–streptomycin–fungizone (PSF, Life Technologies, Inc.) at 37 ^oC overnight. The obtained suspensions were filtered with 70-μm cell strainers, centrifuged at 1,500 rpm for 10 min to form pellets. The cells were seeded at a density of 1×10^4 cells/cm^2 in DMEM supplemented with 10% fetal bovine serum (FBS, Sigma) and 1% PSF in a 37 ^oC incubator with 5% CO_2 and 95% humidity. The medium was changed every 2 days. The cells were subcultured upon 80% confluence to the second passage (P_2) for future use.

4.2.6 Cell encapsulated with the regional DM-ECM hydrogels

The pre-gels were prepared under the sterile condition and stored in an ice bath for cell encapsulation. Fibrochondrocyte suspension was mixed with pre-gels to yield a mixture with the ECM concentration of 10 mg/mL and the cell density of 1.0×10^7 cells/mL. The mixtures were injected into plastic rings (10 mm in diameter) in 24-well plates and incubated at 37 ^oC for 30 min to form cell-encapsulated hydrogels. Subsequently, the rings were removed and 2 mL medium was added to each well. The cell-encapsulated hydrogels were maintained in DMEM with 10% FBS and 1% PSF in

a 37 ^{o}C incubator with 5% CO_2 and 95% humidity for 4 weeks. The medium was refreshed every 2 days. Unless otherwise stated, 100 µL mixture was injected into each ring for the culture. Cell viability was evaluated after 1, 14, and 28 days of culture using the live/dead staining assay (Invitrogen). The stained cells were visualized with a microscope (Eclipse Ti, Nikon). Cell proliferation was assessed by quantifying total cellular DNA using PicoGreen DNA assay and GAG accumulation was determined by DMMB test as described in **3.2.8**. The DNA and accumulated GAG were calculated at the per scaffold level to monitor their total amounts during the culture [92].

4.2.7 Histological analysis

The cell morphology within the hydrogels was determined by histological analysis. Samples of the cell-encapsulated hydrogels were harvested, fixed with 4% paraformaldehyde, O.C.T embedded and then cryosectioned to 7 µm slices for H&E staining.

4.2.8 Contraction and Biomechanical Analysis

To determine the cell-seeded hydrogel contraction and biomechanical properties, 300 µL cell-pregel mixture was injected into each ring and then cultivated for 28 days. Hydrogel contraction was quantified by macroscopic images analysis as reported elsewhere [22]. Briefly, the samples were harvested and their gross appearance was imaged. The surface area of hydrogels was determined by tracing the round border of the sample using Image J (NIH, Bethesda, MD). The contraction was expressed as the percent of the surface areas of the cell seeded ECM hydrogels to the unseeded ECM

hydrogel surface areas (n=3). For the biomechanical analysis, the height of each sample measured by a caliper. Then the compressive stresses and strains of the samples were tested as previously described (n=3).

4.2.9 Statistical analysis

All the data were expressed as mean ± standard deviation and analyzed by one-way analysis of variance (ANOVA) with a Tukey's post hoc test using Statview software. Significant difference was considered at $p < 0.05$.

4.3 Results

4.3.1 Decellularization

Porcine menisci were regionally cut into three zones (Figure 4.1) for decellularization using the PAA-based method as Chapter 3. Apparently, the different zones of the native meniscus exhibited distinct tissue density (Figure 4.2). Overall, all the three tissues of the three zones were very dense with parallel hollows. The cross-section images showed that the inner zones had relatively smaller hollows compared to the middle zones. After decellularization, all the decellularized meniscus ECMs showed a porous structure with little collagen fibers (Figure 4.2). This is consistent with our previous study that showed PAA is relatively gentler for meniscus decellularization compared with SDS and TX.

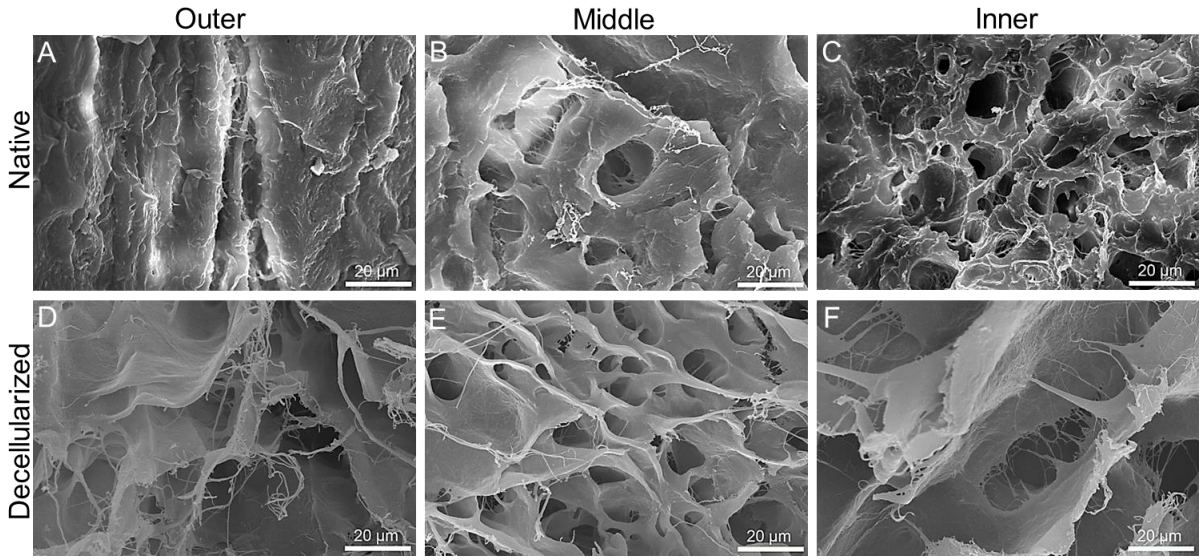

Figure 4. 2 SEM images of the native meniscus tissue the decellularized meniscus ECMs. (A) and (D), outer zone; (B) and (E), middle zone (C), and (F), inner zone.

The residual DNA in the decellularized ECMs was assessed by PicoGreen DNA assay. Figure 4.3 illustrated that all the decellularized ECMs contained negligible DNA residual (~ 0.1 ng/mg). No significant difference in the residual DNA content was observed among the different ECMs.

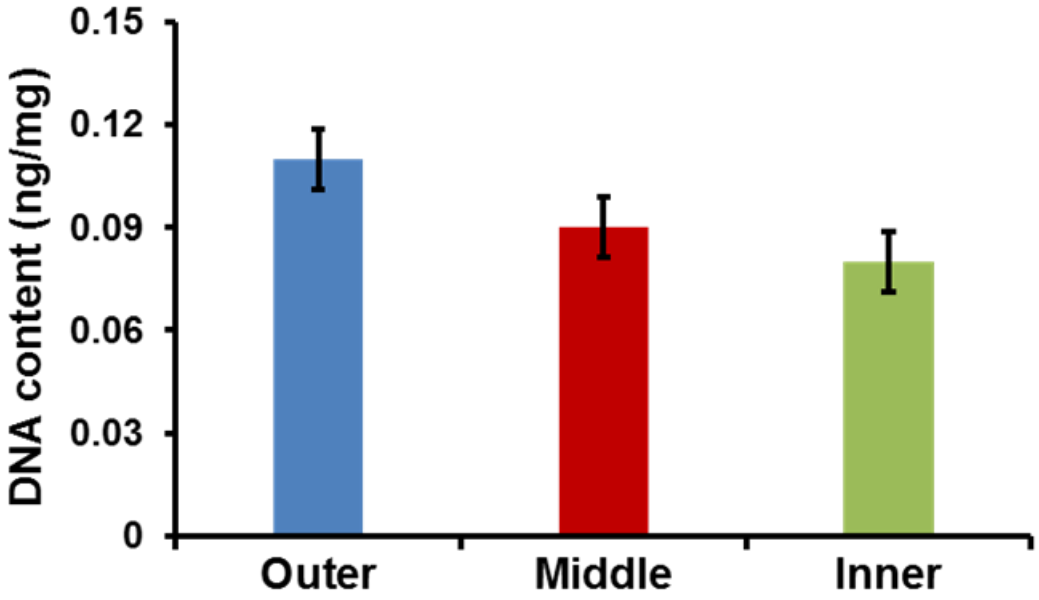

Figure 4. 3 Residual DNA contents of the regionally decellularized ECMs.

Collagen contents of the decellularized ECMs were determined by quantifying the hydroxyproline that makes up 14.3% of collagen. The IM-ECM had a collagen content of 59 ± 7%, which was significantly lower than that of the OM-ECM (86 ± 7%) and MM-ECM (79 ± 6%) (Figure 4.4A). All the decellularized ECMs had higher collagen contents compared to the corresponding native tissues. Notably, the IM-ECM had a significantly greater collagen content than the native inner zone tissue.

Decellularization processes always cause a loss in GAG contents, due to the water-soluble nature of GAG. The PAA-based decellularization process resulted in the loss of GAG for the OM-ECM and MM-ECM to some extent (Figure 4.4B). There significantly decreased GAG contents of the OM-ECM and MM-ECM compared to their corresponding native tissues. Although the IM-ECM showed lower GAG content than the native inner meniscus, there was no significant difference. The IM-ECM (11.1 ± 1.1

mg/µg) had significantly a higher content of GAG than that of the OM-ECM (5.5.1 ± 0.8 mg/µg) and MM-ECM (11.1 ± 1.1 mg/µg).

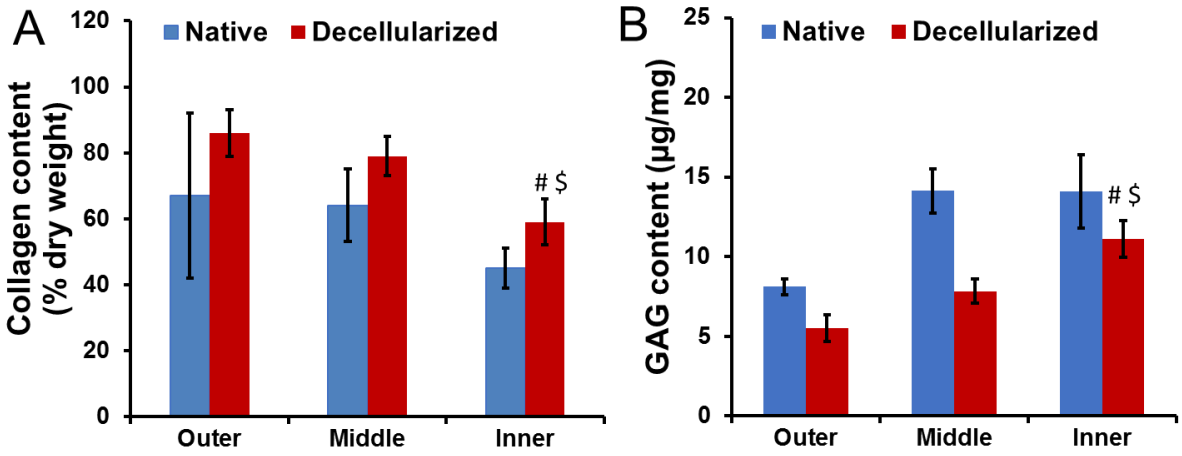

Figure 4. 4 Collagen (A) and GAG (B) contents of the decellularized meniscus ECMs. # vs. Decellularized Outer, $ vs. Decellularized Middle; Significant difference was considered at $p < 0.05$.

SDS-PAGE showed that the regional DM-ECMs contained strong protein bands that present in the collagen lane (Figure 4.5). Multiple faint bands at 100 and 37 kD were observed for the regional DM-ECMs, but they were absent for the collagen, indicating that the DM-ECMs have some lower molecular weight species.

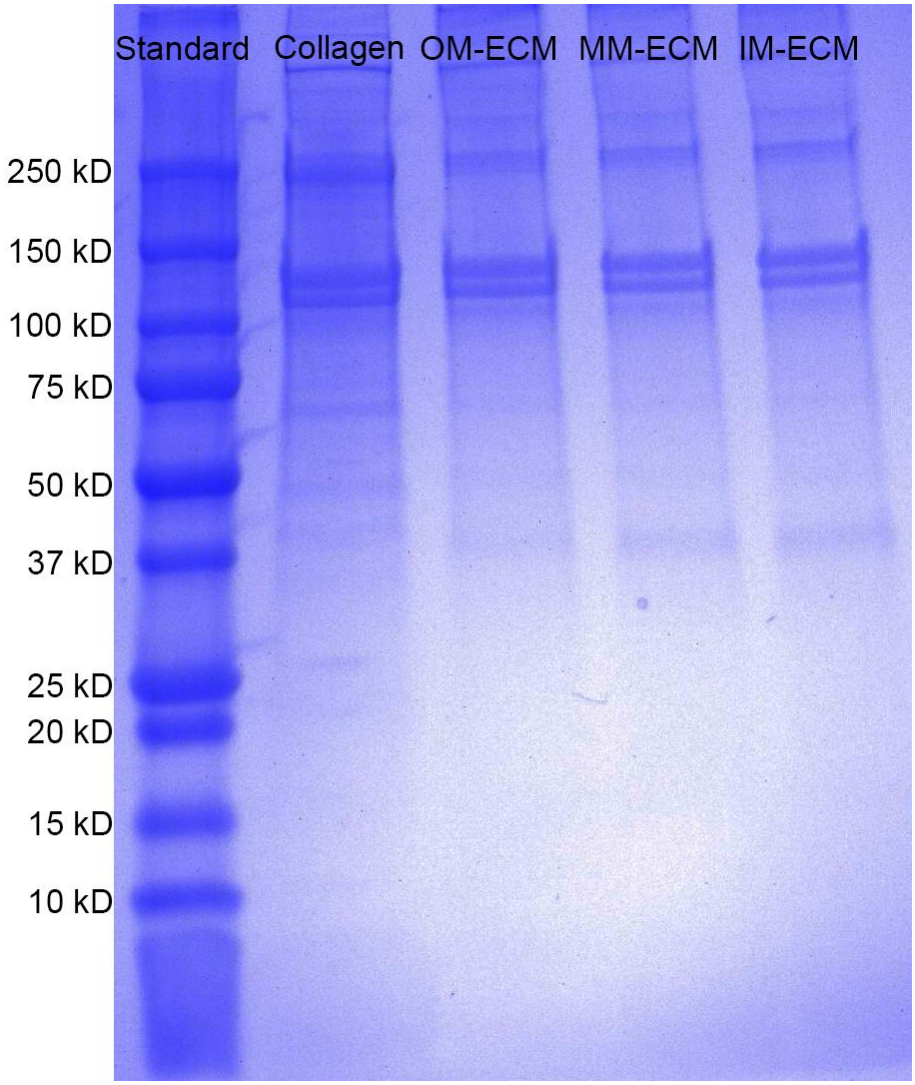

Figure 4. 5 SDS-PAGE analysis of the regional DM-ECMs.

4.3.2 Hydrogel gelation behavior

The gelation behaviors of the meniscus ECM hydrogels were determined using turbidimetric absorbance (Figure 4.6). Sigmoidal shaped curves of the hydrogel gelation kinetic demonstrated the hydrogel formation after a lag phase. No significant difference in gelation behavior was found among the three meniscus ECM hydrogels.

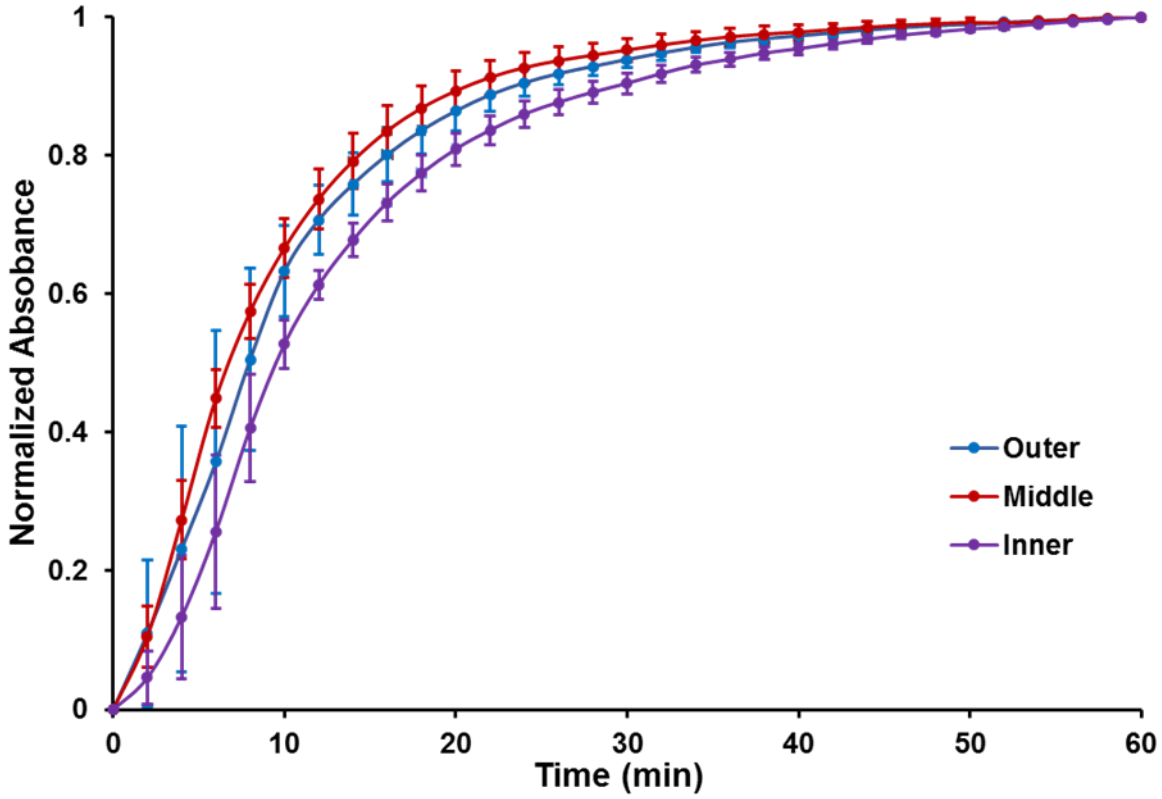

Figure 4. 6 Turbidimetric gelation curves of the decellularized ECM hydrogels.

4.3.3 Hydrogel morphology

Decellularized ECM hydrogels were formed at the ECM concentration of 10 mg/mL and their morphology was observed via SEM. Figure 4.7 showed the morphology of these ECM hydrogels. It was shown that the hydrogels mainly contained fibrous structures with some sheets.

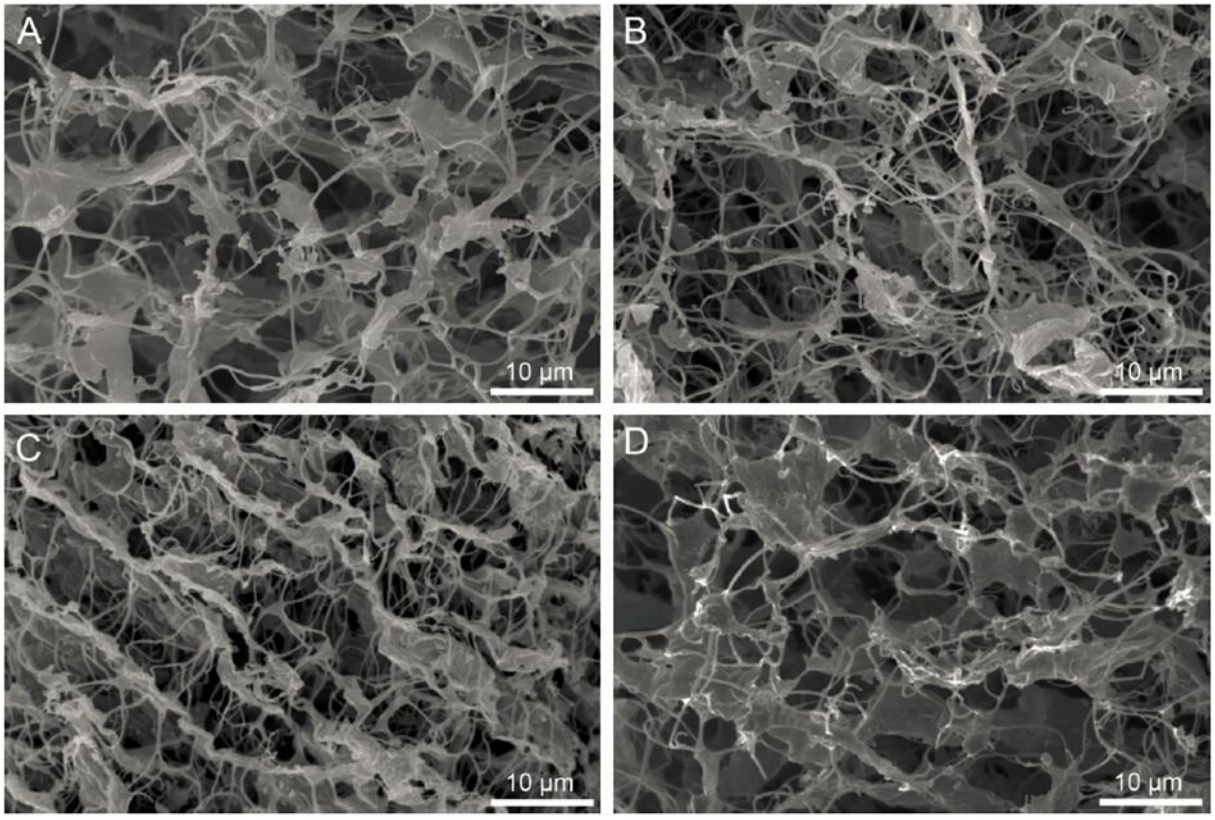

Figure 4. 7 SEM images of the OM-ECM (A), MM-ECM (B), IM-ECM (C) and decellularized whole meniscus ECM (D) hydrogels.

4.3.3 Compressive strengths of hydrogels

Compressive strengths of the decellularized meniscus ECM hydrogels were determined by an unconfined compressive test. The hydrogels were formed at varying concentrations from 6 to 12 mg/mL for the test. Notably, the OM-ECM hydrogels had significantly greater peak compressive strength (Figure 4.8) and initial moduli (Figure 4.9) than the MM-ECM and IM-ECM hydrogels.

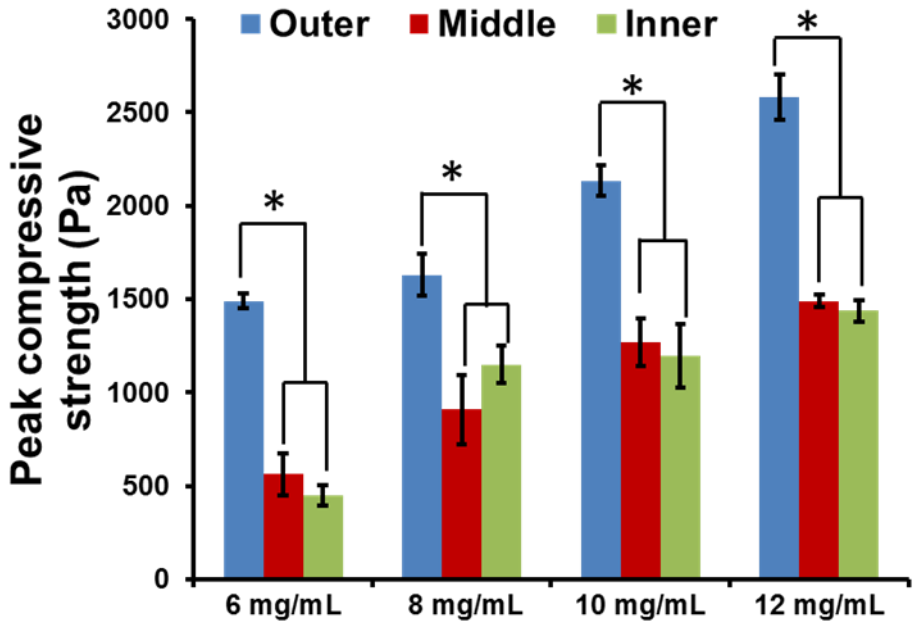

Figure 4. 8 Peak compressive strengths of the regionally decellularized meniscal ECM hydrogels.

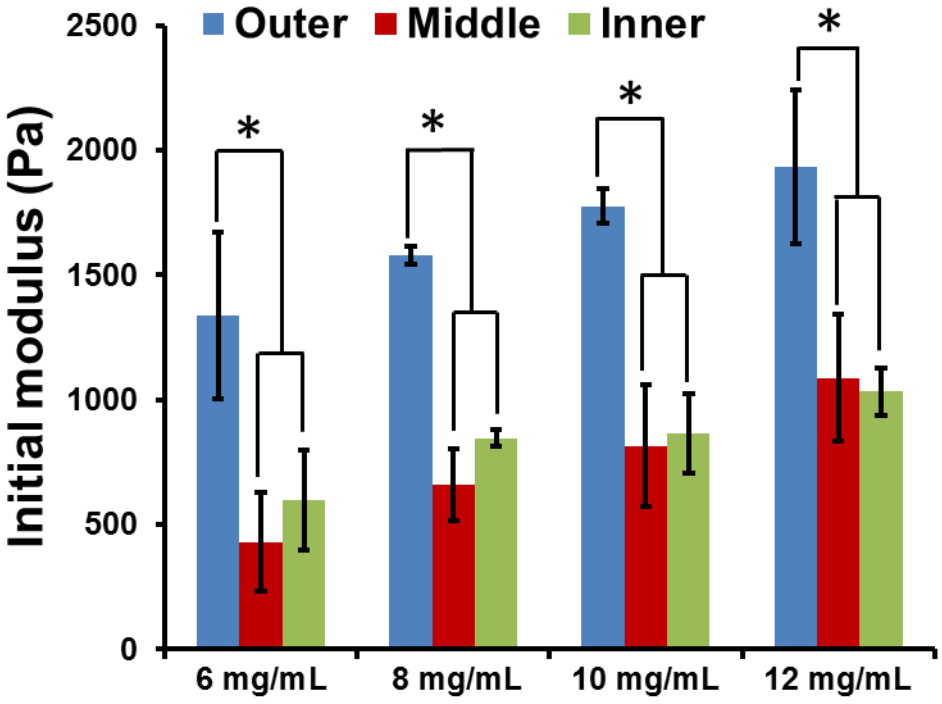

Figure 4. 9 Initial moduli of regionally decellularized meniscal ECM hydrogels.

4.3.4 3D cell growth and GAG accumulation

Cell viability and morphology of encapsulated fibrochondrocytes inside the ECM hydrogels was evaluated by a live/dead staining. Fibrochondrocytes showed a round morphology and homogeneously distributed within the hydrogel without cell aggregation at day 1 (Figure 4.10 A, B, and C). With the culture, fibrochondrocytes retained a predominately round morphology with a few spindle-shaped cells (indicated by white arrows) at day 14 (Figure 4.10 D, E, and F) and day 28 (Figure 4.10 G, H, and I). Encapsulated fibrochondrocytes experienced a high level of viability throughout the culture as most of the cells were live (green dots) and few dead cells (red dots) were observed. No significant difference in cell morphology or cell viability was found among the three cell-seeded hydrogels throughout the culture. These results were consistent with our previous report that bovine chondrocytes had a survival rate of 90% when cultured within meniscal ECM hydrogel [218].

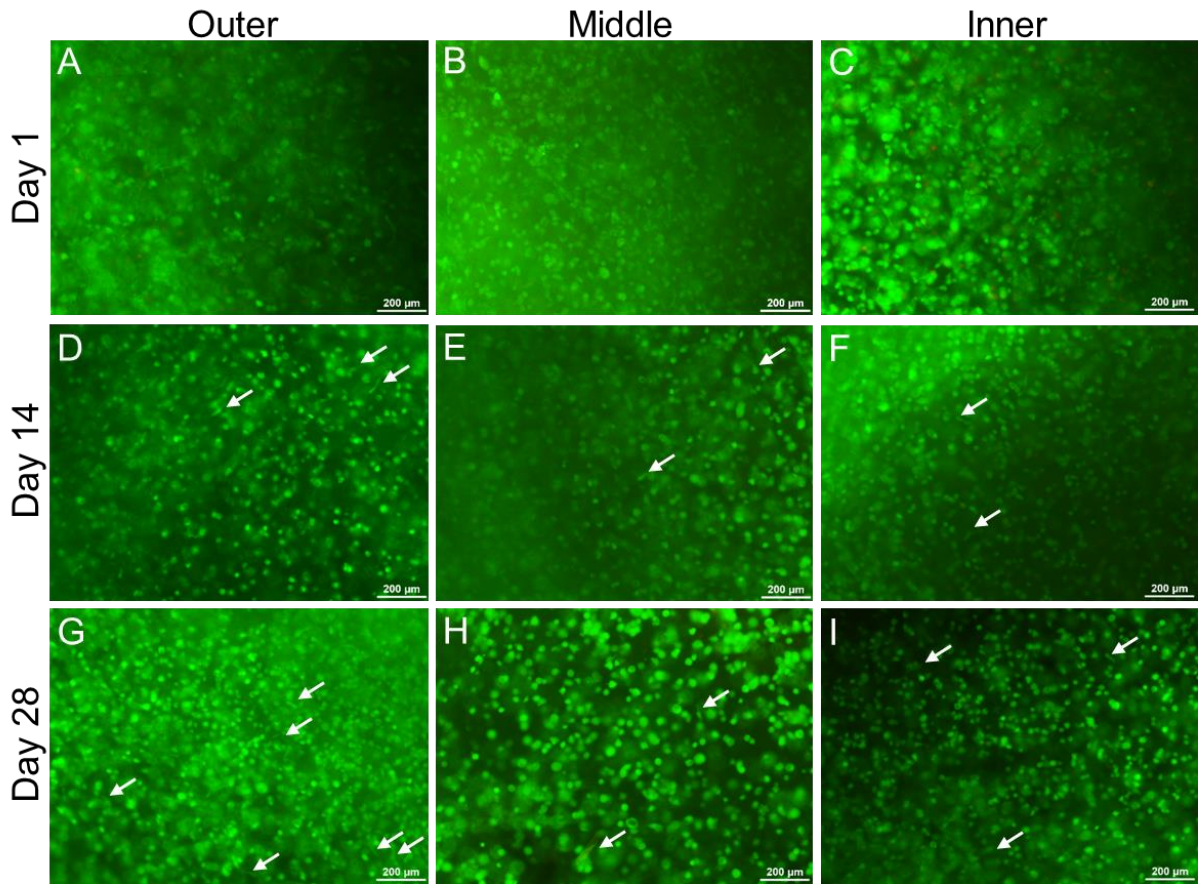

Figure 4. 10 Live/dead staining of fibrochondrocyte-encapsulated meniscal ECM hydrogels at day 1 (A-C), 14 (D-F), and 28 (G-I). White arrows indicate spindle-shaped cells.

The total DNA assay illustrated no significance among the three groups at each time point, indicating all the ECM hydrogels maintained their DNA contents throughout the entire culture period (Figure 4.11A). The largely retained total DNA contents at day 28 compared with that of day 1 indicated that fibrochondrocytes had a great viability inside the hydrogels, which was in line with the live/dead staining. In contrast to the stable levels of the DNA contents, all the ECM hydrogels greatly promoted GAG accumulations over the entire culture period of 28 days (Figure 4.11B). A 5-fold increase in GAG accumulation was found by 14 days compared with day 1, which

continued to increase over time. At day 28, the MM-ECM and IM-ECM hydrogels showed a 9-fold increase in GAG accumulation compared with day 1, which was significantly higher than that of the OM-ECM hydrogel. GAG accumulations of the MM-ECM and IM-ECM hydrogels calculated on the basis of per cell were also significantly greater compared with that of the OM-ECM hydrogel at 28 days (Figure 4.11C).

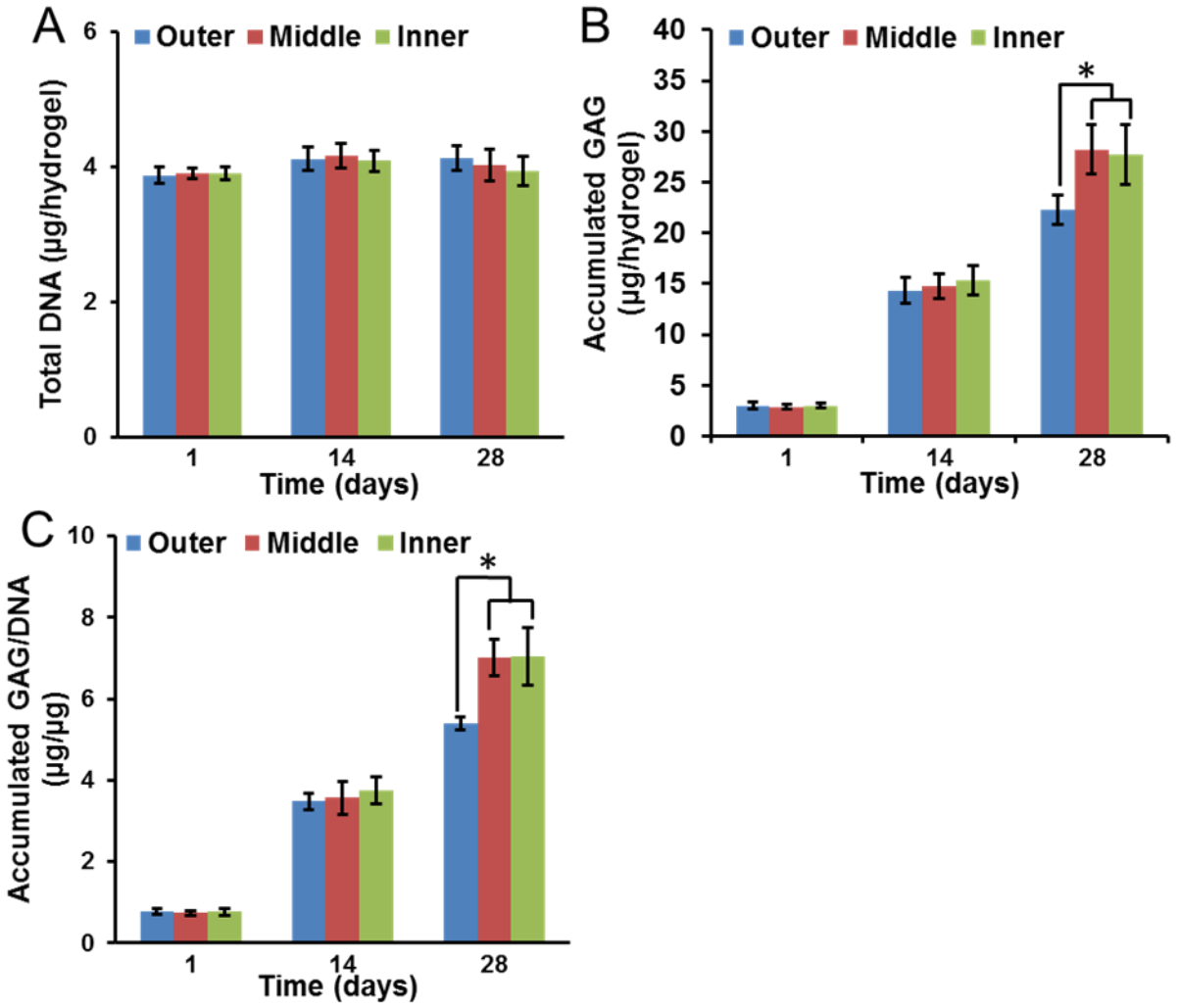

Figure 4. 11 Total DNA (A), accumulated GAG (B), and GAG/DNA ratio (C) of the fibrochondrocyte-encapsulated meniscal ECM hydrogels up to 28 days. * indicate $p < 0.05$.

4.3.5 Histological analysis

H&E staining provided straightforward cell morphology of the cell-seeded hydrogels (Figure 4.12). Fibrochondrocytes presented a predominately oval to round shape with a minor spindle shape at 28 days, which was consistent with the live/dead staining.

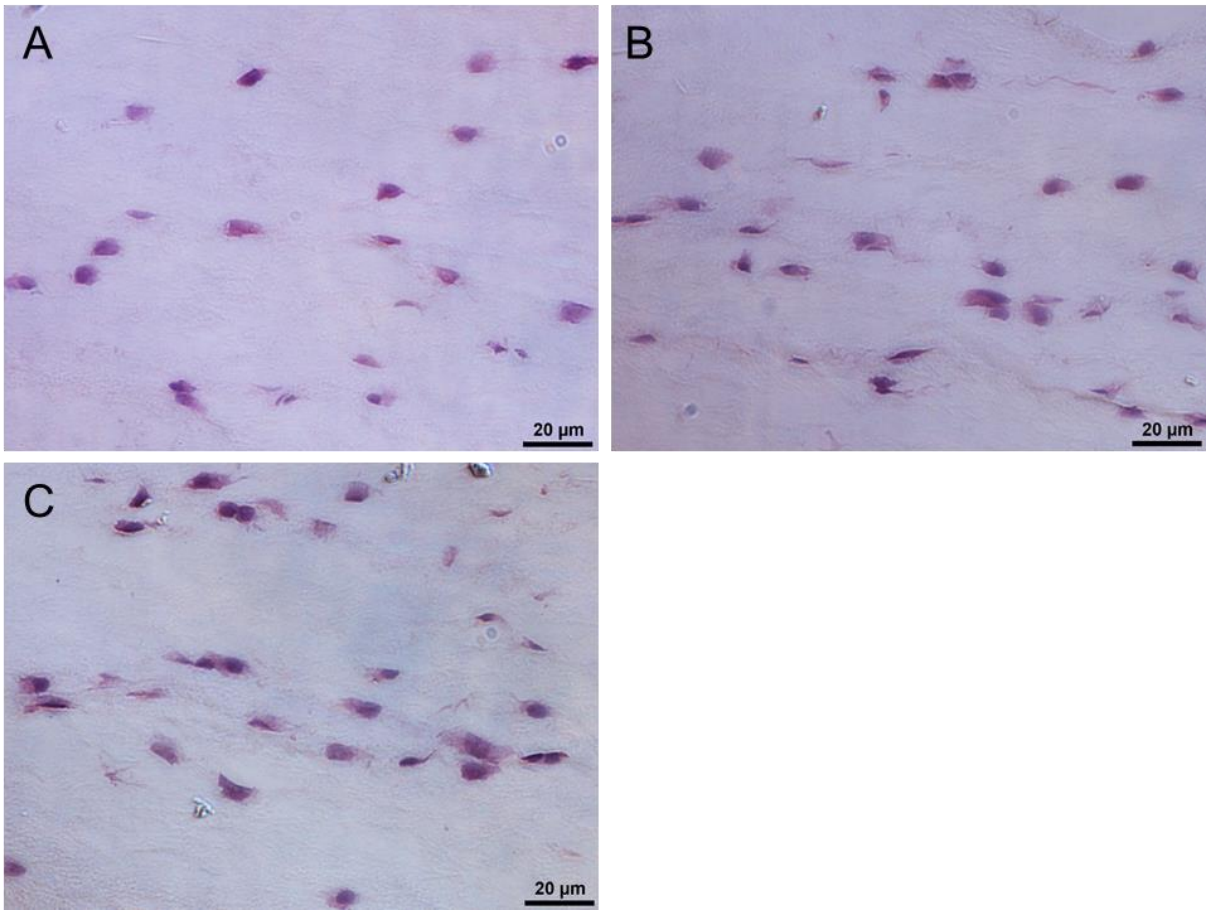

Figure 4. 12 H&E staining of fibrochondrocyte-encapsulated OM-ECM (A), MM-ECM (B), and IM-ECM (C) hydrogels at 28 days.

4.3.6 Contraction of cell-seeded hydrogels

Contraction behavior of cell-seeded collagen hydrogel in the change of surface area is proportional to the change of volume [92]. Therefore, we assessed the

contraction by measuring the surface areas of cell-seeded hydrogels and comparing with unseeded controls. Gross appearance demonstrated that the cell-seeded hydrogels maintained their overall round shapes throughout culture, while they continually contracted over time. The unseeded hydrogels did not show changes in the surface area throughout culture (data not shown). After 28 days, in comparison to the unseeded hydrogels, the cell-seeded OM-ECM hydrogel maintained 60.0 ± 10.0% surface area, while the cell-seeded MM-ECM and IM-ECM hydrogels experienced greater contraction extents of 27.5 ± 4.7% and 16.7 ± 6.7%, respectively (Figure 4.13A).

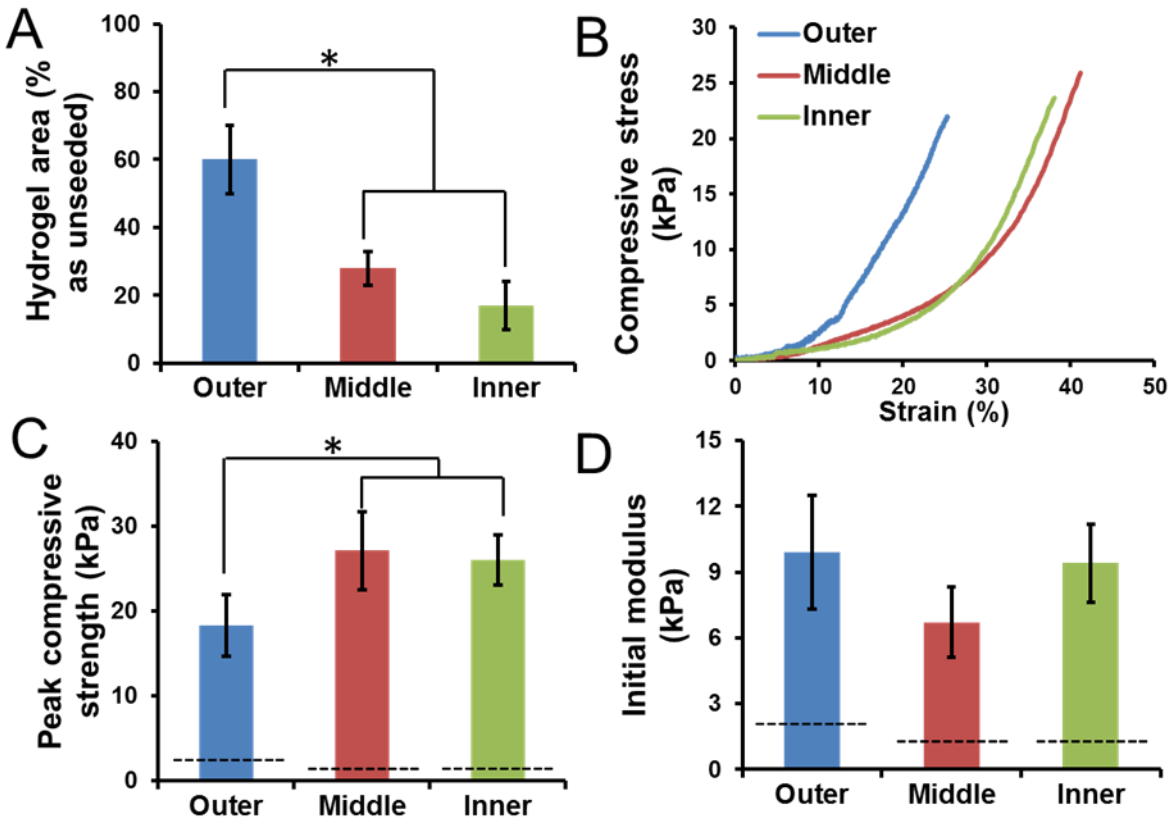

Figure 4. 13 Contraction (A), compressive curves (B), peak compressive strengths (C), and initial moduli (D) of the fibrochondrocyte-encapsulated meniscal ECM hydrogels at

28 days. Dash lines indicate the peak compressive strengths (C) and initial moduli (D) of the non-seeded hydrogels at day 0.

4.3.7 Biomechanics

The biomechanical properties of the fibrochondrocyte encapsulated ECM hydrogels were assessed to illustrate cell-matrix interactions. Although the unseeded hydrogels maintained their original shapes without contraction, they were too weak for compressive test after 28 days, properly due to *in vitro* degradation. Therefore, we compared the compressive strengths and initial moduli (denoted by dash lines across the histogram) of the cell-seeded hydrogels with their corresponding hydrogels at the same ECM concentration (10 mg/mL) without cell seeding (hydrogel only) (Figure 4.13). Biomechanical analysis illustrated that the cell-seeded hydrogels showed great increases in peak compressive stregnths (Figure 4.13C) and initial moduli (Figure 4.13D). Specifically, the cell-seeded OM-ECM hydrogel had a 9-fold increase in peak compressive strengths (18.3 ± 3.6 vs. 2.1 ± 0.1 kPa) and a 6-fold increase in initial modulus (9.9 ± 2.6 vs. 1.7 ± 0.2 kPa) compared to the OM-ECM hydrogel only. The cell-seeded MM-ECM and IM-ECM hydrogels had greater peak compressive strengths than the cell-seeded MM-ECM hydrogel, while the three cell-seeded hydrogels showed comparable initial moduli at 28 days. In comparison to the MM-ECM hydrogel only, the cell-seeded MM-ECM hydrogel experienced a 21-fold increase in peak compressive strengths (27.1 ± 4.6 vs. 1.3 ± 0.1 kPa) and a 9-fold increase in initial modulus (6.7 ± 1.6 vs. 0.8 ± 0.1 kPa). Similarly, the cell-seeded IM-ECM hydrogel achieved a 22-fold

increase in peak compressive strengths (26.0 ± 3.0 vs. 1.2 ± 0.2 kPa) and a 9-fold increase in initial modulus (9.4 ± 1.8 vs. 0.9 ± 0.2 kPa) over the IM-ECM hydrogel only.

4.4 Discussion

We have demonstrated that the major meniscal component, collagen, was enriched but GAGs were significantly depletive in DM-ECM treated with SDS in Chapter 2 [218]. Furthermore, we optimized the decellularization process by comparing the SDS with PAA to yield the DM-ECM with a significantly improved GAG retention and proved that the optimal DM-ECM hydrogel was superior for meniscal repair and regeneration in Chapter 3. In the current study, we use the optimal decellularization method to prepare three meniscal ECM hydrogels from different regions of the porcine meniscus and separately encapsulate them with bovine fibrochondrocytes to investigate the effects of regional meniscal ECMs on the cell behaviors and cell-matrix interactions.

Safety issue should be regarded as the essential consideration for the decellularized ECM materials in clinical applications. Of all the potential sources that could induce immune responses, the cellular DNA was primarily implicated as the cause of inflammatory reactions and host responses [170, 239]. Badylak *et al* summarized the current preclinical studies of biological ECM devices and proposed criteria suffice of residual DNA in ECM materials that acceptable for clinical use: less than 50 ng DNA per mg dry ECM and absent of visible nuclear materials in DAPI or H&E staining [68]. Based on this rule, our PAA was found to be highly effective for

regional meniscal tissue decellularization as regional DM-ECMs retained had DNA contents less than 0.11 ng/mg in dry weight.

In addition to the high efficiency of DNA removal, the PAA treatment was elucidated to be mild for meniscus decellularization with minimal disruption to the ECM structure and high retentions of the biological components. SDS-PAGE analysis demonstrated that, besides collagen, the regional DM-ECMs contained multiple lower weight molecules. This finding indicates the compositional complex of the DM-ECMs, which could play critical roles in cellular behaviors and tissue regeneration. In consistent with a previous study [87], we found the PAA treatment had no side effect on collagen retention. In addition, the resulting OM-ECM and MM-ECM had slightly reduced GAG contents compared to their corresponding native tissue zones, indicating the PAA treatment did pose minor adverse effect on GAG during the decellularization process. However, we found enriched GAG in the IM-ECM after decellularization. The enriched GAG might be associated with the high type II collagen content in the inner zone, as GAG is chemically crosslinked with type II collagen, which contributes to the great elasticity of the native inner meniscal zone [15, 111]. The binding of GAG to type II collagen fibers might prevent GAG from being washed out during decellularization. Meanwhile, some non-collagen proteins were removed in the PAA treatment. Taken together, the PAA treatment yields an enriched GAG in the IM-ECM.

The inner meniscus has higher GAG and type II collagen over the outer meniscus, which emprises the inner meniscus great compressive strength that functions in resisting the compression in the knee joint. Therefore, it is expected that the IM-ECM hydrogel could have greater compressive strength than the OM-ECM hydrogel.

However, the mechanical analysis illustrates that the IM-ECM hydrogel has a much lower compressive strength than the OM-ECM hydrogel. For decellularized meniscus ECM, the major component that self-assemblies into fibers is collagen [218]. At the physiological condition, type I collagen is easier to form hydrogels over the type II collagen. Moreover, type II collagen mainly self-assembles into short fibers and forms hydrogels with less stability compared to type I collagen hydrogel [240]. Thus, it is reasonable that the OM-ECM hydrogel is much stronger than MM-ECM and IM-ECM hydrogels, as OM-ECM contains the highest type I collagen contents among these decellularized meniscal ECMs.

Various injectable hydrogels have emerged for regenerative medicine application [241]. Common features of injectable hydrogels including the capability of filling irregularly shaped defects, forming solid gels *in situ,* and homogeneously encapsulating cells within the scaffolds. Previously, we reported a decellularized meniscus ECM hydrogel that was capable of *in situ* gel formation involved no chemical crosslinking agents, both *in vitro* and *in vivo* [218]. Cells are readily mixed with the pregel solutions and evenly distributed inside the hydrogels without aggregation over 28 days. Together with the thermosensitive nature of decellularized ECM hydrogels, it provides an administration of biological materials and cells in a minimally-invasive manner.

Potential advantages of decellularized ECM hydrogels for therapeutic applications include their great cytocompatibility and biocompatibility as they are composed of naturally-derived molecules such as collagen, GAG, and elastin [242]. Investigations with decellularized ECM hydrogels have demonstrated that the

decellularized ECM materials are noncytotoxic to cells, and are comparable or better in supporting cell proliferation and maintaining cell viability *in vitro* and *in vivo* when compared to type I collagen hydrogel [152, 160, 218, 243]. Decellularized liver ECM hydrogel supported significantly greater viability of hepatocytes in 3D culture for 7 days compared to the type I collagen hydrogel [74]. Human mesenchymal stem cells encapsulated within decellularized lung ECM hydrogels remained equal or higher survival rates than type I collagen hydrogel. We have illustrated that the decellularized meniscal ECM hydrogel was cytocompatible to NIH 3T3 cells and bovine chondrocytes for 7 days *in vitro*, and revoked a minor immune response when subcutaneously injected in mice [218]. In this study, we showed that the regionally decellularized meniscal ECM hydrogels maintained great cell viability of bovine fibrochondrocytes up to 28 days. The fibrochondrocytes encapsulated inside the regional meniscal ECM hydrogels maintained their total cellular DNA without significantly change up to 28 days, this is in accord with a previous report that fibrochondrocytes retained total DNA when encapsulated in type I collagen hydrogels during a 28-day culture period [92]. These results indicate that the regional meniscal ECM hydrogels were equally cytocompatible regardless of the compositional variations.

In addition to the great biocompatibility, decellularized ECM materials hold complex tissue-specific bioactive molecules occurring from constitutive matrices, which are indispensable components of functional tissues and provide a driving force to influence cell behaviors [243]. Many studies have shown that decellularized ECM materials, either used as the bulk scaffolds or processed into injectable hydrogels, promote primary cell function and enhance targeted differentiation of stem cells [74,

162, 225]. Fibrochondrocytes are a class of cells that are oval to round in shape and mainly reside in the avascular zone of inner meniscus [244]. They function to produces collagen and GAG to form crosslinked matrix to provide compressive strength. Our results showed that fibrochondrocytes predominately exhibited a round morphology inside hydrogels throughout the culture, implying that the regional meniscal ECM hydrogels might be beneficial in maintaining the fibrochondrogenesis phenotype of the cells.

Accumulation of GAG is critical for regenerated meniscal tissues executing their protective effects in the knee joint. Compared to 2D culture, the 3D culture of fibrochondrocytes within scaffolds is advantageous for GAG accumulation [244]. Scaffolding materials of hydrogels also affect GAG accumulation. For example, when seeded with fibrochondrocytes, collagen hydrogels preserved more GAG than alginate hydrogels [92]. Progressive increase of GAG was found within the cell-seeded hydrogels over time, and the IM-ECM and MM-ECM hydrogels accumulated significantly greater amounts of GAG than the OM-ECM hydrogel at 28 days. The enhanced GAG accumulation of the IM-ECM and MM-ECM hydrogels over the OM-ECM hydrogels were also found on a per cell basis. Probably, the varying capability of accumulating GAG is associated with the different types of collagens in the regional meniscal ECMs, as outer meniscal tissue mainly makes up of type I collagen, while the middle and inner meniscal tissues contain both type I and type II collagens. As discussed above, GAG is prone to react with type II collagen to form crosslinked matrix, which prevents GAG from diffusing and losing in the hydrogel. While in the OM-ECM hydrogel, GAG appears to have less binding with the matrix and easily lost. Equally

plausible, the difference of GAG accumulation might result from the cell-matrix interactions between the fibrochondrocytes with specific ECM molecules that are variable in amount and/or in presence of the regional meniscal ECMs.

Contraction is the nature of cell-seeded collagen hydrogels and promotes maturation of cell-seeded constructs and enhances wound healing [245-247]. Similar to the collagen hydrogel, regionally decellularized meniscal ECM hydrogels went through significant contractions with decrease in size over time (Figure 4.13A). Reduction in volume yields to the increase in the effective concentrations of GAG and collagen and increases the matrix density, of the cell-seeded regional meniscal ECM hydrogels. Additionally, the contraction indicates the cell-mediated traction is occurring in the hydrogels [247]. The IM-ECM hydrogel contracted to the greatest extent as it contained the highest content of type II collagen that mainly assembles into short fibers.

Cell-matrix interactions and cell-secreted matrix spontaneously affect the biomechanical properties of cell-seeded hydrogels [247]. The cell-seeded hydrogels showed great increases in peak compressive strengths and initial moduli compared to the corresponding hydrogel only control (Figure 4.13 B and C). It is worthy of noting that the GAG accumulation might greatly contribute to the improved mechanical strength. GAG covalently reacts with collagen fibers to improve the density of crosslinking of the matrix. As a result, it substantially increases the mechanical strength and integrity of the cell-seeded hydrogels. In comparison, without the cell-produced GAG, the unseeded hydrogels became extremely weak at 28 days. Enhancement in mechanical strengths could partially result from the contraction, as it gives to a great increase in the matrix density of the cell-seeded hydrogels. Moreover, the cell-

mediated traction may also help to increase the biomechanics of the cell-seeded hydrogels.

While the 3D culture of fibrochondrocytes can achieve significantly greater mechanical properties, the cell-seeded regionally decellularized meniscal ECM hydrogels did not yet achieve that of the native meniscus. Several limitations need to be addressed in the future study. Determination of the fibrochondrogenesis gene expressions and meniscus specific proteins will be performed to identify the phenotype of the encapsulated cells after the long-term culture. Although the fibrochondrocyte-encapsulated hydrogels attained great increases in compressive strength (about 10 ~ 30 kPa) and modulus (about 1 ~ 2 kPa) after 28 day culture, it is much lower than that of the native meniscus (100 ~ 400 kPa in compressive modulus) [248, 249]. Improving the mechanical strength of meniscus ECM hydrogels via chemical crosslinking might be a possible solution to address this problem [225, 250]. Collagen Type I present distinctive fiber length and mechanical properties compared with collagen type II at the physiological condition. Qualitative and quantitative determinations of the type and content of collagen in regionally decellularized meniscal ECMs would be helpful to illustrate the structure-property relationship of the ECM hydrogels. Such collagen determinations will also be applied to the cell-seeded ECM hydrogels to demonstrate the cell-matrix interaction and the biomechanics. Contraction could be either reduced by increasing the ECM concentrations of the hydrogels or be prevented by incorporating the ECM hydrogels with photo-crosslinked hydrogels such as gelatin methacrylamide and polyethylene glycol diacrylate [92, 129, 231]. Also, the introduction of photo-crosslinked hydrogels could greatly improve the mechanical properties of the

ECM hydrogels. Although the regionally decellularized meniscal ECMs might retain some endogenous growth factors, exogenous growth factors could be introduced into the hydrogels to foster cell proliferation and matrix accumulation [251].

4.5 Summary

In this study, we regionally divided porcine meniscus into three zones and decellularized them based on the PAA-treatment. The regionally specific meniscus ECMs were distinct in collagen and GAG contents. These biochemical variations are associated with the varying compressive strengths of the ECM hydrogels. In addition, the biochemical variations have great influence on cell-matrix interactions, ultimately affecting GAG accumulation, contraction, and the biomechanical strengths of the cell-seeded hydrogels. Our *proof-in-concept* investigation shows the feasibility of utilizing region-specific meniscus ECM hydrogels and their potential in meniscus repair and regeneration.

CHAPTER 5

CONCLUSION AND FUTURE WORK

5.1 Conclusions

The meniscus plays critical roles in the maintenance and protection of knee joints. Damage and functional loss of meniscus are intimately associated with knee joint diseases. The current meniscus repair techniques merely effective in treating the damages in the outer vascularized zone of the meniscus. To date, the most popular surgical intervene in treating the inner meniscus lesions is partial meniscectomy, while this technique is not perfect. Post-surgery complications such as cartilage damage and OA frequently occur and significantly reduce the patients' life quality.

In this thesis, we seek to develop naturally derived biomaterials, decellularized meniscus ECMs, and process them into engineered scaffolds for meniscus tissue engineering. Four specific aims, including 1) development of injectable meniscus ECM hydrogel, 2) optimization of the meniscus ECM hydrogel and 3) preparation and comparison of regionally decellularized ECM hydrogels, were performed accordingly from Chapter 2 to 4.

In Chapter 2, a decellularized meniscus ECM was prepared through SDS-based decellularization process and it was processed into an injectable hydrogel. Previous studies mainly focused on the development of decellularized meniscus ECMs and used them as solid scaffolds [79-82, 84-86, 88-91]. These studies demonstrate the decellularized ECMs are biocompatible and bioactive and hold great potential for meniscus replacement. A significant problem of the solid scaffolds of those

decellularized ECMs is the poor cell infiltration that is associated with their dense structure. In addition, a precise size match of the solid scaffold to the meniscus defect is difficult to achieve, and the use of decellularized ECM in the solid form is not compatible with minimally-invasive surgery. In our study, we turned to a smart use of the decellularized meniscus ECM in an injectable form. We found SDS treatment was effective in DNA removal and had a negligible effect on collagen, while it caused great GAG loss. When solubilized by pepsin digestion and NaOH neutralization, the ECM preparation was capable of being injected through a 21-gauge needle and forming solidified hydrogels within 30 min in a 37 ^{o}C incubator or in mouse through subcutaneous injection. The decellularized meniscus ECM hydrogel had a nanofibrous structure with tunable mechanical properties by altering the ECM concentrations. *In vitro* and *in vivo* results indicated the hydrogels was highly biocompatible and supported intensive cell infiltration. In summary, the injectable ECM hydrogel is advantageous in filling meniscus defect via minimally-invasive injection and promoting cell infiltration compared to decellularized solid ECM scaffold.

In Chapter 3, we continued the work of developing injectable meniscus ECM hydrogel based on the findings of Chapter 2, where we found a huge loss of GAG content in the decellularized meniscus ECM. Methodologically, many approaches have been developed for the optimization of tissue/organ decellularization [206-208, 211, 252-254]. We selected three commonly used chemical detergents and compared their efficacies for meniscus decellularization. Our results showed that, despite comparable DNA removal and a similar level of collagen after decellularization, PAA was the most efficient in meniscus decellularization as it yielded the greatest GAG retention

compared to the SDS and TX treatments. The greater GAG content contributed to the significantly higher mechanical strength of the PAA-ECM hydrogel. When encapsulated with bovine meniscus fibrochondrocytes and cultured for 28 days, the PAA hydrogel exhibited much greater compressive strength associated with its higher GAG accumulation. Therefore, we demonstrated an optimal protocol of decellularized meniscus ECM hydrogel preparation.

In Chapter 4, we investigated the regional variation of the meniscus by dividing it into distinct zones and decellularizing them separately via the PAA-based protocol. The cellular and compositional variations of the meniscus have long been noted in the literature [12, 15, 19, 113, 255-258]. Those cellular and compositional variations interact with each other and result in the anisotropic characteristic of the meniscus tissue [11, 259, 260]. We hypothesized that the compositional variations still exist after decellularization and they would influence cell behaviors. We observed the various GAG and collagen contents in the regionally decellularized ECMs. We found the OM-ECM hydrogel had significantly great compressive strength compared with the MM-ECM and IM-ECM hydrogels. We speculated the various compressive strength of hydrogels were due to the distinct collagen types and contents. In summary, we demonstrated the compositional variations of meniscus ECMs after regional decellularization. However, this study is not completed. We are working on the biological performance of those hydrogels by combining them with bovine meniscus cells.

5.3 Preliminary data of future direction

5.3.1 Introduction

Naturally derived ECM materials prepared by decellularization are highly desirable and commonly used to facilitate tissue remodeling and reconstruction in preclinical studies and clinical applications [261]. The ECM materials not only preserve the three-dimensional architectures of native tissues but also harbor multiple bioactive components such as proteins, proteoglycans, elastin, and growth factors [68, 201]. Therefore, these biological materials are capable of modulating a variety of cellular activities including proliferation, migration, gene expression, and differentiation, as well as promoting tissue-specific cell self-assembling to reconstruct tissues and organs [262]. However, the decellularized ECM materials had inherent geometries and intrinsic mechanical properties, which made it tough to process them into scaffolds with appropriate flexibilities and comparable mechanical properties that ideally reassemble the native tissues [263]. In addition to the poor processability, material properties including size, degradation rate and physical shape defined by tissue resource and decellularization processes, could further limit the clinical potential of ECM materials [53, 262, 263].

In contrast to ECM materials, synthetic materials are superior in mechanical properties and more accommodating to various processing methods to produce scaffolds with well-defined microstructures similar to native tissues [263]. Scaffolds prepared from synthetic materials are distinctively characterized in uniform and reproducible mechanical properties, adjustable degradation profiles and controllable sizes and shapes specializing for certain tissues [71]. However, synthetic materials

intrinsically lack the bioactive components and immune modulation capability of ECM materials and were frequently found to elicit severe immune responses and form fibrous encapsulations post implantation [71, 264]. Therefore, to create a biomaterial for a specific tissue, numerical efforts have been addressed in introducing biological cues into synthetic materials to achieve improved bioactivity while maintaining excellent control over the material properties [264-267].

Compromised meniscus function caused by injury and degenerative diseases often results in subsequent complications such as osteoarthritis (OA), which significantly reduce the life quality of patients. Unfortunately, due to the poorly vascular nature, meniscus repair and regeneration still poses a huge obstacle in clinics. Tissue engineering provides an emerging alternative to produce scaffolds conforming biological and mechanical properties of native menisci which could be combined with appropriate cells for meniscus regeneration [28]. A typical routine of meniscal tissue engineering is to partially or entirely replace the injured menisci with synthetic or natural material scaffolds, including collagen sponges, porous foams, polymeric meshes and decellularized ECMs [62]. Although considerable achievements have gained in the existing studies, for example, decellularized meniscal ECM (DM-ECM) scaffold exhibited a chondroprotective effect in a rat model [80], efforts need to thrive and progress further [4]. Electrospinning represents one of the most promising approaches of scaffold preparations and has been elaborative utilized by Mauck colleague to fabricate meniscal scaffolds [29]. Electrospun scaffolds are composed of nanofibers that mimic native meniscal collagen bundles in dimension, which could be easily manipulated to reassemble native meniscal ECM [4]. In addition, adding of biological

cues into synthetic materials would further strengthen electrospun scaffolds with improved performance for meniscal tissue regeneration.

In the present work, we aimed to develop a DM-ECM incorporated nanofibrous scaffold that combines the versatility of synthetic materials and the meniscal tissue-specific components. The DM-ECM was enzymatically digested and lyophilized to allow a completely homogenized DM-ECM/PCL solution for electrospinning. The morphology, wettability, chemical components and mechanical properties of the electrospun scaffold was characterized. The biological performance was evaluated by assessing the cell proliferation and morphology, as well as ECM accumulation of the bovine meniscal fibrochondrocytes on the scaffolds.

5.3.2 Experimental section

5.3.2.1 Materials

PAA, EDTA, HCl, pepsin, PCL, 1,1,1,3,3,3-hexafluoro-2-propanol (HFIP), high glucose DMEM, FBS, and 1,9-dimethyl methylene blue (DMMB) were purchased from Sigma. PSF, rhodamine-conjugated phalloidin and DAPI were supplied by Life Technologies, Inc.

5.3.2.2 Preparation of digested DM-ECM

Porcine DM-ECM was prepared following our previous protocol as Chapter 3. Specifically, menisci were freshly harvested from knee joints of adult pigs (weighing 80 -100 kg) from a local slaughterhouse and snap frozen at -80 ^{o}C. The frozen menisci were sliced into thin pieces, pulverized to coarse particles and then treated with 0.1%

PAA/4% ethanol solution for three days (Figure 5.1). The PAA/ethanol solution was refreshed every 24 h. Subsequently, the meniscal particles were agitated in 0.1% EDTA, thoroughly washed deionized (DI) water and lyophilized to obtain DM-ECM. The DM-ECM was enzymatically digested to yield a uniform solution as ref [218]. Briefly, DM-ECM was agitated in pepsin/0.01 M HCl at the ECM concentration of 15 mg/mL with the DM-ECM/pepsin ratio of 10/1 for 48 h to allow complete digestion. The digest was neutralized with NaOH and then frozen and lyophilized to obtain DM-ECM.

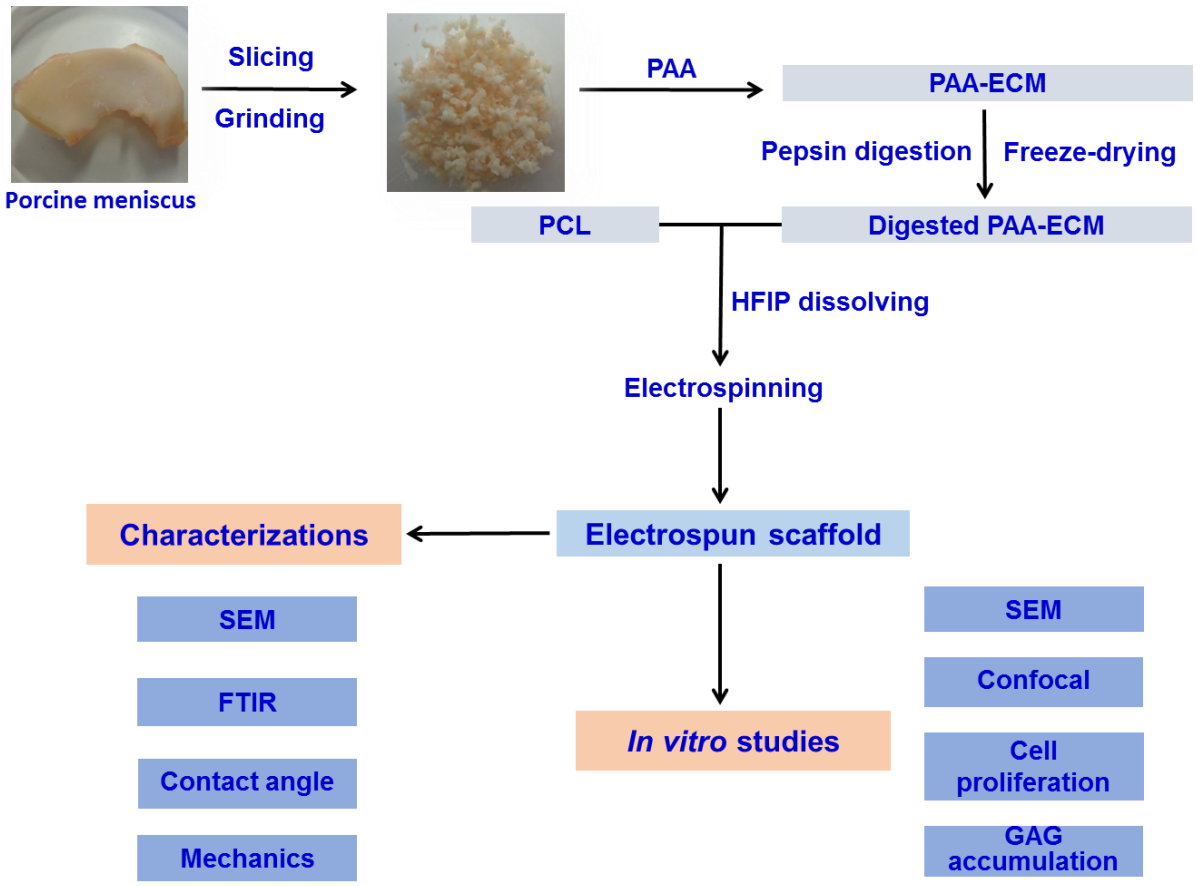

Figure 5. 1 Schematic of the experimental design.

5.3.2.3 Electrospinning of PCL/ECM

The digested meniscal ECM was blended with PCL, at serial PCL/ECM weight ratios of 95/5, 90/10, and 85/15, and dissolved in HFIP at a concentration of 10% (w/v) (Figure 5.2). The blended solution was electrospun at 1.0 mL/h through an 18 G blunt needle with an applied positive charge of 15 kV. The electrospun nanofibers were collected with a negatively charged (-5kV) solid plate at a distance of 20 cm. The resulting nanofibrous sheets with PCL/ECM ratios of 95/5, 90/10, and 85/15 were referred as PCL/ECM-95/5, PCL/ECM-90/10, and PCL/ECM-85/15, respectively. Pure PCL solution (10%w/v) was electrospun under the aforementioned conditions and the obtained PCL scaffold was used as a control.

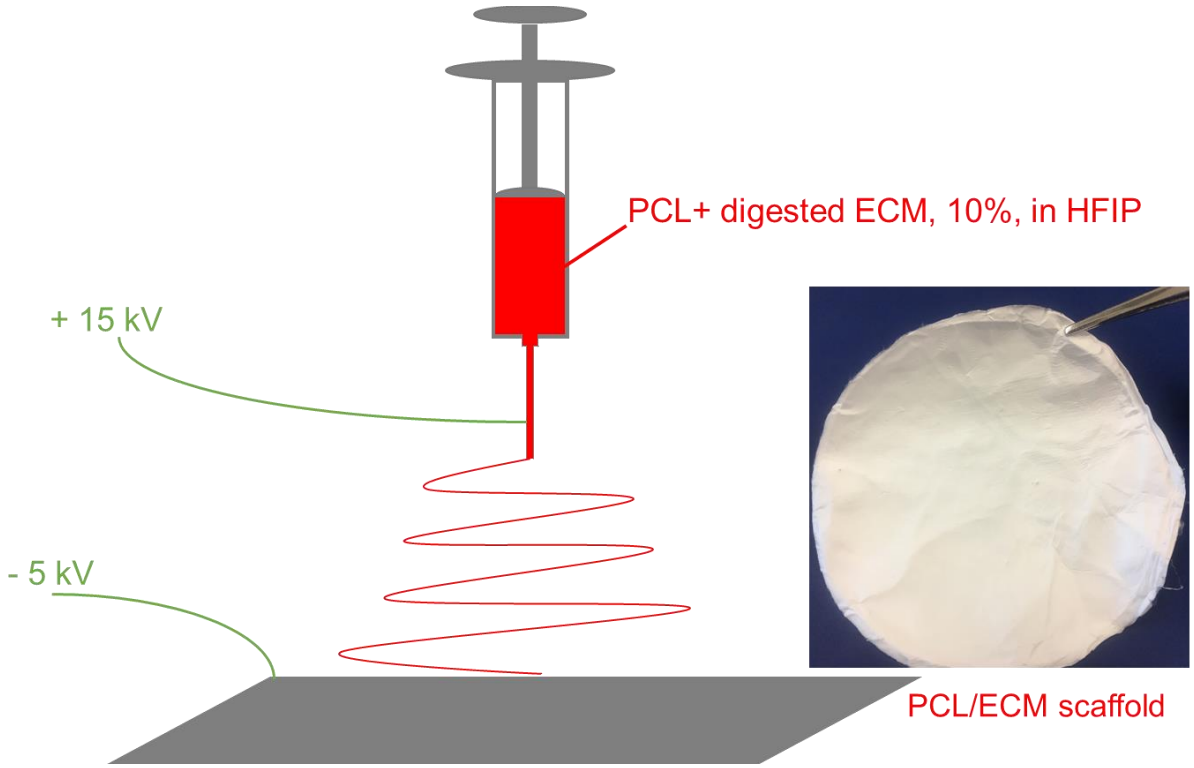

Figure 5. 2 Electrospinning setup (left) of PCL/ECM and a white sheet of the electrospun PCL/ECM scaffold (right).

5.3.2.4 Scaffold characterizations

The surface morphology of the nanofibrous scaffolds was observed using a scanning electron microscope (SEM, S-3000 N, Hitachi). The scaffolds were mounted on conductive tape and sputter coated with silver, and then visualized under SEM at an accelerating voltage of 10 kV. The average fiber diameter was determined by ImageJ software (National Institute of Health, USA). Briefly, one hundred nanofibers of each scaffold were randomly selected and measured from the SEM images to assess the average diameter (n = 3).

Chemical analysis of the DM-ECM powder, PCL and PCL/ECM-90/10 scaffolds were performed by Fourier transform infrared attenuated total reflectance spectroscopy (FTIR-ATR, Nicolet 6700, Thermo Nicolet Corp. Madison, WI) over the range of 2000-800 cm^{-1} at a resolution of 4 cm^{-1}.

To determine the wettability, the contact angles of the scaffolds were assessed using a contact angle measuring system CAM 101 (KSV Instruments). The test was conducted with DI water as the reference and the droplet size was set at 5 µL and read at 5 seconds (n =3). The results were reported as average values with standard deviations.

The nanofibrous scaffolds were cut into 2 × 25 mm strips for uniaxial tensile testing on an MTS Insight machine (MTS, Eden Prairie, MN) with a 500 N load cell at a crosshead speed of 1cm/min. The test was terminated until failure. Four samples of each scaffold were tested (n=5).

5.3.2.5 Cell isolation and seeding

Bovine meniscal fibrochondrocytes were isolated as Ref [125]. Briefly, the knee joint menisci of skeleton maturely calves were obtained from a local abattoir within 24 h of slaughter. The menisci were separated into two zones, the outer 2/3 zone was discarded and the inner 1/3 zone was diced into 1-2 mm^3 particles under sterile condition. The meniscal particles were incubated with 0.2% collagenase type II in high glucose DMEM supplemented with 1% PSF in a 37 ^oC incubator overnight. The digested cell suspension was filtered through a 70-μm cell strainer, washed with PBS, centrifuged at 1500 rpm for 10 min. The cells were seeded in DMEM supplemented with 10% FBS and 1% PSF in 25 cm^2 flasks placed in a 37 ^oC incubator with 5% CO_2 and 95% humidity. The medium was changed three days thereafter for the first refreshment and every two days in the following culture.

The pure PCL and PCL/ECM-90/10 nanofibrous meshes were punched into 15 mm dish scaffolds to fit 24-well plate for cell culture. The scaffolds were disinfected with 70% ethanol for 30 min and thoroughly rinsed with PBS for 5 times prior to cell seeding. Each scaffold was seeded with 1.0×10^4 fibrochondrocytes and maintained in DMEM with 10% FBS and 1% PSF in an incubator with 5% CO_2 and 95% humidity at 37 ^oC up to 14 days. The medium was refreshed every two days.

5.3.2.6 Cell morphology

The morphology of fibrochondrocytes was observed with SEM and confocal laser microscopy image. At pre-determined time points of 1, 7, and 14 days, the samples were harvested, fixed with 4% paraformaldehyde. For SEM, the fixed samples were

dehydrated with gradient ethanol followed by air drying overnight at room temperature. The dried samples were then sputter coated with silver and observed using SEM. For confocal imaging, the fixed samples with permeabilized with 0.1% Triton X-100 (Sigma), rinsed with PBS, and then incubated with DAPI and rhodamine-conjugated phalloidin to stain the nuclei and cell actin filaments into blue and red, respectively. The stained samples were then visualized by a confocal laser scanning microscope (LSM 780, Carl Zeiss).

5.3.2.7 Cell proliferation and GAG accumulation

The cell proliferation was determined by measuring the DNA content using the PicoGreen DNA assay (Life Technologies, Inc.). The samples collected at each time point were stored at -80 ^{o}C. Upon the assays, the frozen samples were thawed, lyophilized and digested with papain (buffered in the solution containing 0.1 M of sodium acetate, 10 mM of cysteine-HCl, and 2.4 mM EDTA, pH 6.8) at 60 ^{o}C for 1 h. Then the DNA and GAG contents were assessed by PicoGreen DNA assay and DMMB test, respectively [218]. Alcian blue staining was performed at day 1, 7, and 14 as Ref [268].

5.3.2.8 Statistical analysis

Data were expressed as means ± standard deviations. Significant differences were assessed by one-way ANOVA followed by a Tukey post hoc test. Significant difference was considered at $p < 0.05$.

5.3.3 Results

5.3.3.1 Electrospun scaffolds

After digestion and lyophilization, the DM-ECM was easily homogenized with PCL by dissolving in HFIP and formed a uniform solution (data not shown), which was then electrospun to nanofibrous scaffolds. The morphology of the scaffolds was observed using SEM and the average fiber diameter was determined by measuring the fiber diameter from the SEM images. Grossly, the SEM images demonstrated the fibrous nature of the electrospun scaffolds without bead formation (Figure 5.3). Compared to the electrospun PCL scaffold with an average diameter of 696 ± 136 nm (Figure 5.3A), the PCL/ECM scaffolds had significantly reduced average fiber diameters (422 ± 806 nm for 5/95, 507 ± 102 nm for 10/90 and 551 ± 76 nm for 15/85 (Figure 5.3B-D).

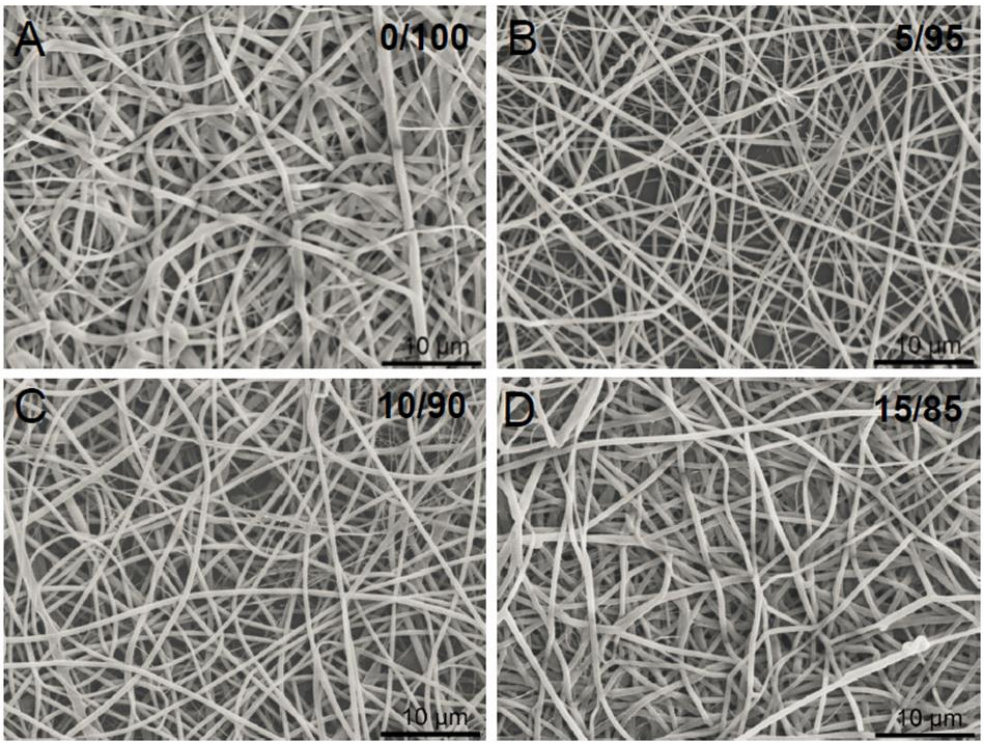

Figure 5. 3 SEM images of the electrospun scaffolds with varying PCL/ECM ratios at 100/0 (A), 95/5 (B), 90/10 (C), and 85/15 (D).

FTIR spectra were shown in Fig. 5.4 to demonstration the addition of DM-ECM components into the scaffold. The PCL and PCL/ECM-90/10 scaffold had a strong peak at 1722 cm^{-1}, which is attributed to C=O stretching. The DM-ECM powder showed two characteristic peaks at 1638 cm^{-1} and 1545 cm^{-1}, which were attributed to amide I and II [269], respectively. Although the amide I and II peaks were slightly shifted, they were observed in the PCL/ECM-90/10 scaffold spectrum, indicating that the DM-ECM was well introduced into the scaffold.

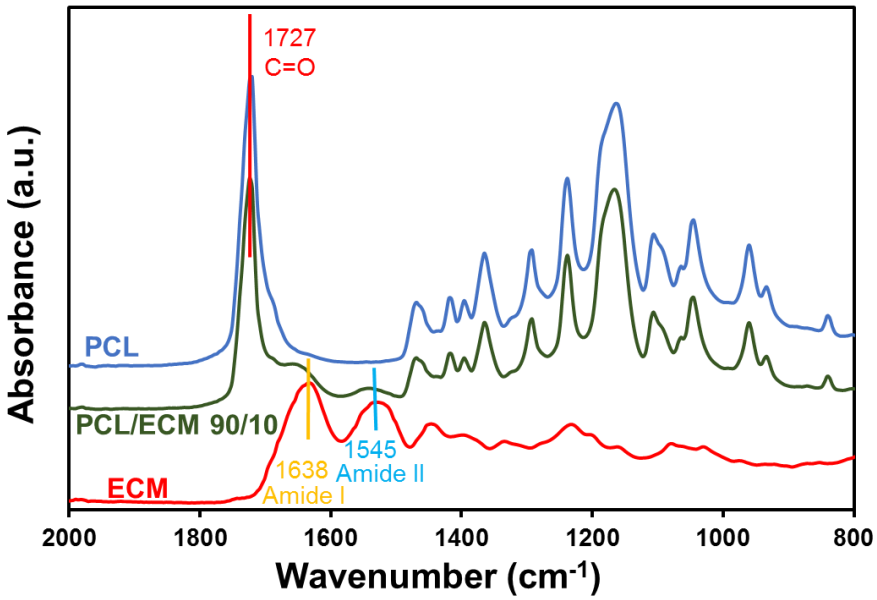

Figure 5. 4 FTIR spectra of the PCL and PCL/ECM-90/10 scaffolds, and DM-ECM.

Figure 5.5 shows the contact angle results of the electrospun scaffolds. As expected, the PCL scaffold had a contact angle of 130 ± 5 ° due to its hydrophobic nature (Figure 5.5A). Incorporation of DM-ECM significantly increased of the wettability that the scaffolds exhibited reduced contact angles ranging from 122 ± 7 ° for 95/5 scaffold (Figure 5.5B) to 70 ± 4 ° for 90/10 scaffold (Figure 5.5C). With the ECM content increasing to 15%, the droplets on the 85/15 scaffold disappeared immediately.

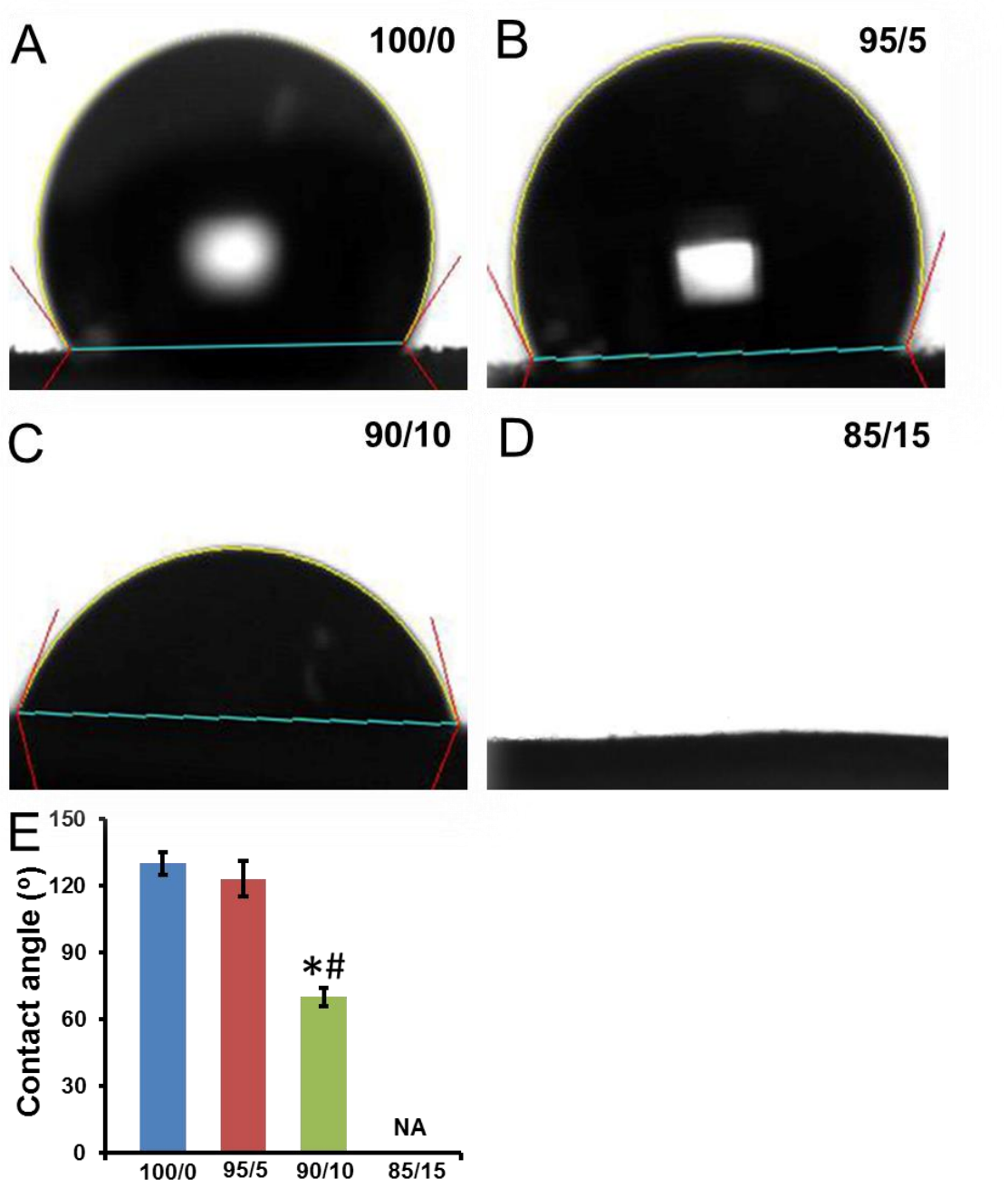

Figure 5. 5 Typical images of contact angles of the electrospun PCL (A), 95/5 (B), 90/10 (C), and 85/15 (D) scaffolds. Increased amount of DM-ECM yields to smaller contact angle as shown in (E).

The results of the scaffold uniaxial tensile testing were shown in Figure 5.6. The PCL/ECM scaffolds had significantly great average peak tensile stresses than of the of

the PCL scaffold (4 ± 1 MPa) (Figure 5.6B). The average peak tensile stresses of the PCL/ECM scaffolds ranged from 10 ± 1 MPa for PCL/ECM-85/15 scaffold to 12 ± 1 MPa for PCL/ECM-95/5 scaffold. The PCL/ECM-90/10 and PCL/ECM-95/5 scaffolds had statistically equivalent average peak stresses. Except the PCL/ECM-90/10 (125 ± 18%) scaffold that had a comparable failure strain to the PCL scaffold (135 ± 19%), the PCL/ECM-95/5 (101 ± 8%) and PCL/ECM-85/15 (99 ± 10%) had significantly smaller failure strains compared to the PCL scaffold (Figure 5.6C). The PCL/ECM scaffolds exhibited greater initial moduli with the increased amount of ECM in the scaffold (Figure 5.6D). No significant difference in the average initial modulus was found between PCL (10 ± 1 MPa) and PCL/ECM-95/5 (12 ± 4 MPa) scaffolds. The PCL/ECM-85/15 (25 ± 3 MPa) and PCL/ECM-90/10 (19 ± 1 MPa) scaffolds had significantly higher initial moduli compared with the PCL and PCL/ECM-95/5 scaffolds.

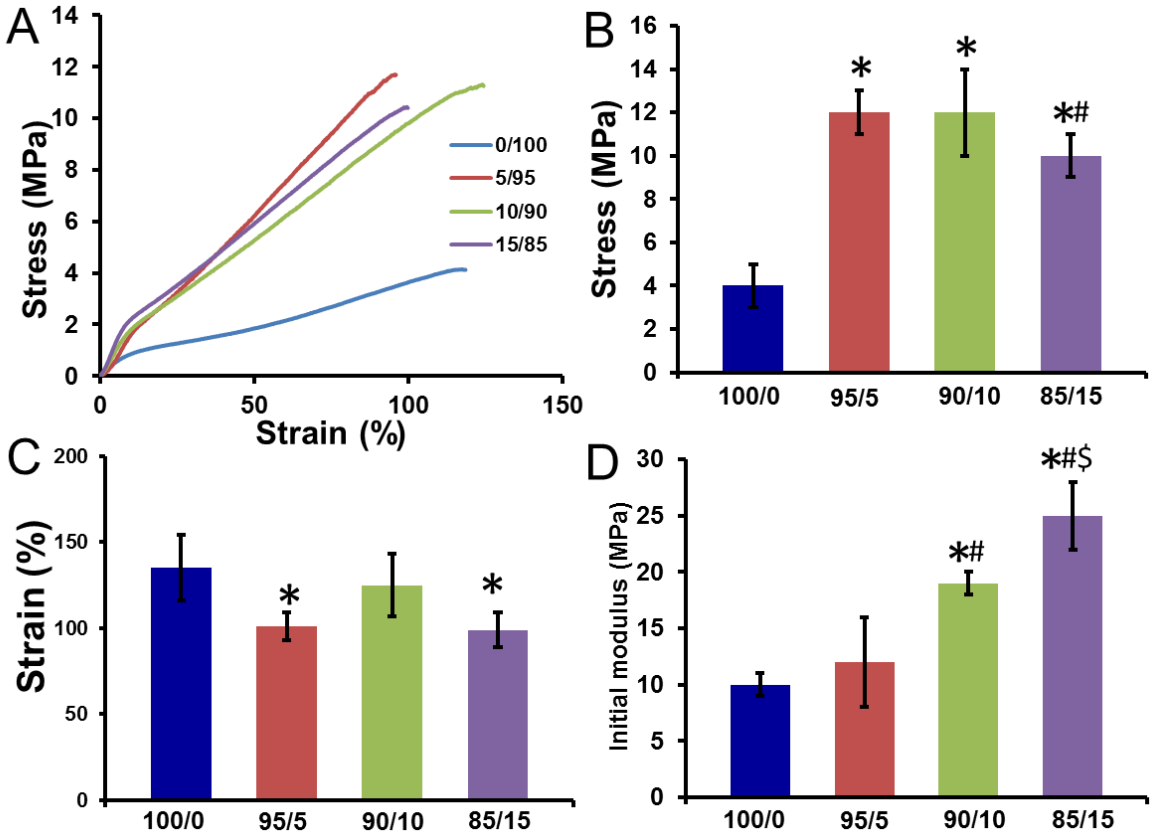

Figure 5. 6 (A) is the typical tensile strength curves of the electrospun scaffolds. (B), (C), and (D) are the tensile strength, strain at failure, and initial modulus of the scaffolds, respectively.

5.3.3.2 Cell morphology

Cell attachment and morphology were visualized by SEM (Figure 5.7) and confocal imaging (Figure 5.8). As shown in Figure 5.7A, bovine fibrochondrocytes well spread out and exhibited a predominant polygonal shape with minor spindle-shaped cells on the PCL/ECM-90/10 scaffold at day 1. In contrast, the cells showed a relatively slower speed of attachment to the PCL scaffold at day 1. Specifically, most of the cells showed round shape with a few cells had spindle shape, indicating the cells initially

adhered to the fibrous substrate and started to spread out on the PCL scaffold. The fibrochondrocytes gradually proliferated with increase cell coverage at day 7 and showed full coverage on the PCL and PCL/ECM-90/10 scaffolds at day 14 (Figure 5.7C). Meanwhile, confocal images indicated that the cells showed polygonal morphology without spindle-shaped cells.

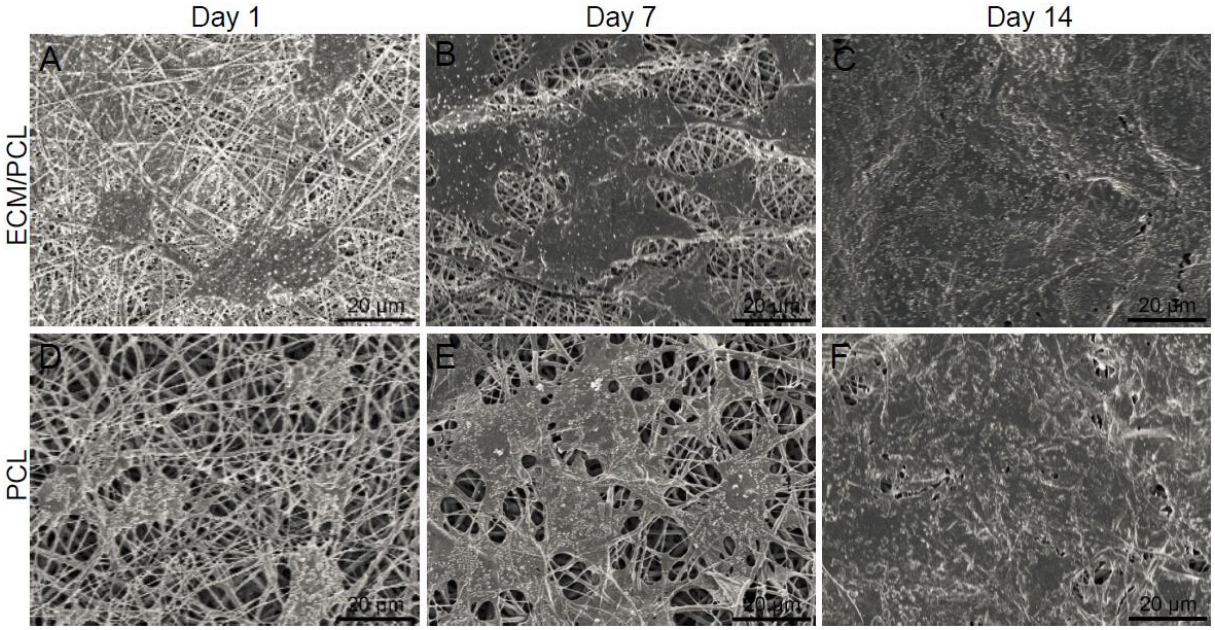

Figure 5. 7 SEM images of the cell morphology of bovine fibrochondrocytes on the PCL/ECM-90/10 (A, B, and C) and PCL (D, E, and F) scaffolds at 1 (A and D), 7 (B and E), and 14 (C and F) days.

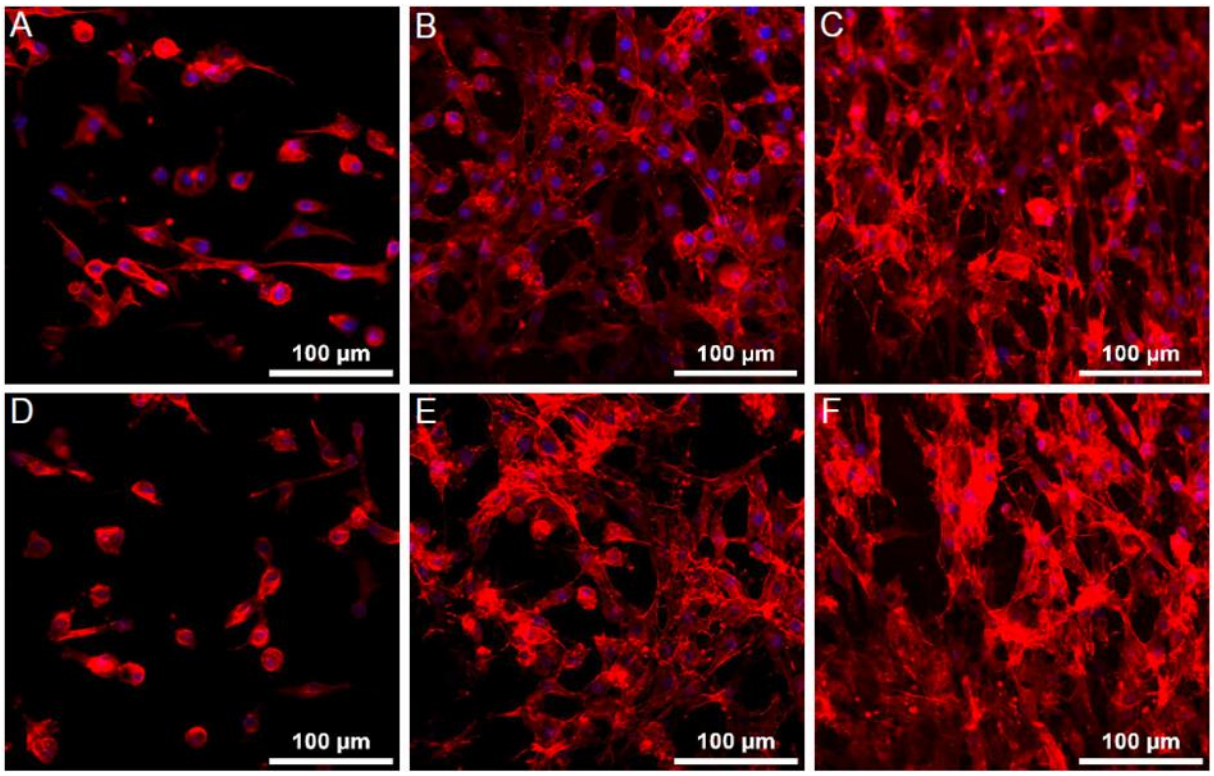

Figure 5. 8 Confocal images of the cell morphology of bovine fibrochondrocytes on the PCL/ECM-90/10 (A, B, and C) and PCL (D, E, and F) scaffolds at 1 (A and D), 7 (B and E), and 14 (C and F) days.

5.3.3.3 Cell proliferation and GAG accumulation

For a specific type cell type, each cell has a consistent amount of DNA. Therefore, we assessed the cell proliferation on the electrospun scaffolds via quantifying the total amount of DNA at each time points during the cell culture period. As shown in Figure 5.9A, the electrospun scaffolds supported progressive DNA increase up to 14 days. No significant difference was found in total DNA between the PCL and PCL/ECM-90/10 scaffolds at each time point. Along with the progressive proliferating, the fibrochondrocytes continuously produced GAG from day 1 to day 14 on the electrospun scaffolds (Figure 5.9B). At day 1, there was negligible GAG accumulation on the

scaffolds, thereafter, increased amounts of GAG were detected throughout the culture. Notably, a significantly higher amount of GAG was found on the PCL/ECM-90/10 scaffold compared with that the of PCL scaffold at day 14. An important indicator of the chondrogenesis capability of fibrochondrocytes is the GAG/DNA ratio. The GAG/DNA ratios of PCL/ECM-90/10 scaffolds were significantly greater than the PCL scaffolds at day 7 and 14 (Figure 5.9C).

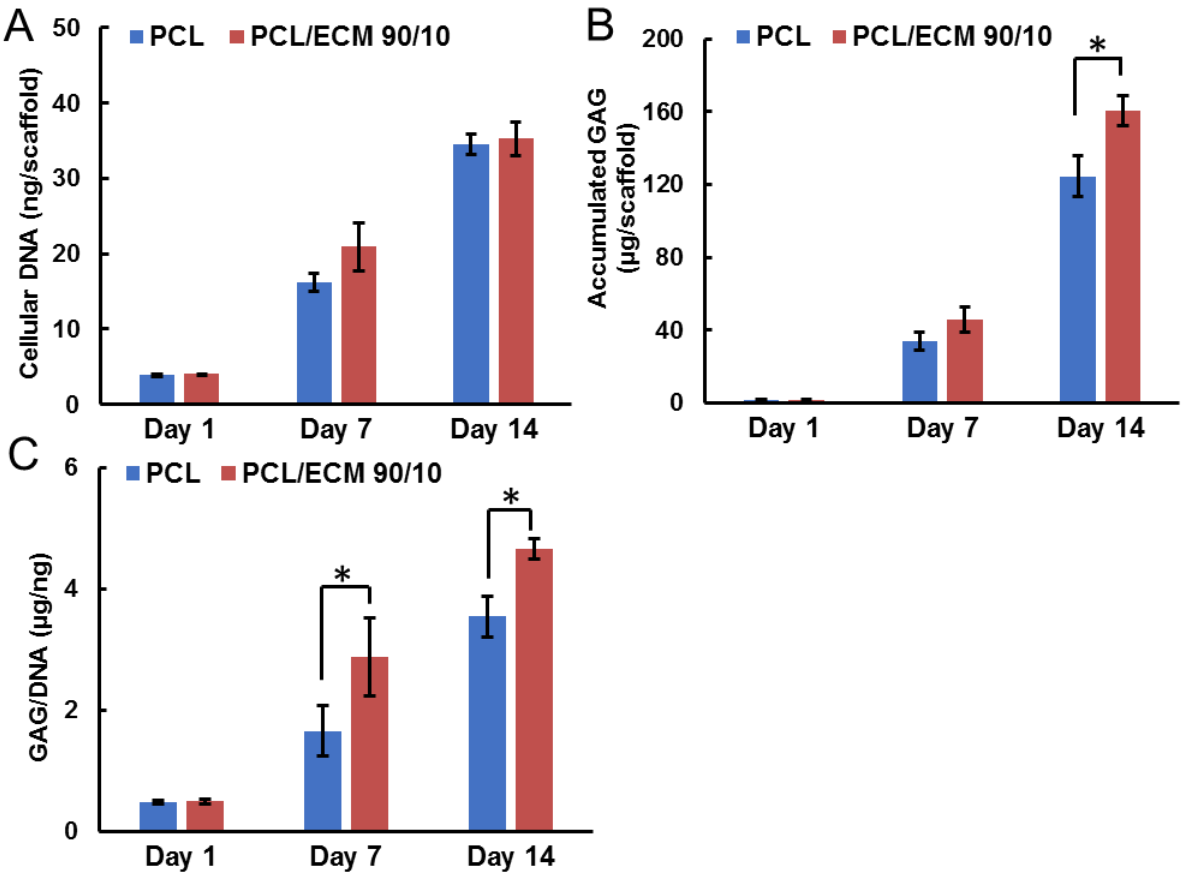

Figure 5. 9 Total DNA (A), GAG accumulation (B), and GAG/DNA ratio of the fibrochondrocyte-seeded electrospun scaffolds up to 14 days.

In addition, Alcian blue staining provided a direct proof of GAG accumulation on the scaffolds (Figure 5.10). At day 1, stained scaffolds with light blue color were observed on the scaffolds (Figure 5.10A). The stained blue got darker over the culture

period from day 7 to 14. The fibrochondrocyte-seeded PCL/ECM-90/10 scaffold had the darkest blue staining at 14 days (Figure 5.10C).

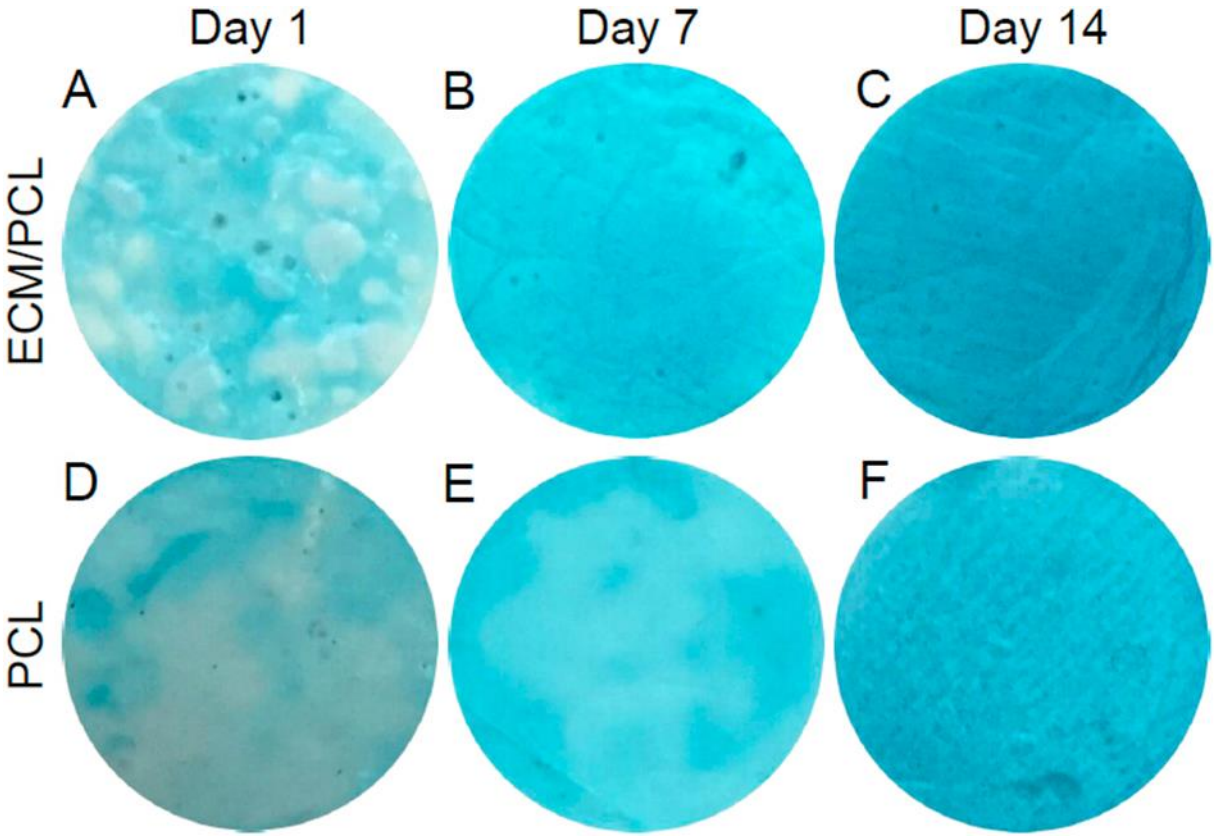

Figure 5. 10 Alcian blue staining of the fibrochondrocyte-seeded PCL/ECM (A, B, and C) and PCL (D, E and D) scaffolds at day 1 (A and D), 7 (B and E) and 14 (C and E).

5.3.4 Discussion

The findings of this study demonstrated that a composite scaffold could be feasibly prepared by single stream electrospinning of PCL/ECM blended solution. This scaffold exhibited significantly improved biological effects on meniscal fibrochondrocyte growth and GAG product accumulation over the pure PCL scaffold. The mechanism of the improved biological performance by incorporating DM-ECM into the electrospun scaffold remains unknown and to be determined in our future study.

Incorporating biological components into electrospun nanofibers can be achieved by direct blending them into solution prior to electrospinning or by surface modifications post electrospinning [262]. Biomolecules such as collagen [49], hyaluronic acid [270] and silk fibroin [50] could be easily dissolved by commonly used electrospinning solvents. They are capable of forming miscible solutions when blended with synthetic polymers, and being electrospun to fibrous mats that have uniform biomolecule distribution within the nanofibers. Unlike the soluble biomolecules, ECM materials derived from tissues/organs, either cellularized or decellularized, are difficult to be dissolved due to their inherent complex composition and dense structure. Especially, ECM materials derived from dense and thick tissues such as cartilage, tendon, and meniscus are not able to be dissolved by electrospinning solvents. One effective approach to incorporate them into electrospun scaffold is to pulverize those ECM materials into nano-to micro-particles and suspend them into a solution for electrospinning [262, 267]. Those ECM-incorporated scaffolds were capable of modulating differentiation of stem cells. One limitation of this method is that the ECM particles might unevenly distribute in the scaffolds, which affects the outcome of those scaffolds toward to regenerative medicine applications. Another method involves a coating process that ECM particles are physically absorbed onto electrospun nanofibers. The coated ECM could significantly influence cell behaviors on the scaffolds [271]. While a drawback is evident that the ECM particles are merely present on the surface and not contained in the core of the scaffold. In addition, the ECM particles appear to experience a huge loss in a short time when immersed in the medium, since they are un-crosslinked to nanofibers.

Recently, decellularized ECMs have been solubilized to flowable solutions by pepsin digestion for the preparation of injectable hydrogels [218]. This leads to the methodology of dissolving enzymatically digested ECMs for electrospinning. The complex extracellular components are enzymatically digested into peptides that are easily dissolved by commonly used solvents, which allows the formation of miscible ECM/synthetic polymer solutions. Electrospinning of such ECM/synthetic polymers solution is easily achievable and the obtained nanofibers have uniform ECM distribution throughout the scaffolds [54]. To our knowledge, this is the first study incorporating DM-ECM into the synthetic polymer to prepare electrospun hybrid scaffold. Our previous study demonstrated that the major component of DM-ECM is collagen [218]. Therefore, we selected HFIP to dissolve pepsin-digested DM-ECM and PCL, as it was reported that collagen was readily soluble in HFIP [272]. As expected, the obtained DM-ECM/PCL solution showed good transparency without insoluble particles similar to the pure PCL solution. DM-ECM/PCL solution could be smoothly electrospun into continuous nanofibers without bead formation on the sheets (Figure 5.1), indicating a good miscibility of DM-ECM and PCL in HFIP.

Electrospinning of natural/synthetic material blended solution often yields nanofibers that have a smaller average diameter compared to electrospun synthetic nanofibers [54, 267, 269, 273]. Reduced fiber diameters of electrospun PCL/ECM scaffolds were observed in our study (Figure 5.1). The addition of natural polymers into synthetic polymer solution could significantly increase the electrical conductivity of the solution, resulting in smaller fiber diameter during electrospinning [269]. Incorporation of natural materials into synthetic polymer also affects the surface wettability of

electrospun scaffolds. Natural materials are known to have excellent hydrophilicity when blended with synthetic polymers, they can greatly increase the wettability of electrospun scaffolds. In our study, we verified the presence of DM-ECM within the electrospun scaffolds via FTIR (Figure 5.2). The incorporated DM-ECM contributes to the significantly increased wettability of the PCL/ECM scaffolds (Figure 5.3), which further benefits the cell attachment and proliferation on the scaffolds.

It is well-established that the adding of natural materials into synthetic polymers can significantly alter the overall mechanical properties of hybrid electrospun scaffolds. Those altering in mechanical strengths could be enhanced [54, 274] or weakened [49, 263, 275] in previous reports. We found enhanced tensile stresses and initial moduli, and decreased failure strains of the PCL/ECM scaffolds when compared to the pure PCL scaffold (Figure 5.4). This altering could be attributed to the high degree of miscibility between ECM and PCL [54]. The increased stiffness and decreased elasticity are associated with the DM-ECM inclusion in the hybrid scaffolds. The tunable mechanical properties of PCL/ECM scaffolds are desirable for scaffold optimization to meet the mechanical requirements of engineered scaffolds in future study.

Excellent engineered scaffolds are capable of promoting cell proliferation and functional product secretion through cell-scaffold interactions [276, 277]. Previous attempts demonstrated that decellularized ECM incorporated scaffolds exhibit improved *in vitro* and *in vivo* results compared to synthetic polymer scaffolds [262, 263, 278]. In consistent with those studies, we found the added DM-ECM into the hybrid scaffolds profoundly affected the meniscal fibrochondrocyte behaviors. Specifically, the cells were more spread out on the PCL/ECM scaffold over the PCL scaffold, though

there was no significant difference in cell proliferation between the two groups of scaffolds. More importantly, the GAG product accumulation on the PCL/ECM scaffold was greater than that of the PCL scaffold on day 28. Additionally, the incorporated DM-ECM significantly improved the normalized GAG/DNA over 28 days. We believe the complex bioactive components including collagen and GAG attributed to these positive effects.

Some limitations of this study should be mentioned. The first concern is the loss of bioactivity during electrospinning as the DM-ECM was directly exposed to HIFP. Although the single-stream electrospinning is feasible and widely used, it compromises the bioactivity of natural materials to some extent when the organic solvent directly contacts with the bioactive nature materials. A two-stream electrospinning/electrospraying process may overcome this drawback by separating the ECM and synthetic polymer that avoids the direct contact of ECM with organic solvents [53]. Another limitation is related to the densely compacted nanofibrous structure of the PCL/ECM scaffold. The fibrochondrocytes can only grow on the surface but not penetrate the scaffold. For meniscus tissue regeneration, a three-dimensional cellularized construct is highly desired. Advanced techniques should be employed to fabricate 3D porous scaffold using DM-ECM material in the future study [67].

5.3.5 Summary

This work describes the preparation of PCL/ECM scaffolds via a single-stream electrospinning. The incorporated DM-ECM significantly affects the properties of the resulting scaffolds, including smaller fiber diameter, increased wettability, and

improved tensile strength. More importantly, the meniscus-specific ECM shows great beneficial effects on meniscus fibrochondrocyte growth and chondrogenesis product accumulation. The electrospun PCL/ECM scaffold holds great potential for meniscus repair and regenerations.

In this study, we present an electrospun PCL/ECM scaffold with randomly oriented nanofibers. Although the PCL/ECM scaffold has greatly improved mechanical and biological performances, its densely compacted nanofibrous structure might impede cellular infiltration into the scaffold. In the future study, we will employ some advanced techniques to enlarge the pore size of the scaffold, making it more conducive for cell penetration and tissue ingrowth [67, 279, 280]. Single-stream electrospinning of DM-ECM and PCL blended solution is feasibly achievable, while the direct contact of DM-ECM with organic solvent unavoidably compromises its bioactivity. A two-stream electrospinning that separates synthetic polymer in an organic phase with the ECM solution in non-organic phase would avoid the loss of bioactivity and obtain loosened fibrous scaffold [53]. This method might provide a great chance to fabricate advanced tissue engineered scaffolds for meniscus repair and regeneration.

5.4 Future work

The decellularized meniscus ECM developed in this thesis offer great potential for meniscus tissue repair and regeneration. The naturally-derived meniscus ECM materials can be processed into hydrogels or combined with synthetic polymers to fabricate hybrid nanofibrous scaffolds. Our results demonstrate that the meniscus ECM is highly biocompatible and bioactive and can promote fibrochondrocyte growth and elevate meniscus-specific product accumulation. Future work will be discussed in this chapter.

5.4.1 Composition of decellularized meniscus ECM

In the thesis, we characterized the composition of decellularized meniscus ECM by determining the collagen and GAG contents. This is regularly conducted in some other related studies [89]. However, little is known about retentions of some other important bioactive components such as elastin and growth factors after decellularization. Those unidentified components might also affect the mechanical and biological properties of the ECM hydrogels. Therefore, future studies need to verify the presence of those bioactive components by ELISA, MS, or proteomics [198, 281].

5.4.2 Inherently weak mechanical properties of meniscus ECM hydrogel

Similar to the ECM hydrogels made from some other tissue resources [160, 163, 165], decellularized meniscus ECM hydrogel possesses lower mechanical strength compared to that of the native meniscus tissue [218]. Obviously, injectable ECM hydrogels are suitable for soft tissue repair and regeneration. In contrast, it is

challenging to use injectable ECM hydrogels for the treatment of diseased or damaged tissues that bear a high level of stress. Meniscal ECM hydrogels have compressive strengths ranged from 0.1 to 0.8 kPa, which is much lower than that of the native meniscus (100-150 kPa). Therefore, it is not suitable for whole meniscus regeneration as it cannot provide sufficient mechanical supports in the knee joint. This decellularized meniscus ECM might be used as an injectable filling material that temporarily takes up the meniscus tear and recruits progenitor cells from neighboring tissue [194, 282].

5.4.3. Animal study

The current work mainly focuses on the preparation, optimization, and characterizations of the DM-ECM hydrogels, and the investigation of their cytocompatibility via 2D and 3D cell culture. In order to illustrate the feasibility of the DM-ECMs as inject materials to fill meniscus defects and their potential to promote meniscus repair and regeneration, *ex vivo* and *in vivo* studies with appropriate animal models will be performed in our future study.

Direct injection of MSCs into partial meniscus defects showed that the cells could adhere to the damaged meniscus tissue and promote tissue repair process in a rat model [283]. However, rats have a relatively higher innate regenerative capability , which brings difficulty to differ the effects of cell and/or scaffold on meniscus tissue regeneration in the experimental group compared with the control group [283, 284]. In addition, the relatively smaller size of rat meniscus and the limited intra-articular space of rat knee joint present great challenge for arthroscopic surgery. Injectable meniscus ECM hydrogel aided delivery of MSCs into bovine meniscus defects for *in vitro* culture

and *in vivo* subcutaneous implantation in a nude rat model demonstrated that the cell encapsulated ECM hydrogel was capable of improving tissue regeneration, preventing the joint from space narrowing, pathologic mineralization, and osteoarthritis development [251]. Evidently, injection of cell-encapsulated ECM hydrogel into the meniscus defects of large animal explants is much feasible than the operation on the rat model. However, growing of cell-encapsulated hydrogel in bovine meniscus explant either *in vitro* or *in vivo* subcutaneous implantation in nude rats lacks the biomechanical stimulus, specifically, the compressive loading that applies to the meniscus in the knee joint.

It seems that large animals such as calf, sheep, and pigs would provide a favorable choice to illustrate the capability of DM-ECM hydrogel on meniscus repair and regeneration. However, economic consideration sometimes comes first in the research community. In contrast to the large animals, rabbits are much cost less. In addition, similar to the human meniscus, the rabbit meniscus presents an inherently limited self-healing and regenerative capability [285]. Rabbit models have been widely used to evaluate the meniscus repair and regenerative capability of cell or scaffold based surgical interventions [109, 284, 286-288]. Therefore, the rabbit will be a great animal model for our future animal study.

Appendix A

Related Publications

Journal Articles

1. Wu J, Ding Q, Dutta A, Wang Y, Huang Y-H, Weng H, Tang L, Hong Y. An injectable extracellular matrix derived hydrogel for meniscus repair and regeneration. *Acta Biomater* 2015;16:49-59.
2. Wu J, Ravikumar P, Nguyen KT, Hsia CCW, Hong Y. Lung protection by inhalation of exogenous solubilized extracellular matrix. *PLoS One* 2017; 12:e0171165.
3. Wu J, Hong Y. Enhancing cell infiltration of electrospun fibrous scaffolds in tissue regeneration. *Bioact Mater* 2016; 1:56-64. (Review article)
4. Xu C, Huang Y-H, Wu J, Tang L, Hong Y. Triggerable degradation of polyurethanes for tissue engineering applications. *ACS Appl Mater Interfaces* 2015;7:20677-88.
5. Jeffords ME[1], Wu J[1], Shah M, Hong Y, Zhang G. Tailoring material properties of cardiac matrix hydrogels to induce endothelial differentiation of human mesenchymal stem cells. *ACS Appl Mater Interfaces* 2015;7:11053-61. (Equal contribution)
6. Huang Y, Zhou J, Wu J, Hong Y, Tang L. An optical probe for detecting chondrocyte apoptosis in response to mechanical injury. Scientific Reports: (Accepted)

Conference Abstracts

1. Wu J, Xu C, Gu X, Hong Y. A tissue-specific matrix-incorporated electrospun scaffold for meniscus tissue engineering. (Oral presentation) Annual Meeting of

Biomedical Engineering Society (BMES). October 5-8th, 2016, Minneapolis, Minnesota.

2. Zhou J, Li S, Huang Y, Wu J, Hong Y, Borrelli J, Tang L. Development of imaging probe for osteoarthritis diagnosis. Annual Meeting of BMES. October 5-8th, 2016, Minneapolis, Minnesota.
3. Xu C, Huang Y, Wu J, Liao J, Tang L, Hong Y. Optimizing anisotropic polyurethane scaffolds to mechanically match with the native myocardium. Annual Meeting of BMES. October 5-8th, 2016, Minneapolis, Minnesota.
4. Wu J, Nguyen KT, Hong Y. A three-dimensional cancer model of decellularized lung extracellular matrix hydrogel for lung tumor engineering. The 10th World Biomaterials Congress. May 17-22nd, 2016, Montreal, Canada.
5. Wu J, Brazile B, Liao J, Hong Y, Electrospun loose-fiber polyurethane scaffolds for tissue engineering applications. Annual Meeting of BMES. October 7-10th, 2015, Tampa, Florida.
6. Punnakitikashem P, Ravikumar P, Wu J, Nguyen KT, Hsia CC, Hong Y. Extracellular matrix coating of nanoparticles modulates uptake and payload release by lung cells. Annual Meeting of BMES. October 7-10th, 2015, Tampa, Florida.
7. Jeffords M, Wu J, Shah M, Hong Y, Zhang G. Accelerated Endothelial Differentiation of Stem Cells on Cardiac Matrix Hydrogel with Tailored Properties. Annual Meeting of BMES. October 7-10th, 2015, Tampa, Florida
8. Wu J, Ravikumar P, Hsia C, Hong Y. Decellularized lung extracellular matrix preparation mitigates acute hyperoxic lung injury. Lung Repair and

Regeneration Consortium (LRRC) Annual Meeting. September 28-29th, 2015, Bethesda, Maryland.

9. Wu J, Huang Y-H, Nguyen, KT, Tang L, Hong Y, Meniscus-derived extracellular matrix hydrogels for meniscus regeneration. The 4th TERMIS World Congress. September 8–11th, 2015, Boston, Massachusetts.

10. Wu J, Ding Q, Dutta A, Hong Y. Optimizing decellularization detergents for meniscus-derived injectable hydrogel. Annual Meeting of the Society For Biomaterials. April 15-18th, 2015, Charlotte, North Carolina.

11. Wu J, Ding Q, Dutta A, Iyer R, Ravikumar P, Hsia C, Hong Y. Lung extracellular matrix solution protects against hyperoxia-induced acute lung injury. The Annual Celebration of Excellence by Students (ACES) Symposium. March 25th, 2015, Arlington, Texas.

12. Wu J, Ding Q, Dutta A, Iyer R, Ravikumar P, Wu L, Hsia C, Hong Y. Nebulizable decellularized lung matrix solution for hyper-induced acute lung injury. Annual Meeting of BMES. October 22-25th, 2014, San Antonio, Texas

13. Jeffords M, Wu J, Ding Q, Hong Y, Zhang G. Tuning material properties of cardiac extracellular matrix for cardiac tissue engineering. Annual Meeting of BMES. October 22-25th, 2014, San Antonio, Texas

14. Wu J, Ding Q, Truong D, Weng H, Tang L, Hong Y. An injectable porcine cartilage-derived hydrogel for cartilage repair and regeneration. Annual Meeting of the Society For Biomaterials. April 16-19th, 2014, Denver, Colorado.

15. Wu J, Hong Y. Naturally derived biomimetic hydrogels for cartilage regeneration. The Annual Celebration of Excellence by Students (ACES) Symposium. March 26th, 2014, Arlington, Texas.

Appendix B

Abbreviations

Abbreviations

ECM	Extracellular matrix
OA	Osteoarthritis
PU	Polyurethane
BMSC	Bone mesenchymal stem cell
PLA	Poly(lactic acid)
PCL	Polycaprolactone
CMI	Collagen meniscus implant
GAG	Glycosaminoglycan
PVA	Poly(vinyl alcohol)
EGF	Endothelial growth factor
TFG-α	Transforming growth factor-α
bFGF	Basic fibroblast growth factor
PDFG-AB	Platelet-derived growth factor AB
IGF-I	Insulin-like growth factor I
VEGF	Vascular endothelial growth factor
SDS	Sodium dodecyl sulfate
SIS	Small intestinal submucosa
rMSC	Rat mesenchymal stromal cell
EDTA	Ethylenediaminetetraacetic acid
PBS	Phosphate-buffered saline
HCl	Hydrogen chloride
NaOH	Sodium hydroxide

DAPI	4’, 6-diamidino-2-phenylindole
O.C.T	Optimal cutting temperature compound
H&E	Hematoxylin and eosin
SEM	Scanning electron microscope
TCPS	Tissue culture polystyrene
TX	Triton X-100
PAA	Peracetic acid
DM-ECM	Decellularized meniscus extracellular matrix
DMMB	1,9-dimethyl methylene blue
GuHCl	Guanidine hydrochloride
PSF	Penicillin–streptomycin–fungizone
SDS-ECM	SDS-treated meniscus extracellular matrix
TX-ECM	TX-treated meniscus extracellular matrix
PAA-ECM	PAA-treated meniscus extracellular matrix
SDS-PAGE	Sodium dodecyl sulfate polyacrylamide gel electrophoresis
OM-ECM	Decellularized outer meniscus extracellular matrix
MM-ECM	Decellularized middle meniscus extracellular matrix
IM-ECM	Decellularized inner meniscus extracellular matrix
HFIP	1,1,1,3,3,3-hexafluoro-2-propanol
FTIR-ATR	Fourier transform infrared attenuated total reflectance

References

1 McNulty A. L., and Guilak F. Mechanobiology of the meniscus. J Biomech 2015;48(8):1469-1478.

2 Aagaard H., and Verdonk R. Function of the normal meniscus and consequences of meniscal resection. Scand J Med Sci Sports 1999;9(3):134-140.

3 Sanchez-Adams J., and Athanasiou K. The knee meniscus: A complex tissue of diverse cells. Cel Mol Bioeng 2009;2(3):332-340.

4 Makris E. A., Hadidi P., and Athanasiou K. A. The knee meniscus: Structure–function, pathophysiology, current repair techniques, and prospects for regeneration. Biomaterials 2011;32(30):7411-7431.

5 Moran C. J., Busilacchi A., Lee C. A., Athanasiou K. A., and Verdonk P. C. Biological Augmentation and Tissue Engineering Approaches in Meniscus Surgery. Arthroscopy 2015;31(5):944-955.

6 Rockborn P., and Gillquist J. Long term results after arthroscopic meniscectomy: The role of preexisting cartilage fibrillation in a 13 year follow-up of 60 patients. Int J Sports Med 1996;17(08):608-613.

7 Pauly H. M., and Haut Donahue T. L., "16 - Bone–meniscus interface," Regenerative engineering of musculoskeletal tissues and interfaces, S. P. Nukavarapu and J. W. F. T. Laurencin, eds., pp. 377-407: Woodhead Publishing, 2015.

8 McDermott I. Meniscal tears, repairs and replacement: their relevance to osteoarthritis of the knee. Br J Sports Med 2011:bjsports81257.

9 Salata M. J., Gibbs A. E., and Sekiya J. K. A systematic review of clinical outcomes in patients undergoing meniscectomy. Am J Sports Med 2010;38(9):1907-1916.

10 Noble J., and Hamblen D. L. The pathology of the degenerate meniscus lesion. J Bone Joint Surg Br 1975;57(2):180-186.

11 Fithian D. C., Kelly M. A., and Mow V. C. Material properties and structure-function relationships in the menisci. Clin Orthop Relat Res 1990;252:19-31.

12 McDevitt C. A., and Webber R. J. The ultrastructure and biochemistry of meniscal cartilage. Clin Orthop Relat Res 1990;252:8-18.

13 Ruiz Ibán M. Á., Comellas Melero N., Martinez-Botas J., Ortiz A., and Diaz Heredia J. Growth Factor Expression After Lesion Creation in the Avascular Zone of the Meniscus: A Quantitative PCR Study in Rabbits. Arthroscopy 2014;30(9):1131-1138.

14 Eyre D. Articular cartilage and changes in Arthritis: Collagen of articular cartilage. Arthritis Res Therapy 2001;4(1):30.

15 Cheung H. S. Distribution of type I, II, III and V in the pepsin solubilized collagens in bovine menisci. Connect Tissue Res 1987;16(4):343-356.
16 Sanchez-Adams J., and Athanasiou K. A. Regional effects of enzymatic digestion on knee meniscus cell yield and phenotype for tissue engineering. Tissue Eng Part C Methods 2012;18(3):235-43.
17 Higashioka M. M., Chen J. A., Hu J. C., and Athanasiou K. A. Building an anisotropic meniscus with zonal variations. Tissue Eng Part A 2014;20(1-2):294-302.
18 Yuan X., Eng G. M., Arkonac D. E., Chao P.-h. G., and Vunjak-Novakovic G. Endothelial cells enhance the migration of bovine meniscus cells. Arthritis Rheumatol 2015;67(1):182-192.
19 Furumatsu T., Kanazawa T., Yokoyama Y., Abe N., and Ozaki T. Inner Meniscus Cells Maintain Higher Chondrogenic Phenotype Compared with Outer Meniscus Cells. Connect Tissue Res 2011;52(6):459-465.
20 Sweigart M., Zhu C., Burt D., Agrawal C., Clanton T., and Athanasiou K. Intraspecies and interspecies comparison of the compressive properties of the medial meniscus. Ann Biomed Eng 2004;32(11):1569-1579.
21 Baker B. E., Peckham A. C., Pupparo F., and Sanborn J. C. Review of meniscal injury and associated sports. Am J Sports Med 1985;13(1):1-4.
22 Hede A., Jensen D. B., Blyme P., and Sonne-Holm S. Epidemiology of meniscal lesions in the knee: 1,215 open operations in Copenhagen 1982-84. Acta Orthop Scand 1990;61(5):435-437.
23 Englund M., Roemer F. W., Hayashi D., Crema M. D., and Guermazi A. Meniscus pathology, osteoarthritis and the treatment controversy. Nat Rev Rheumatol 2012;8(7):412-9.
24 Fox A. J. S., Wanivenhaus F., Burge A. J., Warren R. F., and Rodeo S. A. The human meniscus: A review of anatomy, function, injury, and advances in treatment. Clin Anat 2015;28(2):269-287.
25 Scotti C., Hirschmann M. T., Antinolfi P., Martin I., and Peretti G. M. Meniscus repair and regeneration: review on current methods and research potential. Eur Cell Mater 2013;26:150-70.
26 Drosos G., and Pozo J. The causes and mechanisms of meniscal injuries in the sporting and non-sporting environment in an unselected population. Knee 2004;11(2):143-149.
27 Englund M., Niu J., Guermazi A., Roemer F., Hunter D., Lynch J. et al. Effect of meniscal damage on the development of frequent knee pain, aching, or stiffness. Arthritis Rheum 2007;56(12):4048-4054.
28 Hasan J., Fisher J., and Ingham E. Current strategies in meniscal regeneration. J Biomed Mater Res B Appl Biomater 2014;102(3):619-634.

29 Mauck R., and Burdick J. From Repair to Regeneration: Biomaterials to Reprogram the Meniscus Wound Microenvironment. Ann Biomed Eng 2015;43(3):529-542.
30 Janik H., and Marzec M. A review: Fabrication of porous polyurethane scaffolds. Mater Sci Eng C Mater Biol Appl 2015;48:586-591.
31 de Groot J. H., de Vrijer R., Pennings A. J., Klompmaker J., Veth R. P. H., and Jansen H. W. B. Use of porous polyurethanes for meniscal reconstruction and meniscal prostheses. Biomaterials 1996;17(2):163-173.
32 Stankus J. J., Guan J., Fujimoto K., and Wagner W. R. Microintegrating smooth muscle cells into a biodegradable, elastomeric fiber matrix. Biomaterials 2006;27(5):735-744.
33 Guan J., Wang F., Li Z., Chen J., Guo X., Liao J. et al. The stimulation of the cardiac differentiation of mesenchymal stem cells in tissue constructs that mimic myocardium structure and biomechanics. Biomaterials 2011;32(24):5568-5580.
34 Punnakitikashem P., Truong D., Menon J. U., Nguyen K. T., and Hong Y. Electrospun biodegradable elastic polyurethane scaffolds with dipyridamole release for small diameter vascular grafts. Acta Biomate 2014;10(11):4618-4628.
35 Xu C., Huang Y., Wu J., Tang L., and Hong Y. Triggerable degradation of polyurethanes for tissue engineering applications. ACS Appl Mater Interfaces 2015;7(36):20377-20388.
36 Heijkants R. G. J. C., van Calck R. V., de Groot J. H., Pennings A. J., Schouten A. J., van Tienen T. G. et al. Design, synthesis and properties of a degradable polyurethane scaffold for meniscus regeneration. J Mater Sci Mater Med 2004;15(4):423-427.
37 Liu C., Abedian R., Meister R., Haasper C., Hurschler C., Krettek C. et al. Influence of perfusion and compression on the proliferation and differentiation of bone mesenchymal stromal cells seeded on polyurethane scaffolds. Biomaterials 2012;33(4):1052-1064.
38 Verdonk R., Verdonk P., Huysse W., Forsyth R., and Heinrichs E.-L. Tissue ingrowth after implantation of a novel, biodegradable polyurethane scaffold for treatment of partial meniscal lesions. Am J Sports Med 2011;39(4):774-782.
39 Esposito A. R., Moda M., Cattani S. M., de Santana G. M., Barbieri J. A., Munhoz M. M. et al. PLDLA/PCL-T scaffold for meniscus tissue engineering. Biores Open Access 2013;2(2):138-47.
40 Kon E., Chiari C., Marcacci M., Delcogliano M., Salter D. M., Martin I. et al. Tissue engineering for total meniscal substitution: Animal study in sheep model. Tissue Eng Part A 2008;14(6):1067-80.

41 Gruchenberg K., Ignatius A., Friemert B., von Lübken F., Skaer N., Gellynck K. et al. In vivo performance of a novel silk fibroin scaffold for partial meniscal replacement in a sheep model. Knee Surg Sports Traumatol Arthrosc 2014:1-12.
42 Mandal B. B., Park S.-H., Gil E. S., and Kaplan D. L. Multilayered silk scaffolds for meniscus tissue engineering. Biomaterials 2011;32(2):639-651.
43 Yan L.-P., Oliveira J. M., Oliveira A. L., Caridade S. G., Mano J. F., and Reis R. L. Macro/microporous silk fibroin scaffolds with potential for articular cartilage and meniscus tissue engineering applications. Acta Biomater 2012;8(1):289-301.
44 Stone K. R., Rodkey W. G., Webber R., McKinney L., and Steadman J. R. Meniscal regeneration with copolymeric collagen scaffolds: In vitro and in vivo studies evaluated clinically, histologically, and biochemically. Am J Sports Med 1992;20(2):104-111.
45 Pabbruwe M. B., Kafienah W., Tarlton J. F., Mistry S., Fox D. J., and Hollander A. P. Repair of meniscal cartilage white zone tears using a stem cell/collagen-scaffold implant. Biomaterials 2010;31(9):2583-2591.
46 Rodkey W. G., Steadman J. R., and Li S.-T. A clinical study of collagen meniscus implants to restore the injured meniscus. Clin Orthop Relat Res 1999;367:S281-S292.
47 Zaffagnini S., Giordano G., Vascellari A., Bruni D., Neri M. P., Iacono F. et al. Arthroscopic collagen meniscus implant results at 6 to 8 years follow up. Knee Surg Sports Traumatol Arthrosc 2007;15(2):175-183.
48 Kon E., Filardo G., Tschon M., Fini M., Giavaresi G., Marchesini Reggiani L. et al. Tissue engineering for total meniscal substitution: animal study in sheep model--results at 12 months. Tissue Eng Part A 2012;18(15-16):1573-82.
49 Wu J., Huang C., Liu W., Yin A., Chen W., He C. et al. Cell infiltration and vascularization in porous nanoyarn scaffolds prepared by dynamic liquid electrospinning. J Biomed Nanotechnol2014;10(4):603-614.
50 Wu J., Liu S., He L., Wang H., He C., Fan C. et al. Electrospun nanoyarn scaffold and its application in tissue engineering. Mater Lett 2012;89(0):146-149.
51 Xu Y., Dong S., Zhou Q., Mo X., Song L., Hou T. et al. The effect of mechanical stimulation on the maturation of TDSCs-poly(L-lactide-co-e-caprolactone)/collagen scaffold constructs for tendon tissue engineering. Biomaterials 2014;35(9):2760-2772.
52 Xu Y., Wu J., Wang H., Li H., Di N., Song L. et al. Fabrication of electrospun poly(L-lactide-co-epsilon-caprolactone)/collagen nanoyarn network as a novel, three-dimensional, macroporous, aligned scaffold for tendon tissue engineering. Tissue Eng Part C Methods 2013;19(12):925-36.
53 Hong Y., Huber A., Takanari K., Amoroso N. J., Hashizume R., Badylak S. F. et al. Mechanical properties and in vivo behavior of a biodegradable synthetic

polymer microfiber–extracellular matrix hydrogel biohybrid scaffold. Biomaterials 2011;32(13):3387-3394.

54 Hong Y., Takanari K., Amoroso N. J., Hashizume R., Brennan-Pierce E. P., Freund J. M. et al. An elastomeric patch electrospun from a blended solution of dermal extracellular matrix and biodegradable polyurethane for rat abdominal wall repair. Tissue Eng Part C Methods 2012;18(2):122-32.

55 Baker B. M., Gee A. O., Metter R. B., Nathan A. S., Marklein R. A., Burdick J. A. et al. The potential to improve cell infiltration in composite fiber-aligned electrospun scaffolds by the selective removal of sacrificial fibers. Biomaterials 2008;29(15):2348-2358.

56 Li M., Mondrinos M. J., Gandhi M. R., Ko F. K., Weiss A. S., and Lelkes P. I. Electrospun protein fibers as matrices for tissue engineering. Biomaterials 2005;26(30):5999-6008.

57 Agarwal S., Wendorff J. H., and Greiner A. Progress in the field of electrospinning for tissue engineering applications. Adv Mater 2009;21(32-33):3343-51.

58 Nisbet D. R., Forsythe J. S., Shen W., Finkelstein D. I., and Horne M. K. Review paper: A review of the cellular response on electrospun nanofibers for tissue engineering. J Biomater Appl 2008.

59 Jang J.-H., Castano O., and Kim H.-W. Electrospun materials as potential platforms for bone tissue engineering. Adv Drug Deliv Rev 2009;61(12):1065-1083.

60 Baker B. M., Nathan A. S., Huffman G. R., and Mauck R. L. Tissue engineering with meniscus cells derived from surgical debris. Osteoarthritis Cartilage 2009;17(3):336-345.

61 Baek J., Sovani S., Glembotski N. E., Du J., Jin S., Grogan S. P. et al. Repair of avascular meniscus tears with electrospun collagen scaffolds seeded with human cells. Tissue Eng Part A 2016;22(5-6):436-448.

62 Baek J., Chen X., Sovani S., Jin S., Grogan S. P., and D'Lima D. D. Meniscus tissue engineering using a novel combination of electrospun scaffolds and human meniscus cells embedded within an extracellular matrix hydrogel. J Orthop Res 2015;33(4):572-583.

63 Baker B. M., and Mauck R. L. The effect of nanofiber alignment on the maturation of engineered meniscus constructs. Biomaterials 2007;28(11):1967-1977.

64 Baker B. M., Nathan A. S., Gee A. O., and Mauck R. L. The influence of an aligned nanofibrous topography on human mesenchymal stem cell fibrochondrogenesis. Biomaterials 2010;31(24):6190-6200.

65 Martin J. T., Milby A. H., Ikuta K., Poudel S., Pfeifer C. G., Elliott D. M. et al. A radiopaque electrospun scaffold for engineering fibrous musculoskeletal tissues: Scaffold characterization and in vivo applications. Acta Biomater 2015;26:97-104.

66 Fisher M. B., Henning E. A., Söegaard N., Bostrom M., Esterhai J. L., and Mauck R. L. Engineering meniscus structure and function via multi-layered mesenchymal stem cell-seeded nanofibrous scaffolds. J Biomech 2015;48(8):1412-1419.
67 Wu J., and Hong Y. Enhancing cell infiltration of electrospun fibrous scaffolds in tissue regeneration. Bioact Mater 2016;1(1):56-64.
68 Crapo P. M., Gilbert T. W., and Badylak S. F. An overview of tissue and whole organ decellularization processes. Biomaterials 2011;32(12):3233-3243.
69 Soto-Gutierrez A., Zhang L., Medberry C., Fukumitsu K., Faulk D., Jiang H. et al. A whole-organ regenerative medicine approach for liver replacement. Tissue Eng Part C Methods 2011;17(6):677-686.
70 Monibi F. A., and Cook J. L. Tissue-derived extracellular matrix bioscaffolds: emerging applications in cartilage and meniscus repair. Tissue Eng Part B Rev 2017.
71 Badylak S. F., Freytes D. O., and Gilbert T. W. Extracellular matrix as a biological scaffold material: Structure and function. Acta Biomater 2009;5(1):1-13.
72 Badylak S. F., and Nerem R. M. Progress in tissue engineering and regenerative medicine. Proc Natl Acad Sci U S A 2010;107(8):3285-3286.
73 Agrawal V., Johnson S. A., Reing J., Zhang L., Tottey S., Wang G. et al. Epimorphic regeneration approach to tissue replacement in adult mammals. Proc Natl Acad Sci U S A 2010;107(8):3351-3355.
74 Lee J. S., Shin J., Park H.-M., Kim Y.-G., Kim B.-G., Oh J.-W. et al. Liver extracellular matrix providing dual functions of two-dimensional substrate coating and three-dimensional injectable hydrogel platform for liver tissue engineering. Biomacromolecules 2014;15(1):206-218.
75 Ghaedi M., Calle E. A., Mendez J. J., Gard A. L., Balestrini J., Booth A. et al. Human iPS cell–derived alveolar epithelium repopulates lung extracellular matrix. J Clin Invest 2013;123(11):4950-4962.
76 Mendez J. J., Ghaedi M., Steinbacher D., and Niklason L. E. Epithelial cell differentiation of human mesenchymal stromal cells in decellularized lung scaffolds. Tissue Eng Part A 2014;20(11-12):1735-1746.
77 Ott H. C., Matthiesen T. S., Goh S.-K., Black L. D., Kren S. M., Netoff T. I. et al. Perfusion-decellularized matrix: using nature's platform to engineer a bioartificial heart. Nat Med 2008;14(2):213-221.
78 Valentin J. E., Turner N. J., Gilbert T. W., and Badylak S. F. Functional skeletal muscle formation with a biologic scaffold. Biomaterials 2010;31(29):7475-7484.
79 Yamasaki T., Deie M., Shinomiya R., Izuta Y., Yasunaga Y., Yanada S. et al. Meniscal regeneration using tissue engineering with a scaffold derived from a rat meniscus and mesenchymal stromal cells derived from rat bone marrow. J Biomed Mater Res Part A 2005;75(1):23-30.

80 Yamasaki T., Deie M., Shinomiya R., Yasunaga Y., Yanada S., and Ochi M. Transplantation of meniscus regenerated by tissue engineering with a scaffold derived from a rat meniscus and mesenchymal ttromal cells derived rrom rat bone marrow. Artif Organs 2008;32(7):519-524.

81 Maier D., Braeun K., Steinhauser E., Ueblacker P., Oberst M., Kreuz P. C. et al. In vitro analysis of an allogenic scaffold for tissue-engineered meniscus replacement. J Orthop Res 2007;25(12):1598-1608.

82 Stabile K. J., Odom D., Smith T. L., Northam C., Whitlock P. W., Smith B. P. et al. An acellular, allograft-derived meniscus scaffold in an ovine model. Arthroscopy 2010;26(7):936-48.

83 Gao S., Yuan Z., Xi T., Wei X., and Guo Q. Characterization of decellularized scaffold derived from porcine meniscus for tissue engineering applications. Front. Mater. Sci. 2016:1-12.

84 Stapleton T. W., Ingram J., Fisher J., and Ingham E. Investigation of the regenerative capacity of an acellular porcine medial meniscus for tissue engineering applications. Tissue Eng Part A 2011;17(1-2):231-42.

85 Abdelgaied A., Stanley M., Galfe M., Berry H., Ingham E., and Fisher J. Comparison of the biomechanical tensile and compressive properties of decellularised and natural porcine meniscus. J Biomech 2015;48(8):1389-1396.

86 Stapleton T. W., Ingram J., Katta J., Knight R., Korossis S., Fisher J. et al. Development and characterization of an acellular porcine medial meniscus for use in tissue engineering. Tissue Eng Part A 2008;14(4):505-18.

87 Chen Y.-C., Chen R.-N., Jhan H.-J., Liu D.-Z., Ho H.-O., Mao Y. et al. Development and Characterization of Acellular Extracellular Matrix Scaffolds from Porcine Menisci for Use in Cartilage Tissue Engineering. Tissue Eng Part C Methods 2015;21(9):971-986.

88 Azhim A., Ono T., Fukui Y., Morimoto Y., Furukawa K., and Ushida T., "Preparation of decellularized meniscal scaffolds using sonication treatment for tissue engineering." pp. 6953-6956.

89 Schwarz S., Koerber L., Elsaesser A. F., Goldberg-Bockhorn E., Seitz A. M., Durselen L. et al. Decellularized cartilage matrix as a novel biomatrix for cartilage tissue-engineering applications. Tissue EngPart A 2012;18(21-22):2195-209.

90 Minehara H., Urabe K., Naruse K., Mehlhorn A. T., Uchida K., Sudkamp N. P. et al. A new technique for seeding chondrocytes onto solvent-preserved human meniscus using the chemokinetic effect of recombinant human bone morphogenetic protein-2. Cell Tissue Bank 2011;12(3):199-207.

91 Sandmann G. H., Eichhorn S., Vogt S., Adamczyk C., Aryee S., Hoberg M. et al. Generation and characterization of a human acellular meniscus scaffold for tissue engineering. J Biomed Mater Res Part A 2009;91(2):567-74.

92 Puetzer J. L., and Bonassar L. J. High density type I collagen gels for tissue engineering of whole menisci. Acta Biomater 2013;9(8):7787-7795.
93 Puetzer J. L., and Bonassar L. J. Physiologically distributed loading patterns drive the formation of zonally organized collagen structures in tissue-engineered meniscus. Tissue Eng Part A 2016;22(13-14):907-916.
94 Puetzer J. L., Ballyns J. J., and Bonassar L. J. The effect of the duration of mechanical stimulation and post-stimulation culture on the structure and properties of dynamically compressed tissue-engineered menisci. Tissue Eng Part A 2012;18(13-14):1365-75.
95 Rey-Rico A., Cucchiarini M., and Madry H. Hydrogels for precision meniscus tissue engineering: a comprehensive review. Connect Tissue Res 2017;58(3-4):317-328.
96 Rey-Rico A., Klich A., Cucchiarini M., and Madry H. Biomedical-grade, high mannuronic acid content (BioMVM) alginate enhances the proteoglycan production of primary human meniscal fibrochondrocytes in a 3-D microenvironment. Sci Rep 2016;6:28170.
97 Koh R. H., Jin Y., Kang B.-J., and Hwang N. S. Chondrogenically primed tonsil-derived mesenchymal stem cells encapsulated in riboflavin-induced photocrosslinking collagen-hyaluronic acid hydrogel for meniscus tissue repairs. Acta Biomater 2017;53:318-328.
98 Kobayashi M. A study of Polyvinyl Alcohol - Hydrogel (PVA - H) artificial meniscus in vivo. Biomed Mater Eng 2004;14(4):505-515.
99 Kobayashi M., Toguchida J., and Oka M. Preliminary study of polyvinyl alcohol-hydrogel (PVA-H) artificial meniscus. Biomaterials 2003;24(4):639-647.
100 Kobayashi M., Toguchida J., and Oka M. Development of an artificial meniscus using polyvinyl alcohol-hydrogel for early return to, and continuance of, athletic life in sportspersons with severe meniscus injury. I: mechanical evaluation. Knee 2003;10(1):47-51.
101 Kobayashi M., Chang Y.-S., and Oka M. A two year in vivo study of polyvinyl alcohol-hydrogel (PVA-H) artificial meniscus. Biomaterials 2005;26(16):3243-3248.
102 Chen J.-P., and Cheng T.-H. Thermo-responsive chitosan-graft-poly(N-isopropylacrylamide) injectable hydrogel for cultivation of chondrocytes and meniscus cells. Macromol Biosci 2006;6(12):1026-1039.
103 Chen J.-P., and Cheng T.-H. Functionalized temperature-sensitive copolymer for tissue engineering of articular cartilage and meniscus. Colloids Surf A 2008;313–314(0):254-259.

104 Bakarich S. E., Gorkin R., 3rd, in het Panhuis M., and Spinks G. M. Three-dimensional printing fiber reinforced hydrogel composites. ACS Appl Materials Interfaces 2014;6(18):15998-6006.

105 Chia H. N., and Hull M. Compressive moduli of the human medial meniscus in the axial and radial directions at equilibrium and at a physiological strain rate. J Orthop Res 2008;26(7):951-956.

106 Gunja N. J., Uthamanthil R. K., and Athanasiou K. A. Effects of TGF-β1 and hydrostatic pressure on meniscus cell-seeded scaffolds. Biomaterials 2009;30(4):565-573.

107 Nakata K., Shino K., Hamada M., Mae T., Miyama T., Shinjo H. et al. Human meniscus cell: characterization of the primary culture and use for tissue engineering. Clin Orthop Relat Res 2001;391:S208-S218.

108 Schoenfeld A. J., Jacquet R., Lowder E., Doherty A., Leeson M. C., and Landis W. J. Histochemical analyses of tissue-engineered human menisci. Connect Tissue Res 2009;50(5):307-314.

109 Kang S.-W., Sun-Mi S., Jae-Sun L., Eung-Seok L., Kwon-Yong L., Sang-Guk P. et al. Regeneration of whole meniscus using meniscal cells and polymer scaffolds in a rabbit total meniscectomy model. J Biomed Mater Res Part A 2006;77A(4):659-671.

110 Clark C. R., and Ogden J. A., Development of the menisci of the human knee joint. Morphological changes and their potential role in childhood meniscal injury, 1983.

112 Wilson C. G., Nishimuta J. F., and Levenston M. E. Chondrocytes and meniscal fibrochondrocytes differentially process aggrecan during de novo extracellular matrix assembly. Tissue Eng Part A 2009;15(7):1513-1522.

113 Ryu K., Iriuchishima T., Oshida M., Saito A., Kato Y., Tokuhashi Y. et al. Evaluation of the morphological variations of the meniscus: a cadaver study. Knee Surg Sports Traumatol Arthrosc 2015;23(1):15-19.

114 Fuller E. S., Smith M. M., Little C. B., and Melrose J. Zonal differences in meniscus matrix turnover and cytokine response. Osteoarthritis Cartilage 2012;20(1):49-59.

115 Son M., and Levenston M. E. Discrimination of meniscal cell phenotypes using gene expression profiles. Eur Cell Mater 2012;23:195-208.

116 Stewart K., Pabbruwe M., Dickinson S., Sims T., Hollander A. P., and Chaudhuri J. B. The effect of growth factor treatment on meniscal chondrocyte proliferation and differentiation on polyglycolic acid scaffolds. Tissue Eng 2007;13(2):271-80.

117 de Mulder E. L., Hannink G., Giele M., Verdonschot N., and Buma P. Proliferation of meniscal fibrochondrocytes cultured on a new polyurethane scaffold is stimulated by TGF-ß. J Biomater Appl 2011.

118 Hoben G. M., Hu J. C., James R. A., and Athanasiou K. A. Self-assembly of fibrochondrocytes and chondrocytes for tissue engineering of the knee meniscus. Tissue Eng 2007;13(5):939-46.

119 Kanazawa T., Furumatsu T., Hachioji M., Oohashi T., Ninomiya Y., and Ozaki T. Mechanical stretch enhances COL2A1 expression on chromatin by inducing SOX9 nuclear translocalization in inner meniscus cells. J Orthop Res 2012;30(3):468-474.

120 Furumatsu T., Kanazawa T., Miyake Y., Kubota S., Takigawa M., and Ozaki T. Mechanical stretch increases Smad3-dependent CCN2 expression in inner meniscus cells. J Orthop Res 2012;30(11):1738-1745.

121 Mauck R. L., Martinez-Diaz G. J., Yuan X., and Tuan R. S. Regional multilineage differentiation potential of meniscal fibrochondrocytes: Implications for meniscus repair. Anat Rec 2007;290(1):48-58.

122 Schwartz J. A., Wang W., Goldstein T., and Grande D. A. Tissue engineered meniscus repair: Influence of cell passage number, tissue origin, and biomaterial carrier. Cartilage 2014;5(3):165-171.

123 Verdonk P. C. M., Forsyth R. G., Wang J., Almqvist K. F., Verdonk R., Veys E. M. et al. Characterisation of human knee meniscus cell phenotype. Osteoarthritis Cartilage 2005;13(7):548-560.

124 Croutze R., Jomha N., Uludag H., and Adesida A. Matrix forming characteristics of inner and outer human meniscus cells on 3D collagen scaffolds under normal and low oxygen tensions. BMC Musculoskelet Disord 2013;14(1):353.

125 Gunja N. J., and Athanasiou K. A. Passage and reversal effects on gene expression of bovine meniscal fibrochondrocytes. Arthritis Res Ther 2007;9(5):R93.

126 Marsano A., Millward-Sadler S. J., Salter D. M., Adesida A., Hardingham T., Tognana E. et al. Differential cartilaginous tissue formation by human synovial membrane, fat pad, meniscus cells and articular chondrocytes. Osteoarthritis Cartilage 2007;15(1):48-58.

127 Fox D. B., Warnock J. J., Stoker A. M., Luther J. K., and Cockrell M. Effects of growth factors on equine synovial fibroblasts seeded on synthetic scaffolds for avascular meniscal tissue engineering. Res Vet Sci 2010;88(2):326-332.

128 Yoo J. J., Bichara D. A., Zhao X., Randolph M. A., and Gill T. J. Implant-assisted meniscal repair in vivo using a chondrocyte-seeded flexible PLGA scaffold. J Biomed Mater ResPart A 2011;99A(1):102-108.

129 Visser J., Levett P. A., Te Moller N. C., Besems J., Boere K. W., van Rijen M. H. et al. Crosslinkable hydrogels derived from cartilage, meniscus, and tendon tissue. Tissue Eng Part A 2015;21(7-8):1195-206.

130 Prockop D. J. Marrow stromal cells as stem cells for nonhematopoietic tissues. Science 1997;276(5309):71-74.
131 Lane S. W., Williams D. A., and Watt F. M. Modulating the stem cell niche for tissue regeneration. Nat Biotechnol 2014;32(8):795-803.
132 Nemeth K., and Karpati S. Identifying the stem cell. J Invest Dermatol 2014;134(11):e26.
133 Giai Via A., Frizziero A., and Oliva F. Biological properties of mesenchymal Stem Cells from different sources. Muscles, Ligaments Tendons J 2012;2(3):154-162.
134 Sundaram S., and Niklason L. E. Smooth muscle and other cell sources for human blood vessel engineering. Cells Tissues Organs 2011;195(1-2):15-25.
135 Lau A. N., Goodwin M., Kim C. F., and Weiss D. J. Stem cells and regenerative medicine in lung biology and diseases. Mol Ther 2012;20(6):1116-1130.
136 Bianco P., Cao X., Frenette P. S., Mao J. J., Robey P. G., Simmons P. J. et al. The meaning, the sense and the significance: translating the science of mesenchymal stem cells into medicine. Nat Med 2013;19(1):35-42.
137 Zakrzewski J. L., van den Brink M. R., and Hubbell J. A. Overcoming immunological barriers in regenerative medicine. Nat Biotechnol 2014;32(8):786-94.
138 Baker B. M., Shah R. P., Huang A. H., and Mauck R. L. Dynamic tensile loading improves the functional properties of mesenchymal stem cell-laden nanofiber-based fibrocartilage. Tissue Eng Part A 2011;17(9-10):1445-1455.
139 Vangsness C. T., Jr., Farr J., 2nd, Boyd J., Dellaero D. T., Mills C. R., and LeRoux-Williams M. Adult human mesenchymal stem cells delivered via intra-articular injection to the knee following partial medial meniscectomy: a randomized, double-blind, controlled study. J Bone Joint Surg Am 2014;96(2):90-8.
140 Angele P., Kujat R., Koch M., and Zellner J. Role of mesenchymal stem cells in meniscal repair. J Exp Orthop 2014;1(1):12.
141 Moriguchi Y., Tateishi K., Ando W., Shimomura K., Yonetani Y., Tanaka Y. et al. Repair of meniscal lesions using a scaffold-free tissue-engineered construct derived from allogenic synovial MSCs in a miniature swine model. Biomaterials 2013;34(9):2185-2193.
142 Hatsushika D., Muneta T., Horie M., Koga H., Tsuji K., and Sekiya I. Intraarticular injection of synovial stem cells promotes meniscal regeneration in a rabbit massive meniscal defect model. J Orthop Res 2013;31(9):1354-1359.
143 Imler S. M., Doshi A. N., and Levenston M. E. Combined effects of growth factors and static mechanical compression on meniscus explant biosynthesis. Osteoarthritis Cartilage 2004;12(9):736-744.

144 Forriol F. Growth factors in cartilage and meniscus repair. Injury 2009;40, Supplement 3(0):S12-S16.
145 Kasemkijwattana C., Menetrey J., Goto H., Niyibizi C., Fu F. H., and Huard J. The use of growth factors, gene therapy and tissue engineering to improve meniscal healing. Mater Sci Eng C 2000;13(1):19-28.
146 Becker R., Pufe T., Kulow S., Giessmann N., Neumann W., Mentlein R. et al. Expression of vascular endothelial growth factor during healing of the meniscus in a rabbit model. J Bone Joint Surg Br 2004;86(7):1082-1087.
147 Reckers L. J., Fagundes D. J., and Cohen M. The ineffectiveness of fibrin glue and cyanoacrylate on fixation of meniscus transplants in rabbits. Knee 2009;16(4):290-294.
148 Gillquist J., Hamberg P., and Lysholm J. Endoscopic partial and total meniscectomy: a comparative study with a short term follow up. Acta Orthop Scand 1982;53(6):975-979.
149 Rangger C., Klestil T., Gloetzer W., Kemmler G., and Benedetto K. P. Osteoarthritis after arthroscopic partial meniscectomy. Am J Sports Med 1995;23(2):240-244.
150 Scotti C., Pozzi A., Mangiavini L., Vitari F., Boschetti F., Domeneghini C. et al. Healing of meniscal tissue by cellular fibrin glue: an in vivo study. Knee Surg Sports Traumatol Arthrosc 2009;17(6):645-651.
151 Chiari C., Koller U., Dorotka R., Eder C., Plasenzotti R., Lang S. et al. A tissue engineering approach to meniscus regeneration in a sheep model. Osteoarthritis Cartilage 2006;14(10):1056-1065.
152 Singelyn J. M., DeQuach J. A., Seif-Naraghi S. B., Littlefield R. B., Schup-Magoffin P. J., and Christman K. L. Naturally derived myocardial matrix as an injectable scaffold for cardiac tissue engineering. Biomaterials 2009;30(29):5409-5416.
153 Keeney M., Lai J. H., and Yang F. Recent progress in cartilage tissue engineering. Curr Opin Biotechnol 2011;22(5):734-740.
154 Mollon B., Kandel R., Chahal J., and Theodoropoulos J. The clinical status of cartilage tissue regeneration in humans. Osteoarthritis cartilage 2013;21(12):1824-1833.
155 Gilbert T. W., Sellaro T. L., and Badylak S. F. Decellularization of tissues and organs. Biomaterials 2006;27(19):3675-3683.
156 Badylak S. F., Weiss D. J., Caplan A., and Macchiarini P. Engineered whole organs and complex tissues. Lancet;379(9819):943-952.
157 Singelyn J. M., and Christman K. L. Injectable materials for the treatment of myocardial infarction and heart failure: The promise of decellularized matrices. J Cardiovasc Transl Res 2010;3(5):478-486.

158 Singelyn J. M., Sundaramurthy P., Johnson T. D., Schup-Magoffin P. J., Hu D. P., Faulk D. M. et al. Catheter-deliverable hydrogel derived from decellularized ventricular extracellular matrix increases endogenous cardiomyocytes and preserves cardiac function post-myocardial infarction. J Am Coll Cardiol 2012;59(8):751-763.

159 Seif-Naraghi S. B., Singelyn J. M., Salvatore M. A., Osborn K. G., Wang J. J., Sampat U. et al. Safety and efficacy of an injectable extracellular matrix hydrogel for treating myocardial infarction. Sci Transl Med 2013;5(173):10.1126/scitranslmed.3005503.

160 Wolf M. T., Daly K. A., Brennan-Pierce E. P., Johnson S. A., Carruthers C. A., D'Amore A. et al. A hydrogel derived from decellularized dermal extracellular matrix. Biomaterials 2012;33(29):7028-7038.

161 Duan Y., Liu Z., O'Neill J., Wan L., Freytes D., and Vunjak-Novakovic G. Hybrid gel composed of native heart matrix and collagen induces cardiac differentiation of human embryonic stem cells without supplemental growth factors. J Cardiovasc Transl Res 2011;4(5):605-615.

162 French K. M., Boopathy A. V., DeQuach J. A., Chingozha L., Lu H., Christman K. L. et al. A naturally derived cardiac extracellular matrix enhances cardiac progenitor cell behavior in vitro. Acta Biomater 2012;8(12):4357-4364.

163 Sawkins M. J., Bowen W., Dhadda P., Markides H., Sidney L. E., Taylor A. J. et al. Hydrogels derived from demineralized and decellularized bone extracellular matrix. Acta Biomater 2013;9(8):7865-7873.

164 Freytes D. O., Martin J., Velankar S. S., Lee A. S., and Badylak S. F. Preparation and rheological characterization of a gel form of the porcine urinary bladder matrix. Biomaterials 2008;29(11):1630-1637.

165 Medberry C. J., Crapo P. M., Siu B. F., Carruthers C. A., Wolf M. T., Nagarkar S. P. et al. Hydrogels derived from central nervous system extracellular matrix. Biomaterials 2013;34(4):1033-1040.

166 Quint C., Kondo Y., Manson R. J., Lawson J. H., Dardik A., and Niklason L. E. Decellularized tissue-engineered blood vessel as an arterial conduit. Proc Natl Acad Sci U S A 2011;108(22):9214-9219.

167 Young D. A., Ibrahim D. O., Hu D., and Christman K. L. Injectable hydrogel scaffold from decellularized human lipoaspirate. Acta Biomater 2011;7(3):1040-1049.

168 DeQuach J. A., Yuan S. H., Goldstein L. S. B., and Christman K. L. Decellularized porcine brain matrix for cell culture and tissue engineering scaffolds. Tissue Eng Part A 2011;17(21-22):2583-2592.

169 Elder B. D., Eleswarapu S. V., and Athanasiou K. A. Extraction techniques for the decellularization of tissue engineered articular cartilage constructs. Biomaterials 2009;30(22):3749-3756.
170 Gilbert T. W., Freund J. M., and Badylak S. F. Quantification of DNA in biologic scaffold materials. J Surg Res 2009;152(1):135-139.
171 Woessner J. F. The determination of hydroxyproline in tissue and protein samples containing small proportions of this imino acid. Arch Biochem Biophys 1961;93(2):440-447.
172 Kishimoto H., Akagi M., Zushi S., Teramura T., Onodera Y., Sawamura T. et al. Induction of hypertrophic chondrocyte-like phenotypes by oxidized LDL in cultured bovine articular chondrocytes through increase in oxidative stress. Osteoarthritis Cartilage 2010;18(10):1284-1290.
173 Thevenot P., Nair A., Dey J., Yang J., and Tang L. Method to analyze three-dimensional cell distribution and infiltration in degradable scaffolds. Tissue Eng Part C Methods 2008;14(4):319-331.
174 Ionescu L. C., Lee G. C., Garcia G. H., Zachry T. L., Shah R. P., Sennett B. J. et al. Maturation state-dependent alterations in meniscus integration: implications for scaffold design and tissue engineering. Tissue Eng Part A 2011;17(1-2):193-204.
175 Brightman A., Rajwa B., Sturgis J., McCallister M., Robinson J., and Voytik‐Harbin S. Time‐lapse confocal reflection microscopy of collagen fibrillogenesis and extracellular matrix assembly in vitro. Biopolymers 2000;54(3):222-234.
176 Grant D. S., Leblond C. P., Kleinman H. K., Inoue S., and Hassell J. R. The incubation of laminin, collagen IV, and heparan sulfate proteoglycan at 35 degrees C yields basement membrane-like structures. J Cell Biol 1989;108(4):1567-1574.
177 Stuart K., and Panitch A. Influence of chondroitin sulfate on collagen gel structure and mechanical properties at physiologically relevant levels. Biopolymers 2008;89(10):841-851.
178 Silver F. H. Type I collagen fibrillogenesis in vitro. Additional evidence for the assembly mechanism. J Biol Chem 1981;256(10):4973-4977.
179 Engler A. J., Griffin M. A., Sen S., Bönnemann C. G., Sweeney H. L., and Discher D. E. Myotubes differentiate optimally on substrates with tissue-like stiffness. J Cell Biol 2004;166(6):877-887.
180 Wang N., Tolić-Nørrelykke I. M., Chen J., Mijailovich S. M., Butler J. P., Fredberg J. J. et al. Cell prestress. I. Stiffness and prestress are closely associated in adherent contractile cells. Am J Physiol Cell Physiol 2002;282(3):C606-C616.
181 Saha K., Keung A. J., Irwin E. F., Li Y., Little L., Schaffer D. V. et al. Substrate modulus directs neural stem cell behavior. Biophys J 2008;95(9):4426-4438.

182 Lee K. Y., and Mooney D. J. Hydrogels for tissue engineering. Chem Rev 2001;101(7):1869-1880.
183 Wall S. T., Yeh C. C., Tu R. Y., Mann M. J., and Healy K. E. Biomimetic matrices for myocardial stabilization and stem cell transplantation. J Biomed Mater Res Part A 2010;95(4):1055-1066.
184 Azuma C., Yasuda K., Tanabe Y., Taniguro H., Kanaya F., Nakayama A. et al. Biodegradation of high‐toughness double network hydrogels as potential materials for artificial cartilage. J Biomed Mater Res Part A 2007;81(2):373-380.
185 Busby G. A., Grant M. H., MacKay S. P., and Riches P. E. Confined compression of collagen hydrogels. J Biomech 2013;46(4):837-840.
186 Pereira H., Frias A. M., Oliveira J. M., Espregueira-Mendes J., and Reis R. L. Tissue engineering and regenerative medicine strategies in meniscus lesions. Arthroscopy 2011;27(12):1706-1719.
187 Rongen J. J., van Tienen T. G., van Bochove B., Grijpma D. W., and Buma P. Biomaterials in search of a meniscus substitute. Biomaterials 2014;35(11):3527-3540.
188 Peretti G. M., Caruso E. M., Randolph M. A., and Zaleske D. J. Meniscal repair using engineered tissue. J Orthop Res 2001;19(2):278-285.
189 Peretti G. M., Gill T. J., Xu J.-W., Randolph M. A., Morse K. R., and Zaleske D. J. Cell-based therapy for meniscal repair. Am J Sports Med 2004;32(1):146-158.
190 Blakeney B. A., Tambralli A., Anderson J. M., Andukuri A., Lim D.-J., Dean D. R. et al. Cell infiltration and growth in a low density, uncompressed three-dimensional electrospun nanofibrous scaffold. Biomaterials 2011;32(6):1583-1590.
191 DeLong S. A., Gobin A. S., and West J. L. Covalent immobilization of RGDS on hydrogel surfaces to direct cell alignment and migration. J Control Release 2005;109(1):139-148.
192 Krych A. J., Wanivenhaus F., Ng K. W., Doty S., Warren R. F., and Maher S. A. Matrix generation within a macroporous non-degradable implant for osteochondral defects is not enhanced with partial enzymatic digestion of the surrounding tissue: evaluation in an in vivo rabbit model. J Mater Sci Mater Med 2013;24(10):2429-2437.
193 Ng K. W., Wanivenhaus F., Chen T., Hsu H.-C., Allon A. A., Abrams V. D. et al. A novel macroporous polyvinyl alcohol scaffold promotes chondrocyte migration and interface formation in an in vitro cartilage defect model. Tissue Eng Part A 2012;18(11-12):1273-1281.
194 Agrawal V., Tottey S., Johnson S. A., Freund J. M., Siu B. F., and Badylak S. F. Recruitment of progenitor cells by an extracellular matrix cryptic peptide in a mouse model of digit amputation. Tissue Eng Part A 2011;17(19-20):2435-2443.

195 Gilbert T. W., Stewart-Akers A. M., and Badylak S. F. A quantitative method for evaluating the degradation of biologic scaffold materials. Biomaterials 2007;28(2):147-150.

196 Tottey S., Corselli M., Jeffries E. M., Londono R., Peault B., and Badylak S. F. Extracellular matrix degradation products and low-oxygen conditions enhance the regenerative potential of perivascular stem cells. Tissue Eng Part A 2011;17(1-2):37-44.

197 Sadr N., Pippenger B. E., Scherberich A., Wendt D., Mantero S., Martin I. et al. Enhancing the biological performance of synthetic polymeric materials by decoration with engineered, decellularized extracellular matrix. Biomaterials 2012;33(20):5085-5093.

198 Hoganson D. M., O'Doherty E. M., Owens G. E., Harilal D. O., Goldman S. M., Bowley C. M. et al. The retention of extracellular matrix proteins and angiogenic and mitogenic cytokines in a decellularized porcine dermis. Biomaterials 2010;31(26):6730-6737.

199 Goh S.-K., Bertera S., Olsen P., Candiello J. E., Halfter W., Uechi G. et al. Perfusion-decellularized pancreas as a natural 3D scaffold for pancreatic tissue and whole organ engineering. Biomaterials 2013;34(28):6760-6772.

200 Faulk D. M., Johnson S. A., Zhang L., and Badylak S. F. Role of the extracellular matrix in whole organ engineering. J Cell Physiol 2014;229(8):984-989.

201 Benders K. E. M., Weeren P. R. v., Badylak S. F., Saris D. B. F., Dhert W. J. A., and Malda J. Extracellular matrix scaffolds for cartilage and bone regeneration. Trends Biotechnol 2013;31(3):169-176.

202 Brown B., Lindberg K., Reing J., Stolz D. B., and Badylak S. F. The basement membrane component of biologic scaffolds derived from extracellular matrix. Tissue Eng 2006;12(3):519-526.

203 Melo E., Garreta E., Luque T., Cortiella J., Nichols J., Navajas D. et al. Effects of the decellularization method on the local stiffness of acellular lungs. Tissue Eng Part C Methods 2014;20(5):412-22.

204 Badylak S. F. The extracellular matrix as a biologic scaffold material. Biomaterials 2007;28(25):3587-3593.

205 Wong M. L., and Griffiths L. G. Immunogenicity in xenogeneic scaffold generation: antigen removal vs. decellularization. Acta Biomater 2014;10(5):1806-16.

206 Wallis J. M., Borg Z. D., Daly A. B., Deng B., Ballif B. A., Allen G. B. et al. Comparative assessment of detergent-based protocols for mouse lung de-cellularization and re-cellularization. Tissue Eng Part C Methods 2012;18(6):420-32.

207 Meyer S. R., Chiu B., Churchill T. A., Zhu L., Lakey J. R. T., and Ross D. B. Comparison of aortic valve allograft decellularization techniques in the rat. J Biomed Mater Res Part A 2006;79A(2):254-262.

208 Xu H., Xu B., Yang Q., Li X., Ma X., Xia Q. et al. Comparison of decellularization protocols for preparing a decellularized porcine annulus fibrosus scaffold. PLoS One 2014;9(1):e86723.

209 He M., and Callanan A. Comparison of methods for whole-organ decellularization in tissue engineering of bioartificial organs. Tissue Eng Part B Rev 2013;19(3):194-208.

210 Kajbafzadeh A.-M., Javan-Farazmand N., Monajemzadeh M., and Baghayee A. Determining the optimal decellularization and sterilization protocol for preparing a tissue scaffold of a human-sized liver tissue. Tissue Eng Part C Methods 2013;19(8):642-651.

211 Sheridan W. S., Duffy G. P., and Murphy B. P. Optimum parameters for freeze-drying decellularized arterial scaffolds. Tissue Eng Part C Methods 2013;19(12):981-90.

212 Vavken P., Joshi S., and Murray M. M. TRITON-X is most effective among three decellularization agents for ACL tissue engineering. J Orthop Res 2009;27(12):1612-1618.

213 Cissell D. D., Hu J. C., Griffiths L. G., and Athanasiou K. A. Antigen removal for the production of biomechanically functional, xenogeneic tissue grafts. J Biomech2014;47(9):1987-96.

214 Rieder E., Kasimir M.-T., Silberhumer G., Seebacher G., Wolner E., Simon P. et al. Decellularization protocols of porcine heart valves differ importantly in efficiency of cell removal and susceptibility of the matrix to recellularization with human vascular cells. J Thorac Cardiovasc Surg 2004;127(2):399-405.

215 Yang M., Chen C.-Z., Wang X.-N., Zhu Y.-B., and Gu Y. J. Favorable effects of the detergent and enzyme extraction method for preparing decellularized bovine pericardium scaffold for tissue engineered heart valves. J Biomed Mater Res Part B Appl Biomater 2009;91B(1):354-361.

216 Yang Z., Shi Y., Wei X., He J., Yang S., Dickson G. et al. Fabrication and repair of cartilage defects with a novel acellular cartilage matrix scaffold. Tissue Eng Part C Methods 2009;16(5):865-876.

217 Booth C., Korossis S., Wilcox H., Watterson K., Kearney J., Fisher J. et al. Tissue engineering of cardiac valve prostheses I: development and histological characterization of an acellular porcine scaffold. J Heart Valve Dis 2002;11(4):457-462.

218 Wu J., Ding Q., Dutta A., Wang Y., Huang Y.-h., Weng H. et al. An injectable extracellular matrix derived hydrogel for meniscus repair and regeneration. Acta Biomater 2015;16:49-59.

219 Kheir E., Stapleton T., Shaw D., Jin Z., Fisher J., and Ingham E. Development and characterization of an acellular porcine cartilage bone matrix for use in tissue engineering. J Biomed Mater Res Part A 2011;99A(2):283-294.

220 Remlinger N. T., Czajka C. A., Juhas M. E., Vorp D. A., Stolz D. B., Badylak S. F. et al. Hydrated xenogeneic decellularized tracheal matrix as a scaffold for tracheal reconstruction. Biomaterials 2010;31(13):3520-3526.

221 Barbosa I., Garcia S., Barbier-Chassefière V., Caruelle J.-P., Martelly I., and Papy-García D. Improved and simple micro assay for sulfated glycosaminoglycans quantification in biological extracts and its use in skin and muscle tissue studies. Glycobiology 2003;13(9):647-653.

222 Keane T. J., Londono R., Turner N. J., and Badylak S. F. Consequences of ineffective decellularization of biologic scaffolds on the host response. Biomaterials 2012;33(6):1771-1781.

223 Faulk D. M., Carruthers C. A., Warner H. J., Kramer C. R., Reing J. E., Zhang L. et al. The effect of detergents on the basement membrane complex of a biologic scaffold material. Acta Biomater 2014;10(1):183-193.

224 Adam Young D., Bajaj V., and Christman K. L. Decellularized adipose matrix hydrogels stimulate in vivo neovascularization and adipose formation. J Biomed Mater Res Part A 2014;102(6):1641-1651.

225 Jeffords M. E., Wu J., Shah M., Hong Y., and Zhang G. Tailoring material properties of cardiac matrix hydrogels to induce endothelial differentiation of human mesenchymal stem cells. ACS Appl Mater Interfaces 2015;7(20):11053-61.

226 Arnoczky S. P., and Warren R. F. Microvasculature of the human meniscus. Am J Sports Med 1982;10(2):90-95.

227 Esparza R., Gortazar A. R., and Forriol F. Cell study of the three areas of the meniscus: Effect of growth factors in an experimental model in sheep. J Orthop Res 2012;30(10):1647-1651.

228 Yuan X., Arkonac D. E., Chao P. H., and Vunjak-Novakovic G. Electrical stimulation enhances cell migration and integrative repair in the meniscus. Sci Rep 2014;4:3674.

229 Shimomura K., Bean A. C., Lin H., Nakamura N., and Tuan R. S. In vitro repair of meniscal radial tear using aligned electrospun nanofibrous scaffold. Tissue Eng Part A 2015;21(13-14):2066-2075.

230 Fisher M. B., Henning E. A., Söegaard N., Esterhai J. L., and Mauck R. L. Organized nanofibrous scaffolds that mimic the macroscopic and microscopic architecture of the knee meniscus. Acta Biomater 2013;9(1):4496-4504.
231 Shimomura K., Rothrauff B. B., and Tuan R. S. Region-specific effect of the decellularized meniscus extracellular matrix on mesenchymal stem cell–based meniscus tissue engineering. Am J Sports Med 2016:0363546516674184.
232 Mueller S. M., Shortkroff S., Schneider T. O., Breinan H. A., Yannas I. V., and Spector M. Meniscus cells seeded in type I and type II collagen–GAG matrices in vitro. Biomaterials 1999;20(8):701-709.
233 Calamia V., Mateos J., Fernandez-Puente P., Lourido L., Rocha B., Fernandez-Costa C. et al. A pharmacoproteomic study confirms the synergistic effect of chondroitin sulfate and glucosamine. Sci Rep 2014;4:10.1038/srep05069
234 Englund M., and Lohmander L. S. Patellofemoral osteoarthritis coexistent with tibiofemoral osteoarthritis in a meniscectomy population. Ann Rheum Dis 2005;64(12):1721-1726.
235 Upton M. L., Chen J., and Setton L. A. Region-specific constitutive gene expression in the adult porcine meniscus. J Orthop Res 2006;24(7):1562-1570.
236 Buma P., Ramrattan N. N., van Tienen T. G., and Veth R. P. H. Tissue engineering of the meniscus. Biomaterials 2004;25(9):1523-1532.
237 Ballyns J. J., Wright T. M., and Bonassar L. J. Effect of media mixing on ECM assembly and mechanical properties of anatomically-shaped tissue engineered meniscus. Biomaterials 2010;31(26):6756-6763.
238 Wu J., Ravikumar P., Nguyen K. T., Hsia C. C. W., and Hong Y. Lung protection by inhalation of exogenous solubilized extracellular matrix. PLoS One 2017;12(2):e0171165.
239 Zheng M. H., Chen J., Kirilak Y., Willers C., Xu J., and Wood D. Porcine small intestine submucosa (SIS) is not an acellular collagenous matrix and contains porcine DNA: possible implications in human implantation. J Biomed Mater Res Part B Appl Biomater 2005;73(1):61-67.
240 Yuan L., Li B., Yang J., Ni Y., Teng Y., Guo L. et al. Effects of composition and mechanical property of injectable collagen I/II composite hydrogels on chondrocyte behaviors. Tissue Eng Part A 2016;22(11-12):899-906.
241 Yang J.-A., Yeom J., Hwang B. W., Hoffman A. S., and Hahn S. K. In situ-forming injectable hydrogels for regenerative medicine. Prog Polym Sci 2014;39(12):1973-1986.
242 O'Neill J. D., Anfang R., Anandappa A., Costa J., Javidfar J., Wobma H. M. et al. Decellularization of human and porcine lung tissues for pulmonary tissue engineering. Ann Thorac Surg 2013;96(3):1046-55; discussion 1055-6.

243 Pouliot R. A., Link P. A., Mikhaiel N. S., Schneck M. B., Valentine M. S., Kamga Gninzeko F. J. et al. Development and characterization of a naturally derived lung extracellular matrix hydrogel. J Biomed Mater Res Part A 2016;104(8):1922-35.
244 Tan G. K., Dinnes D. L., Myers P. T., and Cooper-White J. J. Effects of biomimetic surfaces and oxygen tension on redifferentiation of passaged human fibrochondrocytes in 2D and 3D cultures. Biomaterials 2011;32(24):5600-14.
245 Vernon R. B., and Sage E. H. Contraction of fibrillar type I collagen by endothelial cells: a study in vitro. J Cellular Biochem 1996;60(2):185-197.
246 Bell E., Ivarsson B., and Merrill C. Production of a tissue-like structure by contraction of collagen lattices by human fibroblasts of different proliferative potential in vitro. Proc Natl Acad Sci U S A 1979;76(3):1274-1278.
247 Erickson I. E., Huang A. H., Chung C., Li R. T., Burdick J. A., and Mauck R. L. Differential Maturation and Structure–Function Relationships in Mesenchymal Stem Cell- and Chondrocyte-Seeded Hydrogels. Tissue Eng Part A 2008;15(5):1041-1052.
248 Joshi M. D., Suh J.-K., Marui T., and Woo S. L. Y. Interspecies variation of compressive biomechanical properties of the meniscus. J Biomed Mater Res 1995;29(7):823-828.
249 Proctor C. S., Schmidt M. B., Whipple R. R., Kelly M. A., and Mow V. C. Material properties of the normal medial bovine meniscus. J Orthop Res 1989;7(6):771-782.
250 Jang J., Kim T. G., Kim B. S., Kim S. W., Kwon S. M., and Cho D. W. Tailoring mechanical properties of decellularized extracellular matrix bioink by vitamin B2-induced photo-crosslinking. Acta Biomater 2016;33:88-95.
251 Yuan X., Wei Y., Villasante A., Ng J. J. D., Arkonac D. E., Chao P.-h. G. et al. Stem cell delivery in tissue-specific hydrogel enabled meniscal repair in an orthotopic rat model. Biomaterials 2017;132:59-71.
252 He M., Callanan A., Lagaras K., Steele J. A. M., and Stevens M. M. Optimization of SDS exposure on preservation of ECM characteristics in whole organ decellularization of rat kidneys. Biomed Mater Res Part B Appl Biomater 2016;105(6):1352-1360.
253 Brown B. N., Freund J. M., Han L., Rubin J. P., Reing J. E., Jeffries E. M. et al. Comparison of three methods for the derivation of a biologic scaffold composed of adipose tissue extracellular matrix. Tissue Eng Part C Methods 2011;17(4):411-421.
254 Gillies A. R., Smith L. R., Lieber R. L., and Varghese S. Method for decellularizing skeletal muscle without detergents or proteolytic enzymes. Tissue Eng Part C Methods 2011;17(4):383-9.

255 Melrose J., Smith S., Cake M., Read R., and Whitelock J. Comparative spatial and temporal localisation of perlecan, aggrecan and type I, II and IV collagen in the ovine meniscus: an ageing study. Histochem Cell Biol 2005;124(3-4):225-235.
256 Kambic H. E., and McDevitt C. A. Spatial organization of types I and II collagen in the canine meniscus. J Orthop Res 2005;23(1):142-149.
257 Zhang X., Aoyama T., Ito A., Tajino J., Nagai M., Yamaguchi S. et al. Regional comparisons of porcine menisci. J Orthop Res 2014;32(12):1602-1611.
258 Vanderploeg E. J., Wilson C. G., Imler S. M., Ling C. H.-Y., and Levenston M. E. Regional variations in the distribution and colocalization of extracellular matrix proteins in the juvenile bovine meniscus. J Anat 2012;221(2):174-186.
259 Kahlon A., Hurtig M. B., and Gordon K. D. Regional and depth variability of porcine meniscal mechanical properties through biaxial testing. J Mech Behav Biomed Mater 2015;41(0):108-114.
260 Abraham A. C., Edwards C. R., Odegard G. M., and Donahue T. L. H. Regional and fiber orientation dependent shear properties and anisotropy of bovine meniscus. J Mech Behav Biomed Mater 2011;4(8):2024-2030.
261 Badylak S. F., Taylor D., and Uygun K. Whole-organ tissue engineering: decellularization and recellularization of three-dimensional matrix scaffolds. Annu Rev Biomed Eng 2011;13(1):27-53.
262 Gibson M., Beachley V., Coburn J., Bandinelli P. A., Mao H. Q., and Elisseeff J. Tissue extracellular matrix nanoparticle presentation in electrospun nanofibers. BioMed Res Int 2014;2014:469120.
263 Stankus J. J., Freytes D. O., Badylak S. F., and Wagner W. R. Hybrid nanofibrous scaffolds from electrospinning of a synthetic biodegradable elastomer and urinary bladder matrix. J Biomater Sci Polym Ed 2008;19(5):635-652.
264 Ratner B. D., and Bryant S. J. Biomaterials: where we have been and where we are going. Annu Rev Biomed Eng 2004;6:41-75.
265 Baiguera S., Del Gaudio C., Lucatelli E., Kuevda E., Boieri M., Mazzanti B. et al. Electrospun gelatin scaffolds incorporating rat decellularized brain extracellular matrix for neural tissue engineering. Biomaterials 2014;35(4):1205-1214.
266 Levorson E. J., Mountziaris P. M., Hu O., Kasper F. K., and Mikos A. G. Cell-Derived Polymer/Extracellular Matrix Composite Scaffolds for Cartilage Regeneration, Part 1: Investigation of Cocultures and Seeding Densities for Improved Extracellular Matrix Deposition. Tissue Eng Part C Methods 2014;20(4):340-357.
267 Garrigues N. W., Little D., Sanchez-Adams J., Ruch D. S., and Guilak F. Electrospun cartilage-derived matrix scaffolds for cartilage tissue engineering. J Biomed Mater Res Part A 2014;102(11):3998-4008.

268 Song X., Xie Y., Liu Y., Shao M., and Wang W. Beneficial effects of coculturing synovial derived mesenchymal stem cells with meniscus fibrochondrocytes are mediated by fibroblast growth factor 1: increased proliferation and collagen synthesis. Stem Cells Int 2015;2015:926325.
269 Hong S., and Kim G. Electrospun micro/nanofibrous conduits composed of poly(epsilon-caprolactone) and small intestine submucosa powder for nerve tissue regeneration. J Biomater Sci Polym Ed Part B Appl Biomater 2010;94(2):421-8.
270 Ji Y., Ghosh K., Shu X. Z., Li B., Sokolov J. C., Prestwich G. D. et al. Electrospun three-dimensional hyaluronic acid nanofibrous scaffolds. Biomaterials 2006;27(20):3782-3792.
271 Chainani A., Hippensteel K. J., Kishan A., Garrigues N. W., Ruch D. S., Guilak F. et al. Multilayered electrospun scaffolds for tendon tissue engineering. Tissue Eng Part A 2013;19(23-24):2594-2604.
272 Matthews J. A., Wnek G. E., Simpson D. G., and Bowlin G. L. Electrospinning of collagen nanofibers. Biomacromolecules 2002;3(2):232-238.
273 Yin A., Zhang K., McClure M. J., Huang C., Wu J., Fang J. et al. Electrospinning collagen/chitosan/poly(L-lactic acid-co-epsilon-caprolactone) to form a vascular graft: mechanical and biological characterization. J Biomed Mater Res Part A 2013;101(5):1292-301.
274 Zhang K., Wang H., Huang C., Su Y., Mo X., and Ikada Y. Fabrication of silk fibroin blended P(LLA-CL) nanofibrous scaffolds for tissue engineering. J Biomed Mater Res Part A 2010;93A(3):984-993.
275 Powell H. M., and Boyce S. T. Engineered human skin fabricated using electrospun collagen–PCL blends: morphogenesis and mechanical properties. Tissue Eng Part A 2009;15(8):2177-2187.
276 Chen F.-M., and Liu X. Advancing biomaterials of human origin for tissue engineering. Prog Polym Sci 2016;53:86-168.
277 Crowder S. W., Leonardo V., Whittaker T., Papathanasiou P., and Stevens M. M. Material cues as potent regulators of epigenetics and stem cell function. Cell Stem Cell 2016;18(1):39-52.
278 Yoon H., and Kim G. Micro/nanofibrous scaffolds electrospun from PCL and small intestinal submucosa. J Biomater Sci Polym Ed 2010;21(5):553-562.
279 Zhong S., Zhang Y., and Lim C. T. Fabrication of large pores in electrospun nanofibrous scaffolds for cellular infiltration: a review. Tissue Eng Part B Rev 2011;18(2):77-87.
280 Rnjak-Kovacina J., and Weiss A. S. Increasing the pore size of electrospun scaffolds. Tissue Eng Part B Rev 2011;17(5):365-372.

281 Didangelos A., Yin X., Mandal K., Saje A., Smith A., Xu Q. et al. Extracellular matrix composition and remodeling in human abdominal aortic aneurysms: a proteomics approach. Mol Cell Proteomics 2011;10(8):M111 008128.

282 Brennan E. P., Tang X.-H., Stewart-Akers A. M., Gudas L. J., and Badylak S. F. Chemoattractant activity of degradation products of fetal and adult skin extracellular matrix for keratinocyte progenitor cells. J Tissue Eng Regen Med 2008;2(8):491-498.

283 Mizuno K., Muneta T., Morito T., Ichinose S., Koga H., Nimura A. et al. Exogenous synovial stem cells adhere to defect of meniscus and differentiate into cartilage cells. J Med Dent Sci 2008;55(1):101-111.

284 Horie M., Driscoll M. D., Sampson H. W., Sekiya I., Caroom C. T., Prockop D. J. et al. Implantation of allogenic synovial stem cells promotes meniscal regeneration in a rabbit meniscal defect model. J Bone Joint Surg Am 2012;94(8):701-712.

285 Moon M.-s., Kim J., and Ok I. The normal and regenerated meniscus in rabbits. Morphologic and histologic studies. Clin Orthop Relat Res 1983(182):264-269.

286 Walsh C. J., Goodman D., Caplan A. I., and Goldberg V. M. Meniscus regeneration in a rabbit partial meniscectomy model. Tissue Eng 1999;5(4):327-337.

287 Ishida K., Kuroda R., Miwa M., Tabata Y., Hokugo A., Kawamoto T. et al. The regenerative effects of platelet-rich plasma on meniscal cells in vitro and its in vivo application with biodegradable gelatin hydrogel. Tissue Eng 2007;13(5):1103-12.

288 Ruiz-Ibán M. Á., Díaz-Heredia J., García-Gómez I., Gonzalez-Lizán F., Elías-Martín E., and Abraira V. The effect of the addition of adipose-derived mesenchymal stem cells to a meniscal repair in the avascular zone: an experimental study in rabbits. Arthroscopy 2011;27(12):1688-1696.

Biographical Information

Jinglei Wu was born in Wuhan, China. He received his Bachelor Degree in Biotechnology from the Yangtze University, Jingzhou, China, in June 2009. He then received his Master Degree in Biochemistry and Biomolecule from the Donghua University, Shanghai, China, in March 2012. He worked in Dr, Xiumei Mo's laboratory on the project of electrospun nanoyarn scaffolds for cartilage tissue engineering. Then he came to the U.S.A and started his Ph.D. study at the University of North Texas, Denton, TX, in August 2012. Jinglei transferred to the University of Texas at Arlington, Arlington, TX, and began his work under the supervision of Dr. Yi Hong to pursue his Ph.D. in Biomedical Engineering in June 2013. His work focused on the development of decellularized meniscus ECM materials for meniscus repair and regeneration. As a Doctoral student, Jinglei has published five peer-reviewed research articles, one review article, and fifteen conference abstracts. He is still working with Dr. Hong in the preparation of several manuscripts for submission. Jinglei has received several awards including the Enhanced Graduate Teaching Assistantship, the Alfred and Janet Potvin Award for Outstanding Bioengineering Student from the University of Texas at Arlington, and the Travel Award from the NIH Lung Regeneration and Repair Consortium. After graduation, Jinglei plans to continue his research career in biomaterials and tissue engineering.